

INTER- AND INTRA-ANNUAL VARIABILITY IN AN INTERACTIVE OCEAN- ATMOSPHERE CLIMATE SYSTEM

D. D. Houghton and R. G. Gallimore
Co-Principal Investigators

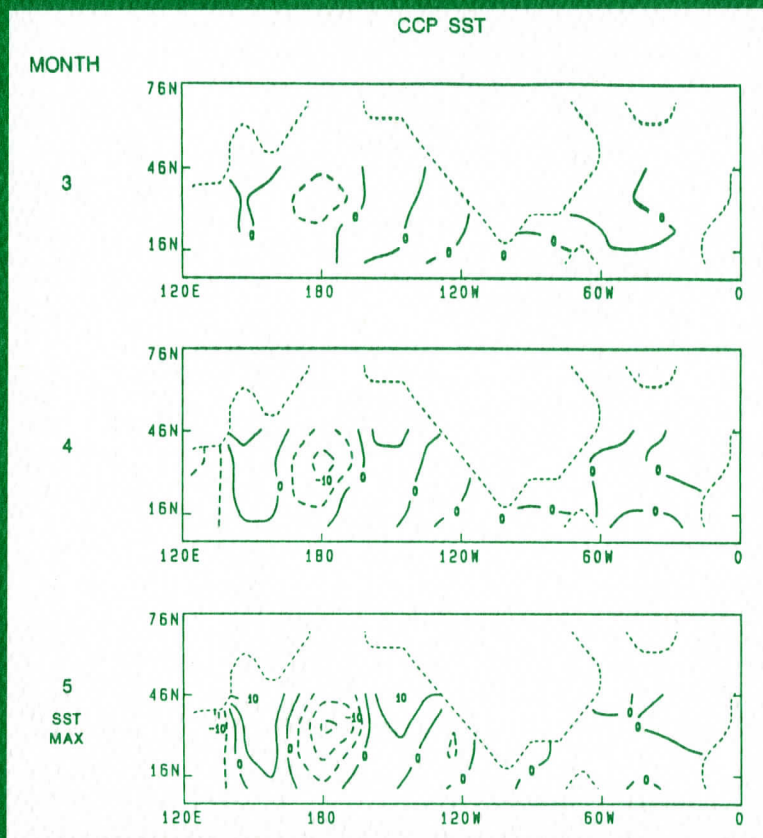
The Stewart/Edger Library
1225 W. Dayton Street
Madison, WI 53706

FINAL TECHNICAL REPORT

NSF Research Grant ATM-8913261
July 1, 1990 to December 31, 1993

Contributions by

M. A. Alexander
D. S. Battisti
U. S. Bhatt
R. G. Gallimore
Y. F. Guo
D. D. Houghton
L. M. Keller
R. E. Moritz
Y. L. Zhu



Department of Atmospheric and Ocean Sciences
University of Wisconsin-Madison
1225 W. Dayton Street
Madison, Wisconsin 53706

Submitted September 30, 1994

INTER- AND INTRA-ANNUAL VARIABILITY
IN AN INTERACTIVE OCEAN-ATMOSPHERE CLIMATE SYSTEM

D.D. Houghton and R.G. Gallimore
Co-Principal Investigators

The Schwerdtfeger Library
1225 W. Dayton Street
Madison, WI 53706

FINAL TECHNICAL REPORT

NSF Research Grant ATM-8913261
July 1, 1990 to December 31, 1993

Contributions by

M.A. Alexander
D.S. Battisti
U.S. Bhatt
R.G. Gallimore
Y.F. Guo
D.D. Houghton
L.M. Keller
R.E. Moritz
Y.L. Zhu

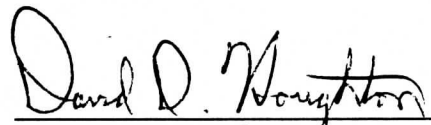
Department of Atmospheric and Oceanic Sciences
University of Wisconsin-Madison
1225 W. Dayton Street
Madison, Wisconsin 53706

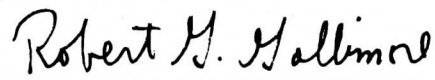
Submitted September 30, 1994

8692678

This report is submitted to satisfy the
National Science Foundation requirements
of a final technical report for
Grant ATM-8913261

Co-Principal Investigators


David D. Houghton


Robert G. Gallimore

September 30, 1994

TABLE OF CONTENTS

I. Introduction	1
II. Nontechnical Summary	1
III. Technical Description of Project and Results	2
IV. Publications	4
V. Data on Scientific Collaborators	5
VI. PhD Theses	5
VII. Copies of Publications	8

I. INTRODUCTION

The research accomplishments are given brief coverage in the nontechnical summary and technical description in the following two chapters. The referenced publications provide the details of the work. Copies of papers yet to appear in print are attached.

II. NONTECHNICAL SUMMARY

Studies were conducted to improve our understanding of the role of ocean-atmosphere interaction in producing natural variability of the ocean-atmosphere climate system. Particular attention was given to investigating variability over the North Atlantic and North Pacific ocean areas and in the summer monsoon region of east Asia and the Indian Ocean.

Primary results were obtained from multi-decadal simulations using numerical climate models. Although of low spatial resolution, these models had a relatively complete representation for the large-scale atmospheric circulations and physical processes. Ocean model formulations were very simple ranging from specified surface temperature conditions to thermodynamic formulations for predicting sea surface temperature.

One main study used a constant depth mixed layer ocean formulation to examine the life cycle and structure of dominant wintertime sea surface temperature anomalies and associated atmospheric circulation in the extratropical North Pacific. Results showed that ocean-atmosphere energy exchange associated with the dominant model anomalous atmospheric flow pattern produced large scale persistent sea surface temperature anomalies across the Pacific basin. Analysis of parallel prescribed sea surface temperature anomaly experiments provided evidence of ocean forcing of the atmosphere in the coupled model experiments.

For the North Atlantic study a more complete variable-depth upper ocean model was used. This study examined the importance of vertical energy transfers within the ocean (e.g. entrainment) for producing variability on interannual timescales. Model results suggest that latent and sensible heat flux anomalies play the most important role in sea surface temperature anomaly development in the mid Atlantic with entrainment being of less significance.

The importance of local and remote effects produced by prescribed sea surface temperature anomalies was highlighted in the monsoon study. Sea surface temperature anomalies over the southern Indian Ocean produced important feedbacks involving atmospheric circulation and large scale hydrological processes (i.e. evaporation, moisture transport, and precipitation). This result documented the complex and potentially important nature of the remote effects of ocean-atmosphere coupling on climate variability.

III. Technical Description of Project and Results

Analysis of numerical model experiments has provided additional understanding of the impacts of ocean-atmosphere interactions on the variability of the ocean-atmosphere climate system. Emphasis has been on intra-seasonal time scales involving, in particular, wintertime conditions in the midlatitude Pacific Ocean area, wintertime conditions in the midlatitude North Atlantic, and summer monsoon variations in the Asian sector. In the first case, fully two-way interactions were examined. In the second case, a study has been completed highlighting atmospheric effects on the ocean, while in the third attention was given to ocean effects on the atmosphere.

Low-resolution numerical models provided the simulations analyzed in these studies. Although of low spatial resolution, these models did have relatively complete representation of large scale circulations, hydrological processes, and the basic components of ocean-atmosphere energy exchange. Ocean model formulations ranged from a simple constant-depth mixed layer with thermodynamic coupling only to a predictive depth mixed layer model including processes associated with the effects of wind stress. The ocean formulation was considered sufficient for representing ocean-atmospheric interactions in extratropical latitudes.

In the North Pacific Ocean study (Gallimore, 1994), a coupled atmosphere-constant depth mixed layer ocean model is used to examine the life cycle and structure of dominant middle latitude wintertime large-scale sea surface temperature anomalies (SSTA) with time scales on the order of 6 months. Model results showed that the cold (warm) phase SSTA consists of a primary negative (positive) SSTA in the central Pacific flanked by anomalies of opposite sign in the western and eastern Pacific. During the growth stage, this primary SSTA develops in 1-2 months in response to the model's dominant atmospheric teleconnection pattern in the extratropics. For the decay stage of the warm SSTA the atmospheric anomalies are essentially of opposite sign to those present during the growth stage and act to rapidly destroy the SSTA. In contrast the atmospheric anomalies during the decay of the cold SSTA phase are of the same sign but weaker than during the growth stage. As a result the atmospheric anomaly structure for the cold SSTA helps maintain, through the process of ocean-atmospheric energy exchange, a more persistent SSTA than for the warm SSTA phase. For the cold SSTA case, there was some evidence of ocean forcing of the atmosphere. This was obtained by comparing the structure of atmospheric anomalies in the interactive model to those found in a one-way forced model where ocean conditions are specified to correspond to the SSTA composite in the interactive model. The differences found between the two-way and one-way forced models suggest that the anomalous response of the atmosphere to sea surface temperature in a coupled model environment may not be the same as that obtained in a one-way forced system.

For the North Atlantic study, Battisti et al. (1994) incorporated more physical processes in the ocean model than in the mixed layer model used in the first study. In particular the depth of the mixed layer is a prognostic quantity along with temperature and salinity in the mixed layer. Physical processes include vertical energy exchange, entrainment, convection, Ekman pumping, and penetrative short wave radiation. The study focused on the atmospheric forcing of the ocean for wintertime conditions. Climatological mean atmospheric conditions were specified from NCAR atmospheric Community Climate Model (CCM1) simulations. The anomalous atmospheric part of the vertical heat fluxes was obtained from the COADS data for years 1950 to 1988.

The model predicted warm and cold SSTA events similar to those observed. Consistent with other studies, the combined sensible and latent heat flux anomalies were shown to contribute substantially to SSTA in the middle latitudes of the North Atlantic, whereas in the subtropics the SSTA were determined primarily by the latent heat fluxes. Generally the effect of entrainment on SSTA formation was relatively small. Isolation of the physical processes was provided by sensitivity studies where the variations in surface air temperature, humidity, and wind speed were separately examined.

The third study (Zhu and Houghton, 1994) expanded our understanding of ocean effects on the atmosphere by examining the remote response in the Asian monsoon region to an SSTA in the southern Indian Ocean. Comparison of ensembles of integrations with the CCM1 for the northern summer season with and without this SSTA isolated both the local and remote impacts of the SSTA. Results showed systematic changes in the large-scale atmospheric conditions and component processes in the Asian summer monsoon. For the negative SSTA the overall intensity of the monsoon was enhanced. The reverse was true for the warm SSTA case. These strong/weak monsoon scenarios are very similar to observed interannual variations of the Asian summer monsoon. For a two-way interactive model, the changes in surface heat fluxes induced by the presence of the prescribed SSTA would tend to dissipate that anomaly over a several month time scale. The study highlights the complexity of understanding systematic remote responses which might occur in fully coupled ocean-atmosphere systems.

IV. PUBLICATIONS

A. Refereed Publications

Battisti, D.S., U. Bhatt, and M.A. Alexander, 1994: A modeling study of the interannual variability of sea-surface temperature in the wintertime N. Atlantic Ocean. J. Climate, submitted.

Gallimore, R.G. and D.D. Houghton, 1990: Simulation of ocean temperature and heat storage from a GCM coupled to a variable depth upper ocean. J. Phys. Ocean., 20, 1312-1332.
[work from previous grant; listed because of page charge support]

Gallimore, R.G., 1994: Simulated ocean-atmosphere interaction in the North Pacific from a GCM coupled to a constant depth mixed layer. J. Climate, accepted conditioned upon revisions.

Houghton, D.D., R.G. Gallimore, and L.M. Keller, 1991: Stability and variability in a coupled ocean-atmosphere climate model: results of 100-year simulations. J. Climate, 4, 557-577.
[work from both previous and current grants]

Zhu, Y.L. and D.D. Houghton, 1994: The impact of Indian Ocean SST on the large-scale Asian summer monsoon and the hydrological cycle. J. Climate, submitted.

B. Conference Paper Reprints

Gallimore, R.G. 1991: Simulated extratropical SST anomalies in the North Pacific from a GCM coupled to a constant depth mixed layer. Preprint volume, Fifth Conference on Climate Variations, AMS, Oct. 14-18, 1991, Denver, CO, pp. 313-316.

Gallimore, R.G. 1994: Simulated extratropical ocean-atmosphere interaction in the North Pacific from a GCM coupled to a constant depth mixed layer ocean. Preprint volume, Sixth Conference on Climate Variations, AMS, January 23-28, 1994, Nashville, TN, pp. 7-11.

Guo, Y.F., and D.D. Houghton, 1991: Interannual variability of July precipitation in an extended 100-year simulation from a coupled ocean-atmosphere climate model. Preprint volume, Fifth Conference on Climate Variations, AMS, Oct. 14-18, 1991, Denver, CO, pp 305-308.

V. DATA ON SCIENTIFIC COLLABORATORS

A. Scientists

Dr. Michael A. Alexander, Co-author on paper, CIRES, University of Colorado, Boulder, CO

Dr. David S. Battisti, Co-investigator, Co-author on paper, Co-advisor for PhD student, currently Assistant Professor, Dept. of Atmospheric Sciences, University of Washington, Seattle, WA

Dr. Robert G. Gallimore, Co-Principal Investigator, Senior Scientist, Dept. of Atmospheric and Oceanic Sciences and Center for Climatic Research, University of Wisconsin-Madison, Madison, WI

Dr. Yufu Guo, Visiting Scientist and Co-author on conference paper, Scientist, Institute of Atmospheric Physics, Beijing, China

Dr. David D. Houghton, Co-Principal Investigator, Professor, Dept. of Atmospheric and Oceanic Sciences, University of Wisconsin-Madison, Madison, WI.

Dr. Richard E. Moritz, Co-Investigator, currently Research Assistant Professor, Department of Atmospheric Sciences, and Oceanographer, Polar Science Center, University of Washington, Seattle, WA

B. Researcher

Ms. Linda M. Keller

C. Students

Uma S. Bhatt
Yunlai Zhu

VI. PhD Theses

Zhu, Yunlai, 1993. The large scale hydrologic cycle and its role in Asian summer monsoon variations induced by Indian Ocean sea surface temperature anomalies. PhD thesis, University of Wisconsin-Madison, 205 pp.

Abstract presented on next two pages

Bhatt, Uma S., 1994. Ocean-atmosphere interactions in the North Atlantic. PhD thesis, University of Wisconsin-Madison (work in progress).

No preliminary abstract available

The Large-scale Hydrologic Cycle and Its Role in Asian Summer Monsoon Variations Induced by Indian Ocean Sea Surface Temperature Anomalies

Yunlai Zhu

Abstract

Characteristic variations of the large-scale hydrological cycle (LHC) and their relationships to the variations of atmospheric circulation and sea surface temperature (SST) during northern summer (Jun-Jul-Aug) are studied using the NCAR CCM1 climate model. The principal focus is on the role of the LHC in monsoon system variations and large-scale atmosphere-ocean interactions. The underlying physical couplings are identified by comprehensive analyses of both the control simulation and the anomaly experiments.

The spatial-temporal variations of the LHC components, viz. evaporation, moisture transport and precipitation in the control simulation are characterized by empirical orthogonal functions. Significant correlations between the dominant modes of the LHC and circulation components on the intraseasonal time scale indicate physically consistent couplings between these

components. This set of coupled covariations in space and time suggest a feedback mechanism between hydrological cycle and monsoon circulation.

Numerical experiments with prescribed SST anomalies in southern Indian Ocean are conducted to test the role of the LHC through its coupling with circulation in influencing the Asian monsoon responses to the remote SST anomalies pertaining to the interannual variations. Significant responses show that the LHC exerts a positive feedback through coupled changes of its component processes similar to those found in the control simulation. The polarity (sign) of the prescribed SST anomaly determines whether the overall monsoon circulation response is enhanced or weakened.

The results from the analyses of both the control simulation and the anomaly experiments are consistent and compare well with observations. These analyses suggest that the positive feedback mechanism highlighted in this study may be partially responsible for some of the variations observed in atmosphere and ocean.

VII. COPIES OF PUBLICATIONS

Three of the five publications listed on Page 4 are duplicated here since they have yet to appear in print. The other two publications were included in the Final Technical Report for NSF Research Grant ATM-8709552.

The three publications reproduced are:

Battisti, D.S., U.S. Bhatt, and M.A. Alexander, 1994: A modeling study of the interannual variability of sea-surface temperature in the wintertime N. Atlantic Ocean. J. Climate, submitted.

Gallimore, R.G., 1994: Simulated ocean-atmosphere interaction in the North Pacific from a GCM coupled to a constant depth mixed layer. J. Climate, accepted conditioned upon revisions.

Zhu, Y.L. and D.D. Houghton, 1994: The impact of Indian Ocean SST on the large-scale Asian summer monsoon and the hydrological cycle. J. Climate, submitted.

A Modeling Study of the Interannual Variability in the wintertime North Atlantic Ocean

by

D.S. Battisti¹, U.S. Bhatt², and M.A. Alexander³

Submitted to the J. of Climate

August 1994

Contribution No. 256 to the Joint Institute for the Study of the Atmosphere and Oceans

-
1. Dept. of Atmospheric Sciences, AK-40, Univ. of Washington, Seattle 98195
 2. Dept. of Atmospheric and Oceanic Sciences, Univ. of Wisconsin, Madison WI 53706
 3. CIRES, Univ. of Colorado, Boulder CO 80309

Abstract

We present a new model for the upper North Atlantic Ocean and use it to hindcast the sea surface temperature (SST) from 1950-1988. The model consists of a matrix of one-dimensional (independent) columns in which a variable depth, bulk mixed layer overlies a diffusive convective thermocline. The climatological annual cycle of heat flux convergence by the oceanic circulation is implicitly included in the formulation of the forcing.

The 38 year control integration of the model includes as surface forcing the shortwave and net longwave radiation from a control integration of the Community Climate Model. Sensible and latent heat fluxes are determined from instantaneous values of surface temperature, humidity and wind speed from the atmospheric model, and the SST simulated by the ocean model using the bulk formulae. The hindcast is performed by repeating the control integration, adding the observed, monthly mean surface anomalies in surface temperature, humidity and wind speed for the period 1950-88. Thus, the simulated SST anomalies are generated explicitly by anomalies in the latent and sensible heat fluxes. A separate hindcast integration is presented, using as forcing the "observed" sensible plus latent heat flux anomalies rather than the surface atmospheric field anomalies to demonstrate the major results are not pre-determined by the formulation of the coupling.

The ability of the model to hindcast the wintertime interannual variations in SST is demonstrated by simple correlations with observed anomalies, and by comparing the composite of warm and cold events observed with those simulated by the model. There is a good quantitative agreement between simulated and observed SST anomalies throughout most of the North Atlantic Ocean. Since the model formulation explicitly excludes any effects due to *anomalies* in the ocean advection, our results confirm the hypothesis that wintertime interannual to sub-decadal variability in SST is mainly due to local anomalies in the air-sea flux of sensible and latent heat and not to anomalies in oceanic advection. Significant disagreement between hindcast and simulated SST anomalies is limited to a small region extending from Cape Hatteras to Nova Scotia along the US coast. Here, the observed surface flux anomalies are anti-correlated with the SST anomalies, implicating important changes in oceanic advection to the interannual wintertime SST anomalies.

Both the sensible and latent heat flux anomalies are shown to contribute substantially to the wintertime anomalies in SST in the subpolar Atlantic, while the heat flux anomalies are predominantly determined by the latent heat flux in the subtropics. Entrainment anomalies contribute to a lesser extent to the mixed layer temperature anomalies throughout the basin. Sensitivity studies are performed to highlight the atmospheric processes and variability that account for the surface heat flux anomalies.

1. Introduction

Bjerknes (1964) was the first to document the dominant concurrent patterns of interannual variability in the wintertime N. Atlantic sea surface temperature (SST) and sea-level pressure (SLP). He found that anomalously warm water in the region north of 40° N is associated with anomalous high SLP in the same region. Concurrent with the anomalously warm water in the northern basin, cold water is found to the south (20°-30° N) where the SLP is anomalously low. More recently, Kushnir (1994) presented composites of the 'warm minus cold' wintertime (December-April mean) climate anomalies in the N. Atlantic on the interannual time scale. Kushnir's results, obtained from a much larger data set, confirmed the earlier results of Bjerknes. In Figs. 1 and 2 we present various composite surface fields from the warm and cold phases of these interannual climate anomalies in the N. Atlantic (see section 3 and Table 1)¹. The concomitant atmosphere and ocean variability depicted in Figs. 1 and 2 is also consistent with the "dipole mode" discussed in Deser and Blackmon (1993). While there is a preferred biennial time scale for this "mode", Deser and Blackmon also note significant power on the decadal time scale.

Bjerknes argued that these interannual climate anomalies are the result of the interaction between the atmosphere and ocean. Specifically, he argued that local thermodynamic processes in the atmosphere and ocean are important for interannual climate anomalies, and that the response of the ocean is confined to the upper ocean. Wallace et al. (1990) and Wallace et al. (1992) present EOF and SVD analyses, respectively, that link the wintertime pattern of SST anomalies in the N. Atlantic with anomalies in the 500 mb height field (Z500). Wallace et al. (1990) determined that the relationship between the anomalies in Z500 and in the SST tendency is stronger than that between the anomalies in Z500 and those in SST. This result is consistent with the hypothesis that on the interannual time scale the dominant thermodynamic processes in the surface ocean are due to local air-sea exchanges. Wallace and Jiang (1987), using lag-correlation analysis, found that the correlations between Z500 and SST anomalies were largest with Z500 anomalies leading the SST anomalies. Davis (1976) and Lanzante (1984) came to similar conclusions using the same analysis technique on the SST with the SLP and Z700, respectively. Together, these studies indicate that the atmospheric anomalies lead the SST anomalies by one to several

1. The amplitudes of the composite fields presented in Figs. 1 and 2 are less than that presented in Kushnir (1994) because of the application of the digital filter.

months, suggesting that the coupled atmosphere/ocean mode, first identified by Bjerknes, is at least initiated by atmospheric circulation anomalies. Furthermore, all of the above studies indicate that the horizontal scale of the SST anomalies is governed by the scale of the associated atmospheric circulation anomalies and not by the synoptic-scale oceanic eddies.

Haney (1985) argued that *local* surface heat flux anomalies are responsible for the interannual SST anomalies in the midlatitude Pacific Ocean, after demonstrating the anomalies in oceanic advection can not account for the amplitude of the observed SST anomalies. In the midlatitudes during winter, the important surface heat flux anomalies are the sensible (Q_S) and latent (Q_L) fluxes: the variance in the shortwave and longwave radiation (and in the net radiation) is small compared with the turbulent transfer of heat (see, e.g., Cayan 1992a). Cayan (1992b) performed an analysis of the interannual variability in the SLP and in the anomalous sensible plus latent (Q_{S+L}) heat flux, averaged monthly during the wintertime in the N. Atlantic. He found that the predominant EOF of SLP anomalies - the North Atlantic Oscillation (NAO; van Loon and Rogers 1978) - is associated with large-scale Q_{S+L} anomalies. Specifically, in one phase of the NAO, an anomalous zonal band of positive heat flux into the ocean at about 50°N is associated with anomalous high SLP to the north. Concurrently, between about 30 and 40°N, a broad region of low pressure associated with the NAO overlies anomalous negative Q_{S+L} . In a follow-up study, Cayan (1992b) presented a composite of the occurrences of the extreme in the index of the NAO and demonstrated that the month-averaged wintertime Q_{S+L} anomalies are consistent with the observed anomalous SST tendency.

Do the observed SST anomalies, in turn, affect the atmospheric circulation? If so, how? The answers to these questions are not so clear. Pitcher et al. (1988) examined the response of the Community Climate Model (CCM0A) to prescribed SST anomalies that were observed in the N. Pacific during wintertime, 1976/77. Experiments were integrated 1200 days using perpetual January insolation to increase the statistical sample. The results from their experiments showed that the atmospheric response resembled that of the observed PNA pattern but the response of the atmosphere (to the polarity of the SST anomaly) was nonlinear. They concluded that 'a North Pacific SST anomaly can produce physically realistic, statistically significant climate anomalies in the northern winter circulation.' Kushnir and Lau (1992) performed similar experiments using the GFDL climate model, focussing on the interaction between the forcing SST anomalies and the baroclinic eddy transport anomalies and the low-frequency variability in the overlying atmosphere. Their results, consistent with Pitcher et al., include a significant low-frequency atmo-

spheric response, but the anomaly patterns and the processes associated with maintaining the anomaly depended on the polarity of the SST anomaly.

Palmer and Sun (1985) presented results from a study where a general circulation model (GCM) is forced by a prescribed anomalous SST field in the N. Atlantic. They conclude that wintertime SST anomalies in the midlatitude N. Atlantic can generate statistically significant anomalies in the midlatitude troposphere, including a displacement of the storm track and downstream anomalies in the 500mb geopotential height field over Europe. This conclusion is supported by the recent results of Peng et al. (1994) and Palmer (personal communication 1993).

Lau and Nath (1990) performed a hindcast of the atmospheric response to the observed global (38°S to 60°N) SSTs from 1950-79 using a version of the GFDL GCM (R15). They also concluded that anomalies in the midlatitude wintertime atmosphere could be attributed, in part, to anomalies in the midlatitude SST. In their study, anomalies in the storm track axes and in the underlying surface fluxes were noted, and significant equivalent barotropic signatures were found in geopotential height in the troposphere. Recently, Lau and Nath (1993) re-ran this hindcast and performed two complimentary hindcasts where the SST anomalies were limited to occur in only the tropical Pacific, or to only in the midlatitudes of the Northern Hemisphere. These results, using a slightly different version of the GFDL GCM, indicate that the midlatitude atmosphere does *not* respond significantly to prescribed midlatitude SST anomalies. [This conclusion is based on a SVD analysis of the observed *hemispheric* midlatitude SST anomalies and the simulated Z500 anomalies.].

Finally, Miller (1992) analyzed the seasonal variability in a simplified coupled model of the global atmosphere and Pacific Ocean. He found that the midlatitude Pacific SST anomalies did influence the atmospheric circulation, and that the persistence of the SST anomalies is enhanced through (Ekman) advection in the ocean.

In this study we test the hypothesis that the wintertime SST anomalies in the N. Atlantic are primarily governed by the local ocean-to-atmospheric energy fluxes and are primarily confined to the upper ocean. To this end, we employ a model of the upper ocean in the N. Atlantic, described in section two, that emphasizes the physics of the mixed layer and implicitly includes the effects of the annual cycle in ocean circulation on the annual cycle of SST. Furthermore, in the model formulation we have assumed that *anomalies* in the circulation of the ocean are, in general, not important for the wintertime anomalies in SST on the interannual time scale. We report in section three the results from a hindcast

simulation of the upper N. Atlantic Ocean response to prescribed observed anomalies in the atmospheric surface variables. The resultant 'sensible plus latent' heat flux (Q_{S+L}) anomalies are calculated using standard bulk formulae and are dependent on the SST calculated from the interactive ocean model. The results are presented in composite form as in Kushnir (1994). Specifically, we composite the simulated SST anomalies for ten winters (defined as the November - April mean) when the observed SST was anomalously warm in the far northern Atlantic; a cold event composite is also presented. The simulated anomalies in SST and heat flux are compared with the SST and heat flux anomalies obtained from a composite of the observations using the same winters. The importance of the anomalies in surface air temperature, wind speed and humidity in determining the total heat flux Q_{S+L} is examined in section four. The conclusions and a discussion are presented in section five.

Finally, our interest in this study is on SST anomalies on the interannual to sub-decadal time scale, hereafter referred to broadly as the "interannual" time scale. Hence, throughout the paper we apply a digital filter (with a 10 year half-power point) to all model and observed fields and to the flux anomalies (estimated from the unfiltered data and using the bulk formulae).

2. The ocean model and experimental design.

The central hypotheses we are testing in this study is that the interannual variability in wintertime SST anomalies in the N. Atlantic Ocean are determined by processes that are inherently associated with local atmosphere-ocean coupling, and the important physics and thermodynamics responsible for these climate anomalies are confined to the mixed layer: we assume changes in SST due to ocean dynamics (advection) become important only for longer time scale (decadal or more) fluctuations. Therefore, we employ an ocean model that has a detailed representation of the mixed layer physics and explicitly exclude deep ocean physics. The advantages of this model over an OGCM include: the model is relatively easy to diagnose, is computationally efficient, and does not require lengthy integrations to obtain a statistically steady state.

a. The ocean model

The ocean model is designed to study the influence of atmospheric forcing and entrainment on SSTs in the North Atlantic Ocean. The ocean model grid, which is aligned with the CCM grid between 20°N and 60°N in the Atlantic, is composed of horizontally

independent column models of the upper ocean. The upper ocean model includes prognostic mixed layer physics and, below the mixed layer and through the permanent thermocline, a convective/diffusive model.

A well mixed surface layer is assumed *a priori*. The temperature of the mixed layer, T_{om} , is controlled by vertical processes including: surface energy fluxes, penetrating solar radiation and entrainment. The salinity in the mixed layer is a time dependent model variable, and is contingent upon precipitation and evaporation at the surface, and entrainment and diffusion at the base of the mixed layer. The mixed layer depth, h , is computed using the formulation of Gaspar (1988) and is a time dependent variable. The mixed layer depth depends on the surface buoyancy forcing, wind stress, penetrating solar radiation and the density jump at the base of the mixed layer. Under stable conditions, the mixed layer will re-form closer to the surface: entrainment is set to zero, and h is computed diagnostically by assuming a balance between turbulent kinetic energy generation, buoyancy forcing and dissipation. When the mixed layer shallows, the temperature and salinity profiles are adjusted according to Adamec et al. (1981), conserving heat, salt and potential energy.

Beneath the mixed layer, heat and salt are affected by convective overturning and vertical diffusion. A Laplacian formulation is used for the vertical diffusion of temperature and salinity: a constant eddy diffusion coefficient of $2 \times 10^{-5} \text{ m}^2/\text{s}$ is used, based on the study of White and Walker (1974; see also Alexander and Deser 1994). The absorption of solar radiation is also included in the convective/diffusive region below the mixed layer using the parameterization of Paulson and Simpson (1977). The convective/diffusive model contains 30 unequally spaced layers between the surface and 1000m depth; the values of the state variables in the layers within the mixed layer are equal to the mixed layer values. Thirteen of the layers are within the first 100m to resolve the sharp summer pycnocline. The temperature of water below the mixed layer, used in the entrainment calculations, is obtained directly from the layer in which h resides.

A similar version of the column model has been used by Alexander and Deser (1994) to simulate the thermal structure of the upper ocean at points in the North Atlantic and North Pacific. A more detailed description of the column model is given in the Appendix.

b. Coupling to the atmospheric fields and the control integration of the ocean model

The formulation of the coupling of the ocean model to atmospheric variables anticipates future studies in which the ocean model will be interactively coupled to an atmo-

spheric GCM, the Community Climate Model (CCM, version 1). Net surface fluxes into the ocean are determined using daily values of the surface atmospheric fields obtained from a five year control run of the CCM1 (R15, Case 256 of Williamson et al. 1987). In this control CCM1 integration, the SST is prescribed to be the observed annual cycle from the Alexander and Mobley (1976) data set. The ocean model is forced with the daily values of the net radiative flux, the momentum flux, the "latent + sensible" Q_{S+L} heat flux, and the precipitation minus evaporation flux. The radiation and momentum fluxes are from the CCM1 control integration (with prescribed climatological SST). Q_{S+L} and the momentum fluxes are determined from the bulk formulae using the prescribed atmospheric variables from the history tapes of the CCM1 control run and the *simulated* SST: the (bulk) flux formulae that are used in calculating Q_{S+L} are identical to that in the CCM1 (Deardorff 1972).

The ocean model, being composed of a matrix of independent mixed layer models, does not explicitly account for the horizontal advection of heat in the ocean. Thus, when forced by the total surface heat flux Q_{tot} (latent + sensible + radiative), the model will not produce a realistic seasonal cycle in regions where surface temperature advection is important. To achieve an accurate seasonal cycle in SST, we have introduced a correction to the observed surface heat flux in tuning the model (see, e.g., Sausen and Ponater 1988). This correction is obtained as follows. The ocean model is integrated for one time step (say from t_1 to t_2) with the forcing determined as stated in the previous paragraph. The simulated SST at t_2 is in general not equal to the climatological temperature at t_2 . A heat flux correction, Q_{corr} , is then calculated as the additional heat that is required to achieve a surface mixed layer temperature equal to the climatological SST at t_2 . The Q_{corr} is then stored and the simulated SST is set to the climatological value. The integration is continued with a Q_{corr} calculated for each day using the surface atmospheric fields from the first year of the CCM1 control run, cycled for six years. Using the daily values of Q_{corr} from the last five years of this integration², a monthly mean climatology of Q_{corr} is assembled. Hence, there are approximately $30 * 5$ daily values of Q_{corr} that go into one monthly average.

In this manner, a monthly averaged Q_{corr} is generated using surface data for each of the five years in the control CCM1 integration. Finally, the five monthly estimates of

2. Since the initial conditions of the mixed layer model are necessarily inconsistent with the atmospheric fields, throughout year one a significant contribution to Q_{corr} results solely from this imbalance and not due to neglected ocean physics or the parameterization of the mixed layer physics. Hence, values of Q_{corr} from the first year of integration are not included in calculating the climatological Q_{corr} .

Q_{corr} are averaged to obtain the monthly average Q_{corr} that is stored and later used in all simulations discussed hereafter. Note that Q_{corr} is applied at each ocean model time step (one day): the value of Q_{corr} is calculated for each day using a cubic spline from the monthly mean Q_{corr} . In all the integrations performed below, Q_{corr} has a fixed annual cycle that is independent of the state of the ocean or atmosphere. The ocean model is henceforth forced at each basin gridpoint with the net heat flux:

$$Q_{net} = Q_L(q_a, V_a, T_{om}) + Q_S(T_a, V_a, T_{om}) + Q_{SW} + Q_{LWnet} + Q_{corr}(t) \quad (1)$$

$$Q_{net} \equiv Q_{tot} + Q_{corr} \quad (2)$$

In Eq. 1, Q_L (Q_S) is the latent (sensible) heat flux, Q_{SW} is the surface shortwave flux into the ocean, and Q_{LWnet} is the net longwave radiative flux at the surface. T_a is the temperature of the air at the lowest model level (at $\sigma = 0.991$), T_{om} the SST from the ocean model, and t is time. V_a is the speed of the surface wind. Q_{tot} ($= Q_{net} - Q_{corr}$) is the sum of all the surface heat flux terms.

We note that *if* the surface energy fluxes that are simulated in the CCM1 were identical to the actual energy fluxes and our ocean basin model accurately represented the physics of the mixed layer, Q_{corr} would represent the horizontal heat flux convergence in the mixed layer due to ocean currents, which are neglected in the model. In a statistically steady state and in the absence of heat transport through the thermocline, averaged over the annual cycle Q_{net} will be zero. Hence, $Q_{tot} \approx -Q_{corr}$ (cf. Fig. 3a and 3c). One anticipates that the heat flux convergence due to the ocean gyre currents should warm (cool) in the northern (southeastern) N. Atlantic Ocean.

The calculated Q_{corr} , averaged over the year, is displayed in Fig. 3c. Throughout the paper, a positive heat flux represents a warming of the water in the mixed layer. Clearly, this heat flux correction, required for the model to simulate the annual cycle, does not resemble the advective oceanic heat flux convergence. In fact, Q_{corr} is due to the neglected advective effects and errors in the surface energy fluxes in the control integration of the CCM1. The latter errors result from errors in the atmospheric model, especially the shortwave radiation incident at the ocean surface, and yield an overestimate of the surface warming (in this case off the northeast US and eastern Canadian coasts) in the subpolar oceans (cf. Fig. 3a and 3b). This is a common problem in many atmospheric GCMs, and stems from an insufficient amount of low-level cloud (e.g., Soden 1992). We note that the calibration of the ocean model was also performed using the ‘‘observed’’ surface fluxes from the COADS long-term mean (Fig. 3b), avoiding the problematic Q_{SW} in the CCM1. In this case, Q_{corr} does indeed have the pattern and amplitude that is consistent with what

one would expect from the oceanic flux convergence. Since the ultimate goal of our work is not to provide a hindcast of the SST, but to examine the interactive atmosphere-ocean coupled system, we develop the ocean model with Q_{corr} based on the CCM1 climatological fields.

c. The control integration of the ocean model.

The control integration is for 38 years whereby the five years of daily atmospheric variables from the CCM1 control integration are prescribed cyclically over the ocean model using (1). The initial conditions for the control integration were obtained from the end-state of an extended ocean model control integration, forced by the CCM1 net surface flux. The climatological SST from the control run of the model is very close to the observed climatology; the drift in simulated SST is less than $0.1\text{ }^{\circ}\text{C}$ over 30 years, except for two isolated grid points approaching $0.17\text{ }^{\circ}\text{C}$ per 30 years, indicating a stable simulation. However, the variance in the simulated wintertime SST from the ocean control integration is about one-half of that from the observations.

Averaged over the annual cycle, one would expect that in a statistical equilibrium the net surface heat flux into the ocean from the atmosphere would be nearly balanced by the convergence of heat by the ocean currents: a small residual flux would be required to compensate for the upward advection of cold water via the thermohaline circulation. The net annual averaged surface energy flux Q_{net} from the control integration of the ocean model implicitly includes the (cyclic) surface advection and is depicted in Fig. 3d. As expected, the net flux is typically less than 15 Wm^{-2} , reaching 25 Wm^{-2} immediately along the east coast of N. America, and acts to warm the ocean.

3. The response of the upper N. Atlantic Ocean to the observed (prescribed) surface atmospheric conditions.

a. The Hindcast

In this section we report on the hindcast of the upper N. Atlantic Ocean response to the observed state of the atmosphere from 1950-1988, using the ocean model described in section two. The model is forced as follows: the observed monthly averaged anomalies in the surface atmospheric air temperature T'_a , the surface specific humidity q'_a , and the average of the instantaneous wind speed V'_a (averaged over the month) are added to the surface atmospheric fields used in the 38 year control integration of the ocean model (i.e.,

added to the daily values of T_a , V_a and q_a from the control integration of the CCM1). The resulting fields are then used to calculate the net heat flux forcing of the ocean model:

$$Q_{net} = Q_L(q_a + q'_a, V_a + V'_a, T_{om}) + Q_S(T_a + T'_a, V_a + V'_a, T_{om}) + Q_{SW} + Q_{LWnet} + Q_{corr}(t) . \quad (3)$$

These atmospheric anomaly data, denoted by ('), are taken from COADS. The atmospheric anomalies are determined using the long-term monthly mean climatological annual cycle from COADS. A digital filter (ten year half power point) is then applied to the 38 year record of anomalies to remove the very low frequency (sub-decadal) variability.

The total flux forcing in the model hindcast is calculated using (3), where the bulk formulae for calculating the sensible and latent heat fluxes are exactly those used in the CCM1. The thermodynamic forcing of the ocean model is explicitly limited to anomalies in Q_{S+L} : the radiative fluxes (Q_{SW}) and Q_{corr} are identical to that in the control integration. The observed anomalies in the momentum flux are also imposed on the ocean model in the hindcast. Due to insufficient observations, however, there are no anomalies in the fresh water flux, precipitation minus evaporation.

A partial measure of the skill of the model is provided by the correlation of the model hindcast SST anomaly with that observed (from COADS). Displayed in Fig.4 are maps of the correlation coefficient based on the monthly mean anomalies for the summer (May - October) and winter (November - April) seasons. The correlation coefficients for the hindcast with the observed SST anomalies generally exceed 0.8 for both the three month and six month (seasonal) average anomalies. Weaker correlations are found in isolated regions in the northwest extremity of the domain and to the west of the Canary Islands (Fig. 4), where the observational data base is relatively sparse. The correlation coefficient is statistically significant at the 1% level almost everywhere in the domain: this criteria is not met in the winter semester for some of the grid points along the northern border of the domain in winter where sea ice - ignored in this study - is observed (see Fig. 4a).

We now present the results of the hindcast in composite form. The years that constitute a composite event are determined in the following manner. An index was formed based on the difference in the wintertime (November to April average) SST anomaly between 40°-60°N and that between 20°-40°N. The index is based on the EOF analysis of SST throughout the Atlantic Basin that highlights a zonally oriented dipole pattern in SST, with centers of opposite polarity in these two regions (see, e.g., Wallace et al. 1990). The twenty extreme values of this index (ten of each polarity) define the years that are consti-

tute the warm and cold composite events, and are listed in Table 1. These years are not strictly a subset of those identified and included in the composites of Kushnir (1994). Kushnir notes that the nature of the composite events is insensitive to the number of cases and specific years that go into the composite. We confirm this conclusion for the composites obtained from the hindcast (not shown).

The composite of the observed events are displayed as anomalies from the climatological mean. Specifically, the anomalies in the atmospheric quantities, the SST and in the “observed” Q_{S+L} anomalies are based on the observed climatological means from COADS (1950 - 1988); the bulk flux formulation is the same that is used in the CCM1 (Deardorff 1972). All anomalies are filtered to remove the low frequency (decadal) variability.

For the events that comprise the hindcast composites (see Table 1), the model SST and mixed layer depth anomalies are calculated by subtracting time series of the variable obtained in the ocean model 38 year control integration from that obtained in the hindcast. Similarly, surface Q_{S+L} flux anomalies are obtained by subtracting the net surface flux obtained in the 38 year control integration (see section 2c) from that obtained in the hindcast integration:

$$Q_{net}(hindcast) - Q_{net}(control) = Q_{S+L}(hindcast) - Q_{S+L}(control) = Q'_{S+L}$$

Q_{net} is defined in Eq. 3³.

b. The composite warm event

The composite warm event from the observations (Fig. 1a) features warm water throughout most of the domain, except in the southwestern quadrant extending off the southeast US where the SST anomalies are negative (-0.2°C). The warm anomalies are centered off the east coast of Canada with amplitude exceeding about $+0.3^{\circ}\text{C}$. The spatial structure of the concomitant surface air temperature anomaly (cf. Fig. 1a and 1c) is very similar to the SST anomaly pattern. The observed air temperature anomalies are typically

3. Note that the anomalies in the hindcast integration are not anomalies from the mean annual cycle of the control integration because the resultant anomalies would then include both the prescribed COADS signal and anomalies inherent to the CCM1 fields.

50 to 100% greater than the SST anomalies in the center of both the warm and cold anomalies (cf. Figs. 1a, 1c and 5b). In the southern half of the domain, the anomalies in the surface air temperature are very similar in pattern to the SST anomalies, though only about 50% greater in amplitude.

The composite of the local surface Q_{S+L} heat flux anomalies, calculated from observations and depicted in Fig. 5a, is consistent in pattern with the SST anomalies. Anomalous heating of the ocean is found coincident with the maximum SST anomalies and exceeds 20 Wm^{-2} . The net heating anomalies are due to anomalies in both sensible and latent heating. Consistent with other studies (e.g., Alexander 1990; Cayan 1992a), these two components of heat flux are highly correlated (e.g., cf. Fig. 5c and 5d). South of about 35° to 40°N , the latent heat flux is the dominant flux. North of this latitude, the sensible heat flux is almost comparable to the latent heat flux. In general, the pattern and sense of the heat flux anomalies and SST anomalies is consistent with the hypothesis that the SST anomalies result from a local interaction between the atmosphere and the oceanic mixed layer (see also, Wallace and Jiang 1987; Alexander 1990; Wallace et al. 1990, Wallace et al. 1992, Cayan 1992b).

The low level atmospheric circulation that accompanies the warm composite is summarized in Figs. 1b, 1d and 5e. Anomalously high (low) SLP is found in the northern (southern) half of the domain and the overall pattern has a dipole structure. A more complete description of the observed atmospheric anomalies and their role in the net surface heat flux anomalies is deferred to section 4a.

The composite warm event simulated by the ocean model is obtained by averaging the same years from the hindcast integration that have gone into the observed composite warm event (see Table 1). The simulated composite warm event is summarized in Fig. 6. In general, the SST anomalies from the ocean model are quantitatively consistent with those in the observed composite warm event (cf. Fig. 6a and 1a). Positive anomalies exceeding 0.25°C are found in the northwestern portion of the domain, with negative anomalies in the southern half of the domain (exceeding in absolute value 0.20°C in the southwest). As in the observations, the sensible and latent heat anomalies are in phase throughout the domain. In both the observed and simulated composites, the pattern of latent and sensible heat anomalies are similar: in the northern half of the domain, the sensible heat anomalies are about equal to that of the latent heat anomalies, while in the subtropics, the latent heat anomalies are much greater than sensible. The pattern of the net

Q_{S+L} anomalies from the hindcast are similar to that "observed", albeit with weaker simulated fluxes in the northwestern domain (cf., Fig. 5a and 6e).

Typically, the mixed layer (Fig. 6g) is anomalously shallow (deep) where the SST anomalies are positive (negative) in the composite model warm event. The anomalous flux of heat into the mixed layer from below Q_w (via changes in entrainment and convection) is displayed in Fig. 6f. Only in an isolated region in the far northwestern section of the domain ($55^\circ, 45^\circ\text{W}$) are the anomalies in the entrainment heat flux comparable to the net surface flux anomalies. Otherwise, anomalies in the entrainment flux are less than 40% of the anomalies in the net surface heat flux. Unfortunately, on the basin scale there are insufficient observations to estimate the actual anomalies in either the mixed layer depth (from XBTs) or subsurface heat flux anomalies to the surface layer. Finally, it is interesting to note, in general, entrainment reinforces the surface cooling anomalies in the subtropics and enhances the warming anomalies in the northern part of the domain.

c. The composite cold event

The observation-based composite cold event features cold water throughout most of the North Atlantic (Fig. 2a). The maximum negative SST anomaly exceeds -0.4°C and is located in the northwestern part of the basin. As in the warm event, the pattern of the air temperature anomalies is similar to the SST anomalies: the atmosphere minus ocean temperature difference is, typically, half of the SST anomaly (cf. Fig 7a, 2a and 2c).

The heat flux anomalies that accompany the composite cold event from observations are displayed in Fig. 7 (panel a, c, and d). Negative heat flux that cools the ocean is found in the northern half of the domain and is consistent with the observed negative SST anomalies. There exists a region of anomalous warming of the subtropical ocean, centered upon $50^\circ\text{W}, 30^\circ\text{N}$. Along the northeast US seaboard, however, the observed fluxes are cooling the ocean locally where anomalously warm water is found (see Figs. 2a and 7a). Throughout the domain in the cold composite event, the latent heat flux anomalies are in phase with the sensible heat flux anomalies (e.g., cf. Fig. 7c and 7d). As in the warm composite event, both flux components contribute importantly to the net heat flux anomalies in the northern half of the domain, while the latent fluxes are about triple the sensible fluxes in the subtropics because of larger moisture deficit (capacity) associated with the warmer air (see also Alexander 1990).

The composite cold event from the hindcast integration is displayed in Fig. 8. Overall, the simulated and observed cold composite SST anomalies are in good agreement in the

northern half of the domain. In the southwestern corner of the domain the simulated warming is only about one half of the observed warming. As in the warm composite event, in the northern half of the domain the anomalies in "surface air temperature minus SST (or T_{mix})" are about half that of the anomalies in SST. The pattern and amplitude of the individual and net surface heat flux anomalies simulated by the model are, overall, consistent with those observed (cf. Figs. 7c and 8c, 7d and 8d, and 7a and 8e). As in the simulated composite warm event, the mixed layer depth is anomalously shallow (deep) where the surface ocean is anomalously warm (cold) (Fig. 8g). Also, for the cold event, the winter-time (six month average) anomalies in the subsurface fluxes into the mixed layer (Fig. 8f) are generally small ($\sim 25\%$) compared with the anomalies in the net (sensible plus latent) surface heat flux. We note, however, during early autumn the heating anomalies due to anomalous entrainment are larger (not shown) than the anomalies in the net surface flux (Q_{S+L}).

4. Sensitivity studies

a. The role of varying surface air temperature, humidity and wind speed

In this section we repeat the hindcast experiment of section two, using only selected atmospheric fields as forcing. Recall that the heat flux anomalies in the hindcast of section two result from the prescribed (observed) monthly mean anomalies in surface air temperature, humidity and daily mean wind speed. We report the results from three additional hindcast integrations. In the first hindcast ("NT"), we prescribe only the observed anomalies in q and V_a ; the air temperature is held fixed at climatology ($T_a = 0$). A second experiment ("NQ") is performed whereby anomalies in T_a and V_a are prescribed and q is set to climatology ($q'_a = 0$). Finally, a third hindcast integration ("NW") is performed setting V_a to climatology and prescribing the observed monthly anomalies in T_a and q . As in the hindcast integration of section three, the warm and cold composite events are formed from each integration and are plotted in Figs. 9 and 10.

For both the cold and warm event composites, monthly mean anomalies in the monthly average of the instantaneous wind speed are seen to have very little effect on the simulated SST anomalies. On the other hand, withholding the information on the anomalies in either T_a or q significantly degrade the hindcast in both the warm and cold cases.

b. The composite hindcast events using prescribed flux anomalies.

In this section we obtain the composite warm and cold events using the same ocean model but now force the model with the net surface forcing anomalies Q_{S+L} that are estimated entirely from the observations of the surface atmospheric fields and the *observed* SST: the flux anomalies are independent of the response of the ocean model. Hence, the composite formed from these integrations are referred to as “one-way forced” composites. For convenience, the hindcast of section 3b, which uses atmospheric fields and simulated SST in calculating the forcing, will be referred to as the partially coupled (PC) hindcast.

We proceed as follows. For each of the winters listed in Table 1 the “observed” flux anomalies are calculated from COADS using the bulk parameterization of Deardorff (1972). For each year that goes into the composite event (see Table 1), the “observed” monthly averaged Q_{S+L} flux anomalies are added to the net surface heat flux obtained from the ocean model control integration. The model is then integrated for eight months, starting on September first for each year that goes into the warm and cold composite events: the initial conditions for the ocean temperature $T(z)$ are from the appropriate September first from the partially coupled hindcast. The composite warm and cold event anomalies (in h and T_{om}) are then obtained by subtracting the model response from that obtained in the control run (described in section 2c).

The “one-way forced (OWF) warm composite” SST and mixed layer depth anomalies are displayed in Fig. 11a,b. The spatial pattern of the OWF composite warm event is qualitatively similar to that from the PC hindcast integration (cf. Figs. 11a and 6a and 1a) though the OWF composite is somewhat noisier than that observed or that from the PC hindcast. Differences between simulated and observed SST anomalies are noted along the northeast US coast, from Cape Hatteras to Nova Scotia (see the discussion in section 5). The amplitude of the warm anomaly centered in the northwestern of the domain is about double that from the PC hindcast of section 3b. The pattern of the mixed layer depth anomalies in the PC hindcast is similar to that obtained in the OWF hindcast (cf. Fig. 11b and 6g), though the amplitude of the h anomalies are larger in the latter case (see Alexander 1992) because of the increase in the buoyancy (SST) anomalies in the OWF case.

The composite cold event obtained from the hindcast using the OWF coupling is displayed in Figs. 12a,b. The observation based composite displays cold water throughout the northern half of the basin, and warm water in the southwest domain (Fig. 2a). The composite SST anomaly pattern from the PC hindcast of section 3b is very similar to the observed composite (cf., Fig 2a and 8a). In the OWF cold composite hindcast, however,

the agreement between simulated and observed SST anomalies is only qualitative. Along the far northern border of the domain, the amplitude of the simulated cold anomaly is about half the observed. A cold anomaly is simulated in the southeast (35°N, 20°W) where the observed SST is near normal but slightly positive. Furthermore, in the OWF simulation there is a strip of cold water along the northeastern US seaboard where observations show warm anomalies (cf. Fig. 2a and Fig. 12a). Mixed layer depth anomalies are negative (shallow) in the northern domain and positive in the southern half of the domain, mainly due to changes in the buoyancy forcing.

5. Discussion

Throughout most of the model domain, the hindcast OWF and PC composite warm and cold events are similar to their observed counterparts. The region of largest disagreement between the simulated and observed SST anomaly is located in the wedge of ocean between Cape Hatteras and just south of Nova Scotia, extending offshore about one grid box (about 400 km). This region is exactly where surface oceanic temperature advection is largest. The simulated SST anomalies for both the warm and cold composite cases are *opposite* than expected from the anomalies in the surface energy budget. The qualitative disagreement between the simulated and observed SST anomalies suggests that the SST anomalies in this region are due primarily to processes that are neglected. The neglected surface fluxes anomalies (e.g., radiation) are small compared with Q_{S+L} . This region is, however, characterized by strong oceanic temperature gradients and ocean currents. Hence, it is likely that an important process for generating wintertime SST anomalies in this small region along the coast is anomalous advection in the ocean.

The weak dependence of the surface flux anomalies on the monthly mean anomalies in the daily wind speed $V_a \equiv |\bar{V}_a|$ is understood from the Taylor series expansion of the net heat flux:

$$Q'_S \propto \bar{V}_a (T'_a - T_{om}) + V_a (\bar{T}_a - \bar{T}_{om}) \quad (4)$$

$$-Q'_L \propto \bar{V}_a (q'_s - q'_a) + V_a (\bar{q}_s - \bar{q}_a) \quad (5)$$

In Eqs. (4) and (5), the overbar denotes the monthly mean climatological value; (prime) denotes the monthly mean anomaly and the nonlinear terms have been neglected. Comparing the terms on the right hand side in the N. Atlantic basin, we find (typically)

$$\left| \frac{\bar{V}_a (T'_a - T_{om})}{V_a (\bar{T}_a - \bar{T}_{om})} \right| \sim \frac{10 \times 0.5}{1 \times 2} = 2.5 \quad \text{and} \quad \left| \frac{\bar{V}_a (q'_s (T_{om}) - q'_a)}{V_a (\bar{q}_s (T_{om}) - \bar{q}_a)} \right| \sim \frac{10 \times 1}{1 \times 3} \sim 3.$$

The secondary role of the anomalous wind speed, V_a in generating SST anomalies in the midlatitudes was also noted by Haney et al. (1983) and Luksch and von Storch (1992).

The significant role of air temperature anomalies in generating SST anomalies was pointed out in section 4b. It is important to note that implicit in the prescribed air temperature anomaly T_a is the process of atmospheric advection; specifically, advection by high frequency (unresolved) synoptic scale eddies in the atmosphere. It is indeed likely that a large fraction of the monthly mean surface heat flux anomaly is, in general, due to the cumulative effect of meridional advection of air with differing temperature and moisture by baroclinic eddies. [We note that a monthly mean anomaly in T_a and q could be attributed to synoptic events without observing a significant change V_a .] It is likely, however, that prescribing the monthly mean atmospheric variables provides a reasonable estimate of the monthly mean surface flux attributed to the synoptic scale storms (a related discussion is found in Trenberth et al. 1989).

It has been argued that by prescribing the atmospheric surface anomaly fields in concert with the bulk formulae representation for surface heat flux anomalies, the SST will be inextricably tied to the air temperature anomalies. To avoid prescribing the atmospheric fields Luksch and von Storch (1992) designed an advective atmosphere model of the (non-divergent) surface flow over the N. Pacific. In their model, the observed air temperatures at the edge of the model domain were prescribed and advected as a tracer that experienced climatological damping and was influenced by the flux of sensible and latent heat to the ocean. The observed monthly mean winds are then imposed on the model. While the point of the model was to allow air temperatures to evolve more freely, it is puzzling that their sensitivity experiments (their section 5) did *not* indicate the heat flux anomalies were important in modifying the surface air temperature.

The coupling methodology (PC) we have used in section 3b ensures that *if* atmospheric circulation anomalies are indeed modified by the fluxes between the media, then *a priori* the observed atmospheric variables explicitly contain this information (see section two). The methodology is thus identical to the experiments whereby SST anomalies are prescribed under an atmospheric GCM. Nonetheless, because the surface air temperature and SST anomalies closely track one another (e.g., cf. Fig. 1a and 5b) and a key flux (sensible) for interannual climate fluctuations is formulated in terms of the difference between air temperature and SST, it is possible that the simulated SST anomalies are overly constrained by the PC formulation of coupling. The good agreement between the OWF and observed composite warm and cold event SST anomalies alleviates this concern.

Finally, we note the magnitude of the observed SST anomalies tend to be greater (less) than those in the PC (OWF). This indicates that the true negative feedback resulting from air-sea interaction lies in between the strong damping in the PC simulations and the absence of any feedback in the OWF simulations.

6. Conclusions

In this paper we examine the hypothesis that the interannual variability in wintertime North Atlantic sea surface temperature (SST) is due to the variability in the surface heat flux, dominated by the variability in the sensible and latent heat flux. The hypothesis is tested by performing a hindcast integration of a upper ocean model of the North Atlantic Ocean, forcing the model with surface heat and momentum fluxes calculated using the bulk formulae and the observed state of the atmosphere at the air-sea interface, from 1950-1988. The ability of the model to accurately hindcast the wintertime interannual variations in SST is demonstrated by simple correlations with the observed anomalies and, following Kushnir (1994), by comparing the composite of warm and cold events observed in the N. Atlantic with those simulated by the model. The composite of SST, sensible and latent heat flux anomalies from the observations are compared with those obtained from the ocean model hindcast. In addition, the entrainment and mixed layer depth anomalies from the ocean model hindcast are presented and discussed.

There is a good quantitative agreement between simulated and observed SST anomalies throughout most of the North Atlantic Ocean. Consistent with conclusions of other observational studies (e.g., Cayan 1992a,b), both sensible and latent heat flux anomalies are shown to contribute substantially to the wintertime anomalies in SST in the N. Atlantic, while in the subtropics the heat flux anomalies are predominantly determined by the latent heat flux term. Entrainment anomalies contribute to a lesser extent to the mixed layer temperature anomalies throughout the domain (typically 33% or less of the net surface heat flux anomalies).

Since in the model formulation we explicitly exclude any effects due to *anomalies* in the ocean advection, our results confirm the hypothesis that wintertime interannual variability in the North Atlantic SST is mainly due to local anomalies in the air-sea flux of sensible and latent heat and not to anomalies in horizontal oceanic advection. There is significant disagreement between hindcast and simulated SST anomalies only in a small region extending from Cape Hatteras to Nova Scotia along the US coast. In this region, the observed surface flux anomalies are anti-correlated with the SST anomalies, implicating

important changes in oceanic advection to the interannual wintertime SST anomalies along the seaboard. We note Haney (1985) and Miller (1992) found ocean current anomalies also play a secondary role ocean in generating interannual SST anomalies throughout the midlatitude Pacific Ocean (cf. Luksch 1994).

Sensitivity studies are performed to highlight the variability in the atmosphere and the atmospheric processes that account for the surface heat flux anomalies. We find the anomalies in air temperature and humidity are fundamental to the net surface flux anomalies. The monthly mean anomaly in the monthly average of the instantaneous wind speed has little effect on either the surface fluxes or on the simulated SST anomaly.

The hindcast presented in this paper is a test of the ocean model, and is a necessary step in our ultimate goal: to examine the interaction between the ocean and the atmosphere in the midlatitudes and how this interaction affects circulation anomalies in the midlatitude atmosphere. Thus, the formulation in the coupling of the ocean to the atmosphere used in the hindcast of section three is designed to facilitate the next step: the interactive simulation using the ocean model and an atmospheric GCM. As a result, the heat fluxes that drive the ocean model depend on the difference between the atmospheric surface temperature and the simulated SST *via* the bulk formulae for the fluxes. To reassure the reader that the model response was not pre-determined by the formulation of the coupling, we presented in section 4c the composite cold and warm events from the model when it was forced by the "observed" heat flux anomalies, estimated exclusively from COADS (using the bulk formula and the observed interfacial fields) and independent of the response of the ocean model.

Acknowledgments

This work was funded by a grant from the NOAA Office of Global Change Programs and grants from the National Science Foundation (ATM ATM-8913261 and ATM-9302884).

Appendix: Model Description

Following Niiler and Kraus (1977), the upper ocean in midlatitudes is represented by a well mixed surface layer with uniform temperature and salinity and a sharp discontinuity

in these quantities at the base of the mixed layer. Integrating the continuity equations for heat and salt over the mixed layer depth yields:

$$\frac{\partial T_{om}}{\partial t} = w_e (T_b - T_{om}) / h + \frac{(Q_{tot} - Q_{SWH})}{\rho_0 C_p h} + \frac{v_H \partial T_{om}}{h \partial z} \Big|_{z=h} \quad (A1)$$

$$\frac{\partial S_{om}}{\partial t} = w_e (S_b - S_{om}) / h + \frac{S_{om} (E - P)}{\rho_0 h} + \frac{v_S \partial S_{om}}{h \partial z} \Big|_{z=h} \quad (A2)$$

where T is the temperature, S salinity, t is time, w_e the entrainment rate, h the mixed layer depth, ρ_0 the reference density, C_p the specific heat, z the vertical coordinate (positive down), E the evaporation rate, P the precipitation rate, Q_{SWH} the penetrating solar radiation, and v_H (v_S) is the molecular diffusion coefficient for heat (salt). Subscripts om and b represent conditions within and below the mixed layer, respectively. The net surface heat flux is given by:

$$Q_{tot} = Q_L + Q_S + Q_{SW} + Q_{LWnet} \quad (A3)$$

where the fluxes are positive downwards and Q_{SW} is the shortwave radiation, Q_{LWnet} the net longwave radiation, and Q_S (Q_L) is the sensible (latent) heat flux. The parameterizations used to compute the four components of Q_{net} are discussed in section 3b. The heat flux below the surface is due to penetrating solar radiation and is prescribed following Paulson and Simpson (1977):

$$Q_{SWH} = Q_{SW} (R \cdot \exp(-z/\xi_1) + (1 - R) \cdot \exp(-z/\xi_2)) \quad (A4)$$

The constants R , ξ_1 and ξ_2 depend on the optical water type (see Jerlov 1967) for which values over the N. Atlantic have been obtained from Simonot and Le Treut (1986). At the base of the mixed layer, the water properties T_b and S_b are obtained directly from the layer in which h resides; below the mixed layer, temperature and salinity evolve according to:

$$\frac{\partial T}{\partial t} = \frac{1}{\rho_0 C_p} \frac{\partial Q}{\partial z} + v_H \frac{\partial^2 T}{\partial z^2} \quad (A5)$$

$$\frac{\partial S}{\partial t} = v_S \frac{\partial^2 S}{\partial z^2} \quad (A6)$$

There are two additional processes that influence the temperature and salinity within the model: convective overturning and an adjustment to conserved model properties. Con-

vective adjustment occurs when the density of a layer exceeds the density of the layer below. The temperature of both layers is subsequently set to the mass-weighted mean. The conservation of heat, salt and potential energy is ensured by adjusting T_{om} and T_b according to

$$T_m = T_m + \frac{(D_k - h - D_m) h (T_m - T_b)}{D_k D_m} \quad (A7)$$

$$T_b = T_b + \frac{(h - D_m) h (T_m - T_b)}{D_k (D_k - D_m)} \quad (A8)$$

where $D_k = \sum_{l=1}^k \Delta z_l$ and $D_m = \max(h, D_k - \Delta z_k)$. Salinity is analogously adjusted.

The entrainment rate is derived from vertically integrating the turbulent kinetic energy equation over the mixed layer depth and then parameterizing the resulting terms using the known variables. The formula, common to most mixed layer models, can be expressed as follows:

$$w_e = \frac{m u_*^3 - 0.5 h B(h) - h \epsilon}{q^2 + 0.5 (h \Delta b - s \Delta \uparrow)} \quad (A9)$$

where

$$B(h) = \frac{\alpha g}{\rho_{ref} C_P} \left(Q_{tot} + Q_{SWH} - \frac{2}{h} \int_0^h Q dz \right) + \frac{\beta g S_m}{\rho} (P - E) \quad (A10)$$

$$\Delta b = \alpha g \Delta T - \beta g \Delta S \quad (A11)$$

$\Delta = \{ ()_{om} - ()_b \}$ represents the discontinuity at the base of the mixed layer, u_* is the friction velocity, ϵ the turbulent dissipation rate, \uparrow the velocity, q^2 the mean turbulent kinetic energy, and m and s are constants determined from observations. The thermal expansion coefficients α and β are determined from the international equation of state for sea water. The three terms in the numerator of (A9) represent the effects of wind stirring, changes in the buoyancy due to surface fluxes and penetrating solar radiation, and the dissipation of energy within the mixed layer. The terms in the denominator of (A9) are the energy required to agitate entrained water, and the buoyancy jump at the base of the mixed layer. The instability term resulting from the shear across the base of the mixed layer is not

included due to the transient nature of this term. The mean turbulent kinetic energy is parameterized according to Kim (1976):

$$q = 9 \cdot \max\left(10^{-4} m^2 s^{-2}, u_*^2\right) \quad (\text{A12})$$

Dissipation is an important process in the mixed layer: several approaches have been used to parameterize this term (cf., Niiler and Kraus 1977; Garwood 1979; Gaspar 1988). We use the formulation of Gaspar, as his model is designed for use in extended integrations (i.e., for integrations longer than a season). In addition, the model with this formulation of entrainment simulates better the depth of the mixed layer in summer. When $w_e \geq 0$, $\frac{dh}{dt} = w_e$ and w_e in (A9) becomes a function of the mixed layer depth, the Monin-Obukov length and the Ekman length scale. When the mixed layer shallows, h is solved iteratively until a balance is reached between the wind stirring and the net buoyancy forcing over the depth of the mixed layer.

Numerical methods, model constraints and initial conditions

The prognostic equations for T_{om} , S_{om} and h are solved using a fourth order Runge-Kutta scheme, which requires information at only one previous time step. All prognostic model equations are integrated using a one-day time step. Below the mixed layer, the integration is a forward differencing scheme in time.

The mixed layer depth is constrained to be greater than 10m and less than 850m to ensure computational stability. While long-lived mixed layer depths less than 10m are extremely rare in Nature, there is the potential for the model to simulated such shallow mixed layers in summer, as there are processes that act to keep the mixed layer away from the surface (e.g., surface wave mixing) that are not included in the model. In the hindcast integrations presented in section 3 of this paper, the mixed layer is initialized with the climatological values of T and S from Levitus (1982).

References

- Ademec, D., R.L. Elsberry, R.W. Garwood and R.L. Haney, 1981: An embedded mixed-layer-ocean model. *Dyn. Atmos. Oceans*, 6, 69-96.
- Alexander, M. A., 1990: Simulation of the response of the north Pacific Ocean to the anomalous atmospheric circulation associated with El Nino. *Climate Dyn.*, 5, 53-65.

- Alexander, M. A., 1992: Midlatitude atmosphere-ocean interaction during El Niño. Part I: the North Pacific Ocean. *J. Climate*, 5, 944-58.
- Alexander, M.A., and C. Deser, 1994: A mechanism for the recurrence of wintertime mid-latitude SST anomalies. To appear, *J. Phys. Oceanogr.*
- Alexander, R.C., and R.L. Mobley, 1976: Monthly average sea-surface temperature and ice-pack limits in a 1° global grid. *Mon. Wea. Rev.*, 104, 143-148.
- Bjerknes, J., 1964: Atlantic air-sea interaction. *Adv. Geophys.*, 20, 1-82.
- Cayan, D.R, 1992a: Variability of latent and sensible heat fluxes estimated using bulk formulae. *Atmos-Ocean*, 30, 1-42.
- Cayan, D.R., 1992b: Latent and sensible heat flux anomalies over the Northern Oceans: Driving the sea surface temperature. *J. Phys. Oceanogr.*, 22, 859-881.
- Davis, R.E., 1976: Predictability of sea surface temperature and sea-level pressure anomalies over the North Pacific Ocean. *J. Phys. Oceanogr.*, 6, 249-266.
- Deardorff, J., 1972: Parameterization of the planetary boundary layer for use in general circulation models. *Mon. Wea. Rev.*, 100, 93-106.
- Deser, C., and M.L. Blackmon, 1993: Surface climate variations over the North Atlantic Ocean during winter: 1900-89. *J. Climate*, 6, 1743-1753.
- Garwood, R.W., 1977: An oceanic mixed layer model capable of simulating cyclic states. *J. Phys. Ocean.*, 7, 455-468.
- Gaspar, Ph., 1988: Modeling the seasonal cycle of the upper ocean. *J. Phys. Oceanogr.*, 18, 161-180.
- Haney, R.L., B.H. Houtman, and W.H. Little, 1983: The relationship between wind and sea surface temperature anomalies in the mid-latitude north Pacific Ocean. *Atm.-Ocn.*, 21, 168-186.
- Haney, R.L., 1985: Midlatitude sea surface temperature anomalies: A numerical hindcast. *J. Phys. Oceanogr.*, 15, 787-799.
- Isemer, H.-J., and L. Hasse, 1987: *The Bunker climatic atlas of the North Atlantic. Volume 2: air-sea interactions*. Springer-Verlag, Berlin, 252 pp.

- Jerlov, N., G., 1976: *Marine Optics*, Elsevier Oceanogr. Ser., Vol 14, New York, 231 pp.
- Kim, J., 1976: A generalized bulk model of the oceanic mixed layer. *J. Phys. Oceanogr.*, 6, 686-695.
- Kushnir, Y.: 1994: Interdecadal variations in North Atlantic sea surface temperature and associated atmospheric conditions. *J. Climate*, 7, 141-157.
- Kushnir, Y. and N.-C. Lau: 1992: The general circulation model response to a North Pacific SST anomaly: Dependence on time scale and pattern polarity. *J. Climate*, 5, 271-283.
- Lanzante, J.R., 1984: A rotated eigenanalysis of the correlation between 700 mb heights and sea surface temperatures in the Pacific and Atlantic. *Mon. Wea. Rev.*, 112, 2270-2280.
- Lau, N.-C., and M.J. Nath, 1990: A general circulation model study of the atmospheric response to extratropical SST anomalies observed in 1950-79. *J. Climate*, 3, 965-989.
- Lau, N.-C., and M.J. Nath, 1993: A modeling study of the relative roles of tropical and extratropical SST anomalies in the variability of the global atmosphere-ocean system. Submitted, *J. Climate*.
- Levitus, S. 1982: Climatological atlas of the world ocean. NOAA Professional Paper 13. US Govt. Printing Office, Washington DC, 173 pp.
- Luksch, U., 1994: Simulation of North Atlantic low-frequency SST variability. Submitted, *J. Climate*.
- Luksch, U. and von Storch, H, 1992: Modeling the low-frequency sea surface temperature variability in the North Pacific. *J. Climate*, 5, 893-906.
- Miller, A.J, 1992: Large-scale ocean-atmosphere interactions in a simplified coupled model of the midlatitude wintertime circulation. *J. Atmos. Sci.*, 49, 273-286.
- Niiler, P.P., and Kraus, E., B., 1977: Modeling and prediction of the upper layers of the ocean. One-Dimensional models of the upper ocean, Kraus, E., B., Ed., Pergamon Press, Oxford, 143-172.

- Palmer, T.N., and Z. Sun, 1985: A modeling and observational study of the relationship between sea surface temperatures in the northwest Atlantic and the atmospheric general circulation. *Quart. J. Roy. Meteor. Soc.*, 111, 947-975.
- Paulson, C.A. and J.J. Simpson, 1977: Irradiance measurements in the upper ocean. *J. Phys. Oceanogr.*, 7, 952-956.
- Peng, S., L. Mysak, H. Ritchie, J. Derome and B. Dugas, 1994: On the difference between early and middle winter atmospheric responses to sea surface temperature anomalies in the northwest Atlantic. Submitted to *J. Climate*.
- Pitcher, E.J., M.L. Blackmon, G. Bates and Munoz, 1988: The effect of North Pacific sea surface temperature anomalies on the January climate of a general circulation model. *J. Atmos. Sci.*, 45, 173-188.
- Sausen, R. and Ponater, 1988: Reducing the initial drift of a GCM. Contributions 15-24. to *Atmospheric Physics*, 63, 15-24.
- Simonot, J.-Y., and H.L. Le Treut, 1986: Climatological field of mean optical properties of the world ocean. *J. Geophys. Res.*, 91, 6642-6646.
- Trenberth, K.E., W.G. Large and J.G. Olson, 1989: The effective drag coefficient for evaluating wind stress over the oceans. *J. Climate*, 2, 1507-16.
- Soden, B.J., 1992: Validation of cloud forcing simulated by the National Center for Atmospheric Research Community Climate Model using observations from the Earth Radiation Budget Experiment. *J. Geophys. Res.*, 97, 18137-18159.
- van Loon, H. and J.C. Rogers, 1978: The seesaw in winter temperatures between Greenland and northern Europe. Part I: General description. *Mon. Wea. Rev.*, 106, 296-310.
- Wallace, J.M., and Q. Jiang, 1987: On the observed structure of the interannual variability of the atmosphere/ocean climate system. *Atmospheric and oceanic variability*, H. Cattle, Ed., *Roy. Meteor. Soc.*, Bracknell, Berkshire, 17-43.
- Wallace, J.M., C. Smith, and Q. Jiang, 1990: Spatial patterns of atmosphere-ocean interaction in the northern winter. *J. Climate*, 3, 990-998.
- Wallace, J.M., C. Smith, and C.S. Bretherton, 1992: Singular Value Decomposition of wintertime sea surface temperature and 500-mb height anomalies. *J. Climate*, 3, 990-998.

White, W.B. and A.E. Walker, 1974: Time and depth scales of anomalous subsurface temperature at Ocean Weather Stations P, N, and V in the North Pacific. *J. Geophys. Res.*, 79, 4517-4522.

Williamson, D.L., J.T. Kiehl, V. Ramanathan, R.E. Dickinson and J.J. Hack, 1987: *Description of NCAR Community Climate Model (CCM1)*. NCAR Tech. Note, NCAR/TN-285+STR, National Center for Atmospheric Research, Boulder CO NTIS PB87-203782/AS, 112 pp.

TABLE 1. The years that define the warm and cold composite events. Years that do not appear in Kushnir's composite events are indicated by (*).

Warm Event	Cold Event
1950-51	1953-54*
1952-53	1956-57*
1954-55	1958-59
1957-58	1960-61
1964-65	1971-72
1965-66	1972-73
1967-68	1973-74
1968-69*	1974-75
1969-70	1979-80*
1980-81	1985-86

Figure Captions

Figure 1. A composite of observed wintertime (November to April) interannual “warm” events in the N. Atlantic. (a) SST anomaly (contour interval, c.i., is 0.1°C); (b) Sea Level Pressure (SLP), in mb; (c) Surface air temperature anomaly, T_a (c.i. 0.1°C); (d) surface wind vector anomaly. The observations are from COADS. The years that constitute the composite are listed in Table 1. Solid contours are positive.

Figure 2. As in Figure 1, but for the composite *cold* event.

Figure 3. The annual average of the climatological surface heat flux (in Wm^{-2}). (a) The total surface heat flux Q_{tot} (= radiation + latent + sensible) from the community climate model (CCM1) control integration. (b) As in (a), but from COADS observations and the bulk formulae of Isemer and Hasse (1987) (latent, sensible). (c) The annual average heat flux “correction” Q_{corr} applied to the ocean model (see section 2). (d) The annual average of the net surface forcing that results from the control run of the ocean model: $Q_{net} \equiv Q_{tot} + Q_{corr}$.

Figure 4. The correlation coefficients for the observed with the hindcast SST anomaly during (a) winter and (b) summer. Winter (summer) is defined as the November through April (May through October) mean. The integration spans 1950-1988.

Figure 5. Selected fields important for the net anomalous wintertime surface heat flux in the N. Atlantic during the composite *warm* event (from observations). (a) The anomalous “sensible + latent” heat flux (c.i. 5Wm^{-2}); (b) the anomalous air-sea temperature difference (c.i. 0.1°C); the anomalous (c) sensible and (d) latent heat flux (c.i. 5Wm^{-2}); (e) the wintertime mean daily wind speed anomaly (c.i. 0.2ms^{-1}).

Figure 6. A composite of wintertime (November to April) interannual “*warm*” events in the N. Atlantic as simulated by the upper ocean model. (a) SST (T_{om}) anomaly (c.i. 0.1°C). (b) The anomalous air-sea temperature difference ($T_a - T_{om}$; c.i. 0.1°C). The anomalous fluxes of heat (c.i. 5Wm^{-2}) into the ocean mixed layer: (c) sensible Q'_S , (d) latent Q'_L , (e) “sensible + latent” Q'_{S+L} and (f) entrainment Q'_w . Positive represents a heat gain in the mixed layer. (g) The anomalies in the mixed layer depth, h (c.i. 5 m; solid contours for thicker-mixed layer).

Figure 7. As in Figure 5, but for the observed composite “*cold*” event.

Figure 8. As in Figure 6, but for the composite “*cold*” event from the hindcast using the ocean model.

Figure 9. The hindcast SST in the composite *warm* event that is obtained when selected anomalies in the atmosphere are withheld from the forcing of the ocean. (a) All anomalies used (same as Fig. 6a); (b) hindcast with $T_a = 0$; (c) hindcast with $q'_a = 0$; (d) hindcast with $V_a = 0$. The contour interval is 0.1°C ; positive contours are solid.

Figure 10. As in Figure 9, but for the hindcast *cold* event. Panel (a) is identical to Fig. 8a.

Figure 11. A composite of wintertime (November to April) interannual *warm* events in the N. Atlantic as simulated by the upper ocean model, forced by the “observed” surface “sensible plus latent” heat flux anomalies. (a) SST (T_{om}) anomaly (c.i. 0.1°C); (b) the anomalies in the mixed layer depth, h (c.i. 5 m; solid contours for thicker mixed layer). The anomalous heat flux into the ocean mixed layer is plotted in Fig. 5a.

Figure 12. As in Figure 11, but for the hindcast *cold* event. The anomalous heat flux into the ocean mixed layer is plotted in Fig. 7a.

Figure 1.

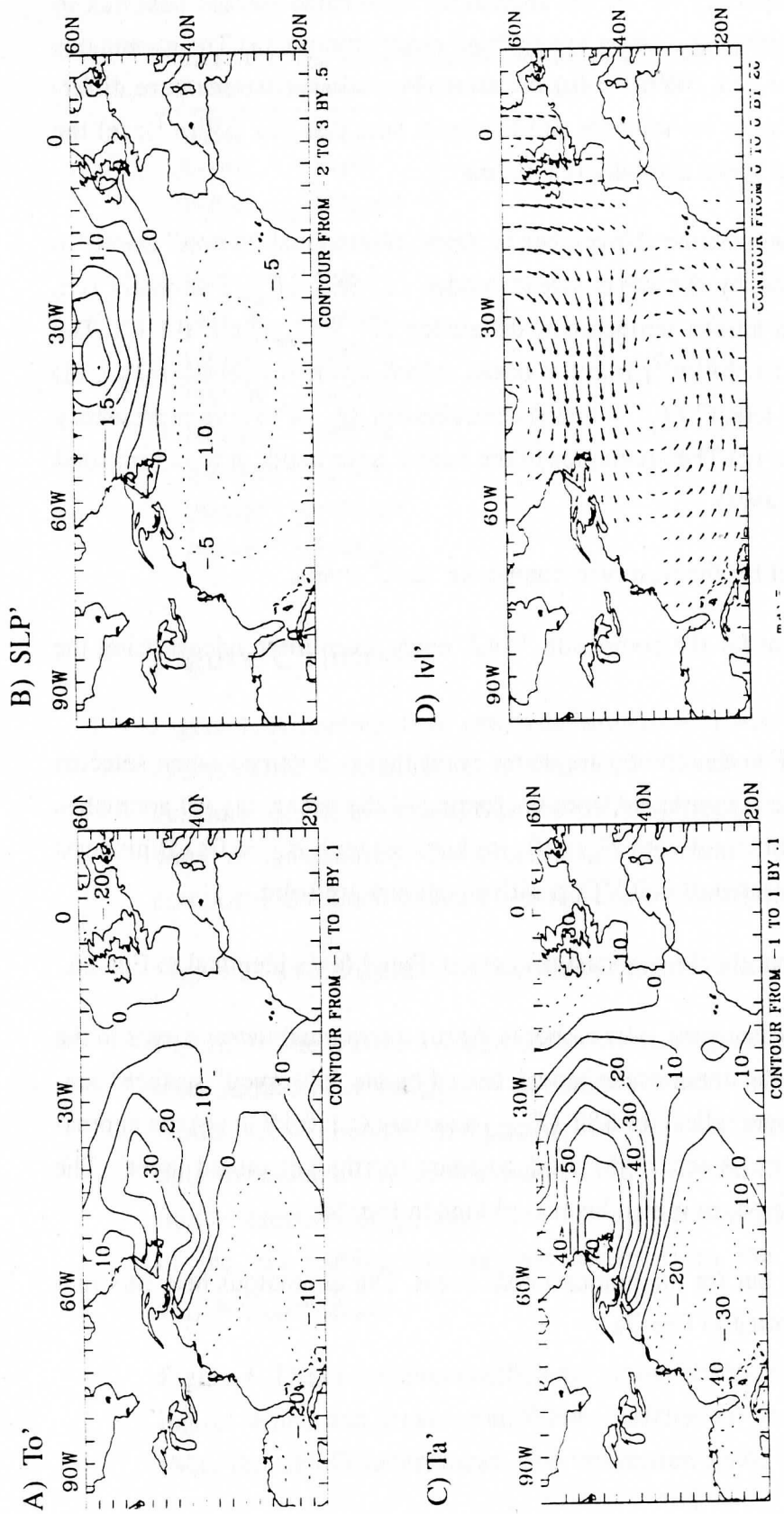
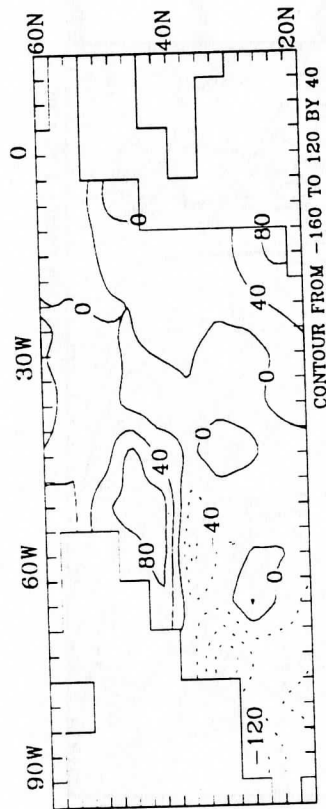
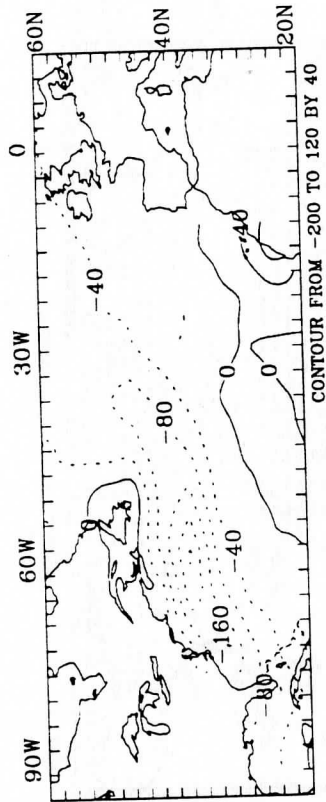


Figure 3.

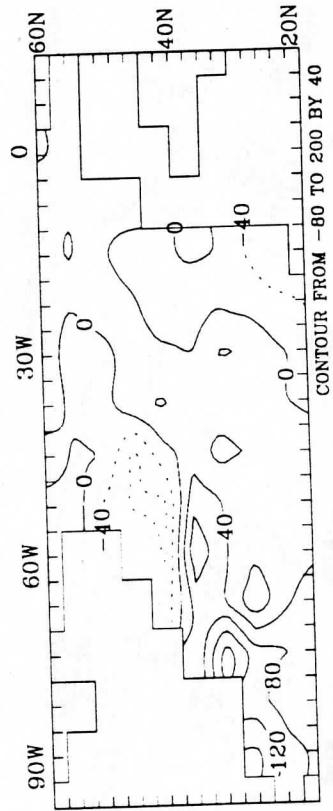
A) Q_{tot}



B) Q_{COADS}



C) Q_{corr}



D) Q_{net}

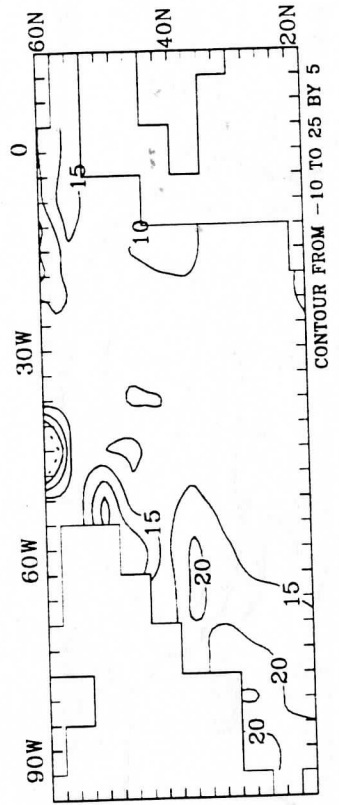
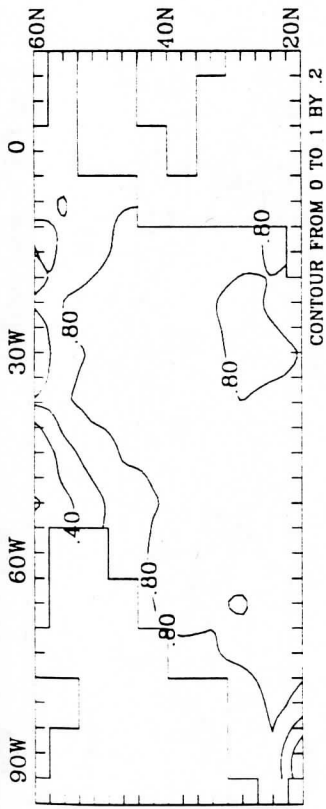


Figure 4.

A) November-April



B) May-October

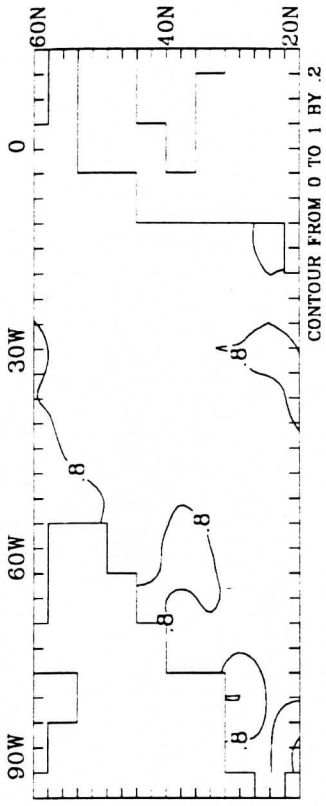
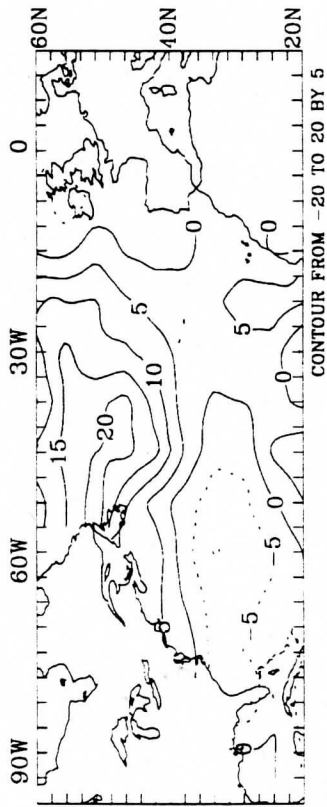
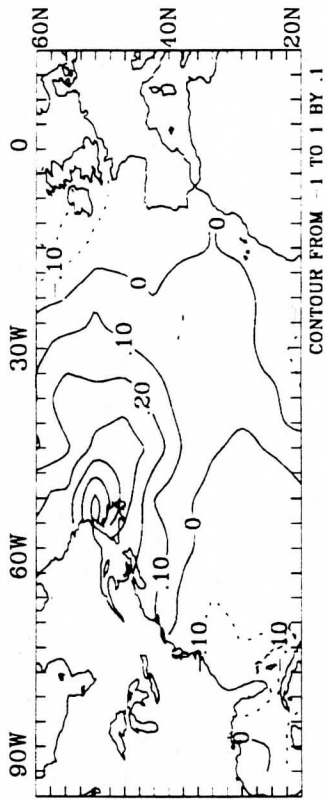


Figure 5.

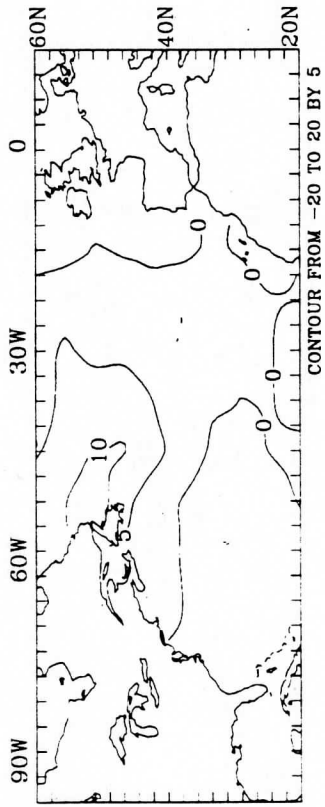
A) $Q_s + I'$



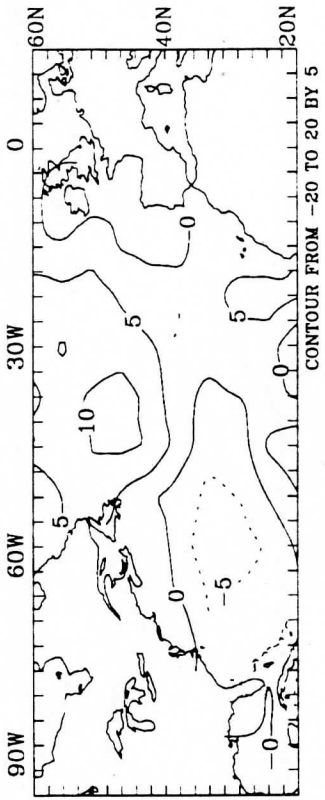
B) $Ta' - To'$



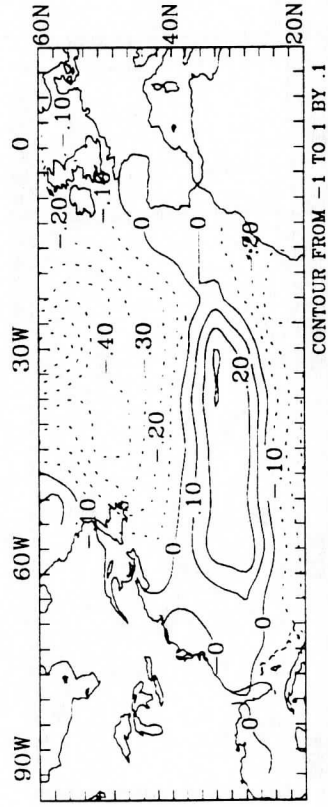
C) Q_s'



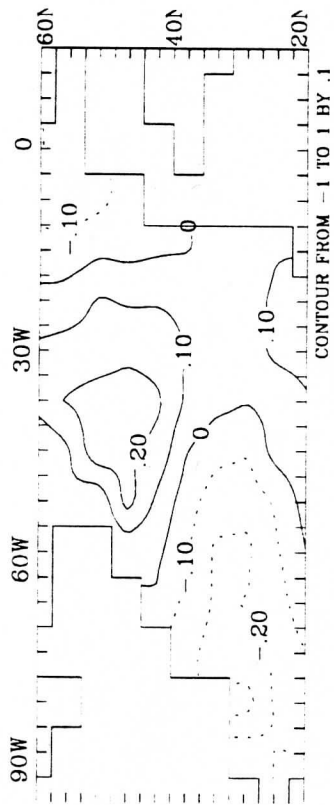
D) QI'



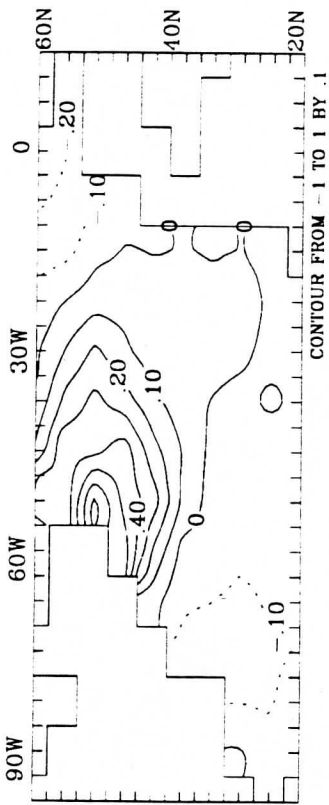
E) $|v|'$



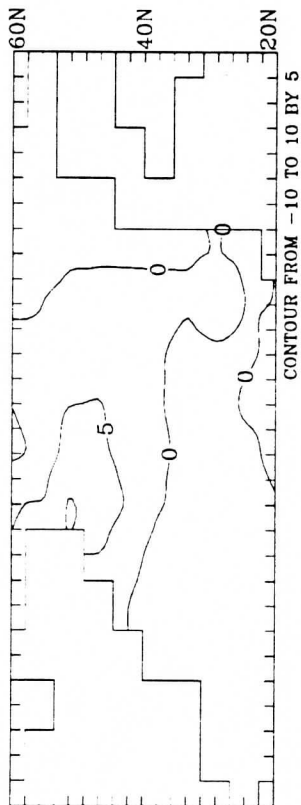
A) Tom'



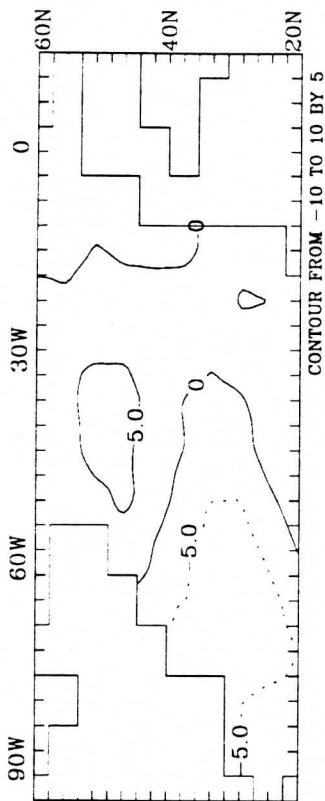
B) Ta'-Tom'



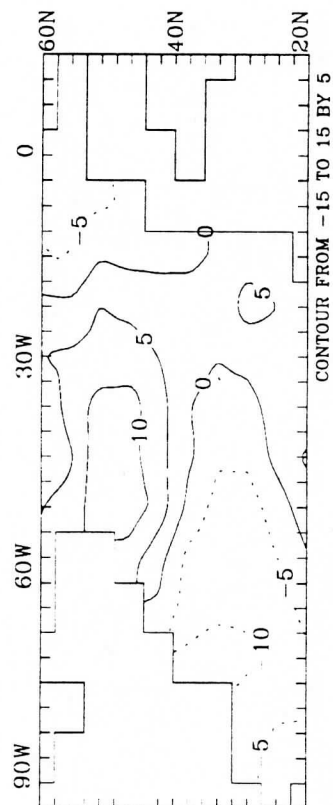
C) Qs'



D) QI'



E) Qs+I'



F) Qwe'

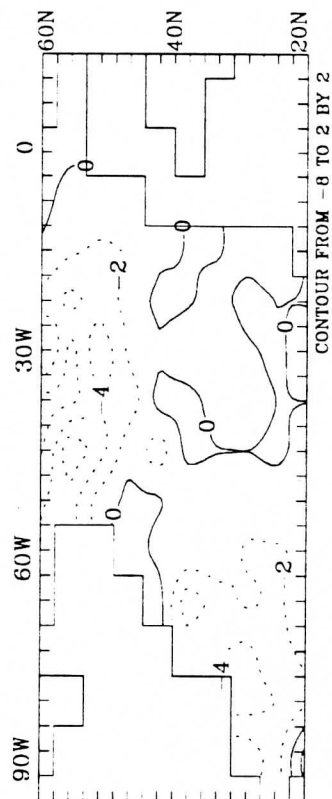


Figure 6 (cont).

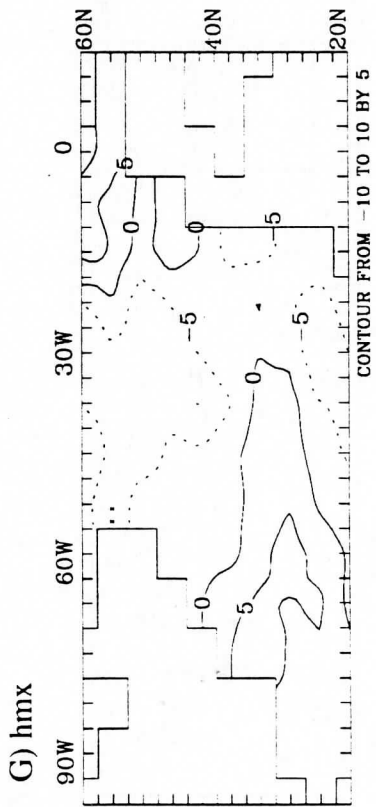


Figure 7.

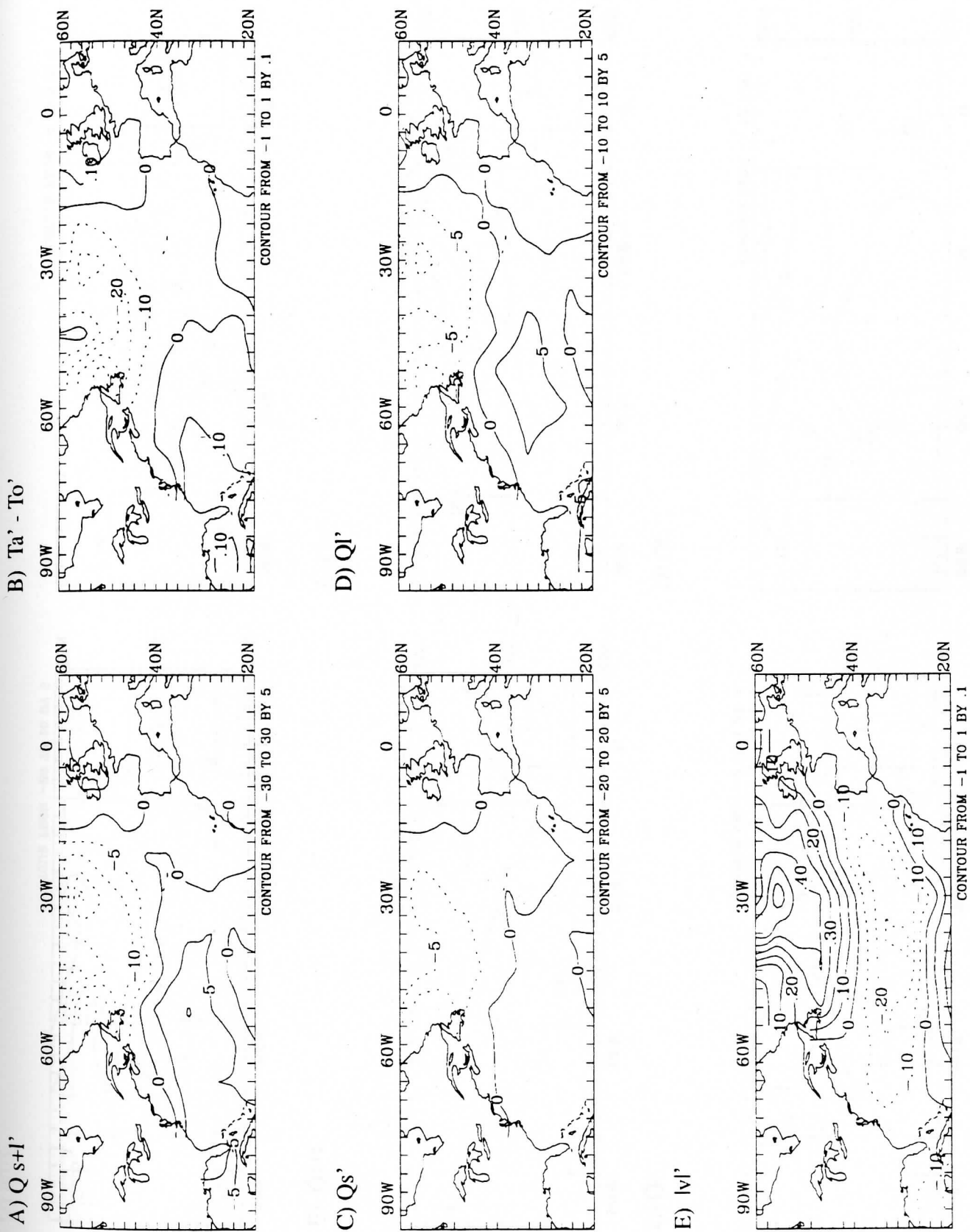
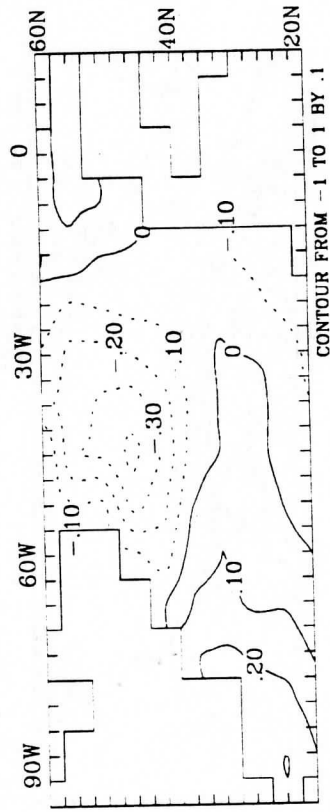
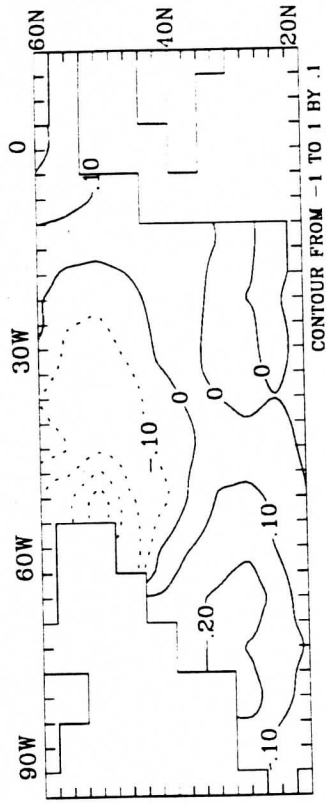


Figure 8.

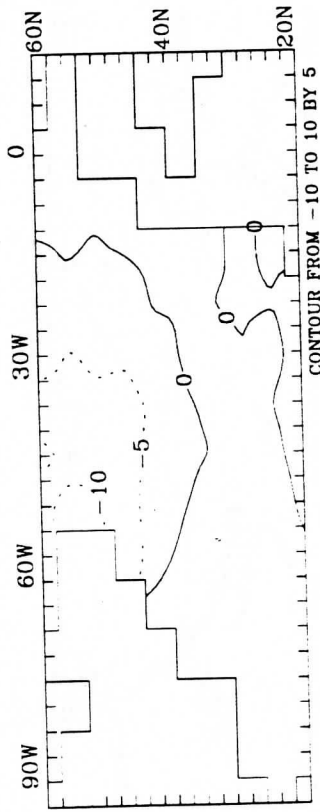
A) Tom'



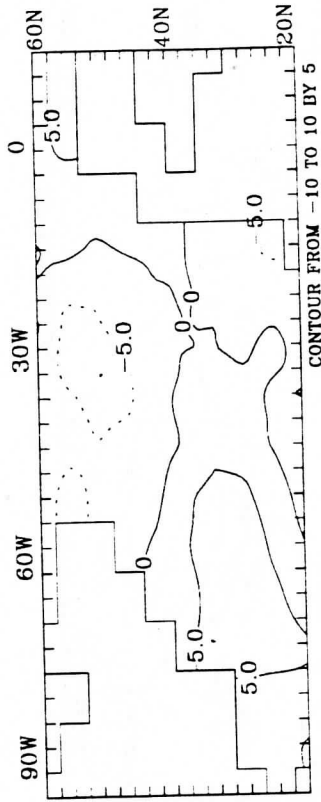
B) Ta' - Tom'



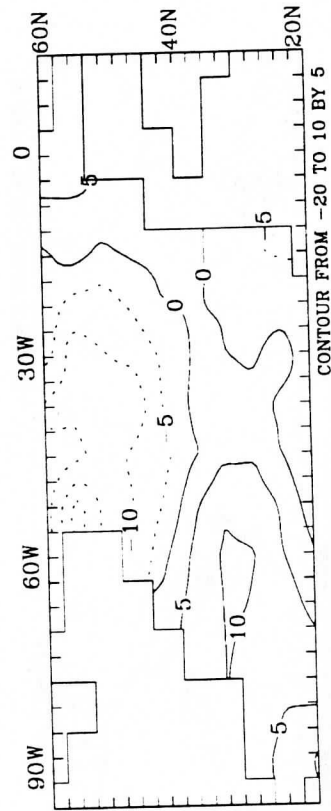
C) Qs'



D) Ql'



E) Qs+I'



F) Qwe'

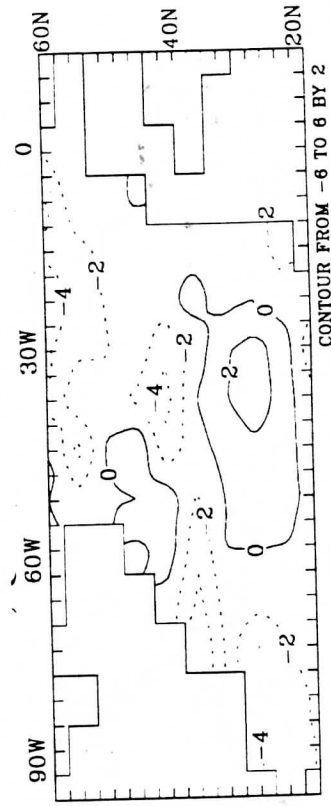


Figure 8 (cont).

G) hmx'

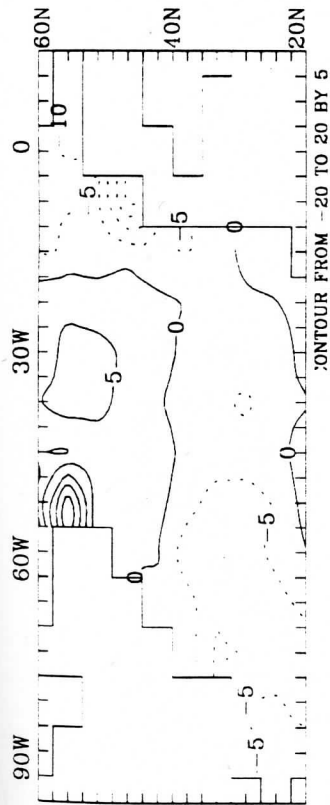
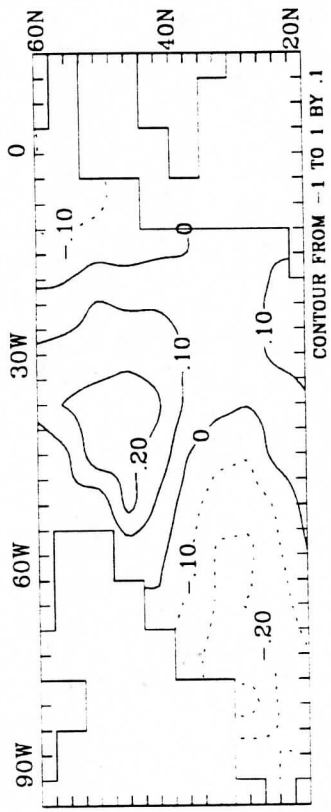
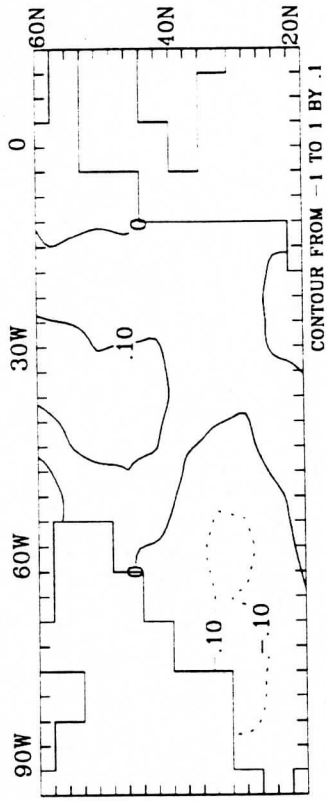


Figure 9.

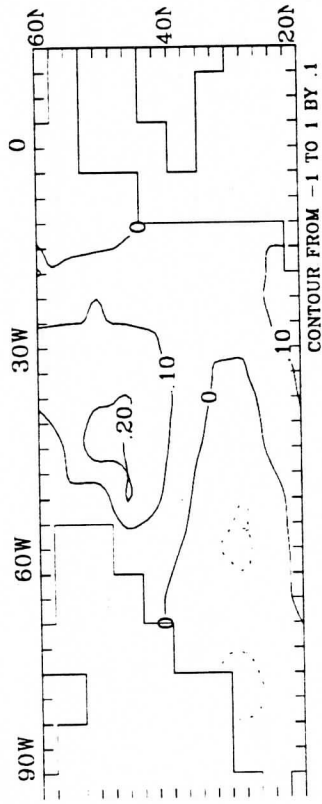
A) Tom'



B) NT



C) NQ



D) NW

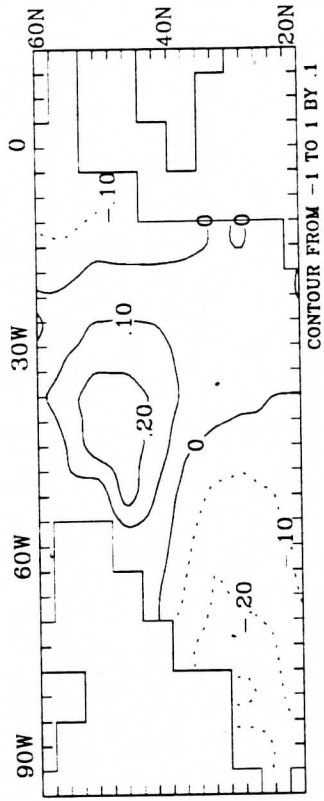
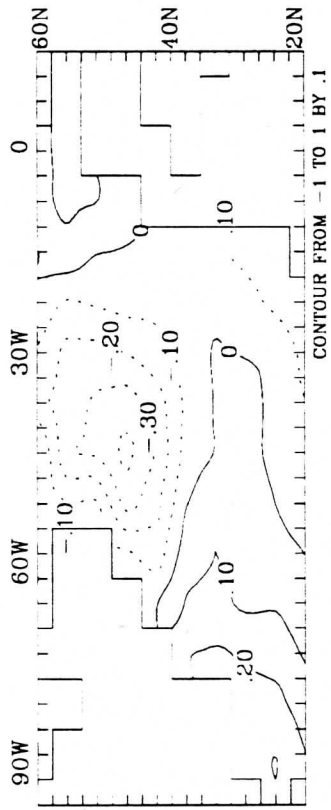
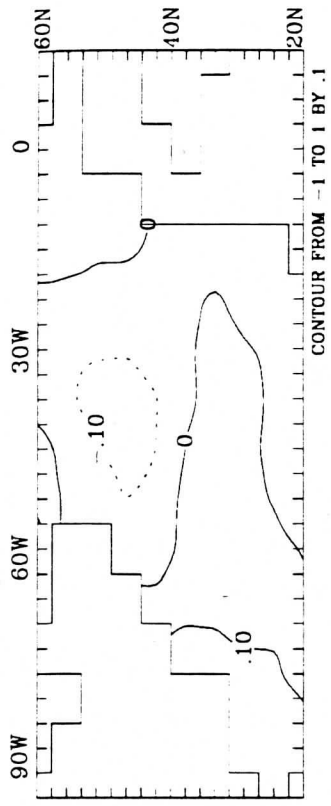


Figure 10.

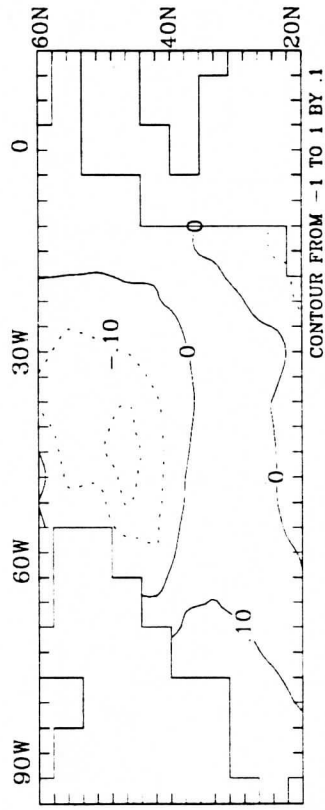
A) Tom'



B) NT



C) NQ



D) NW

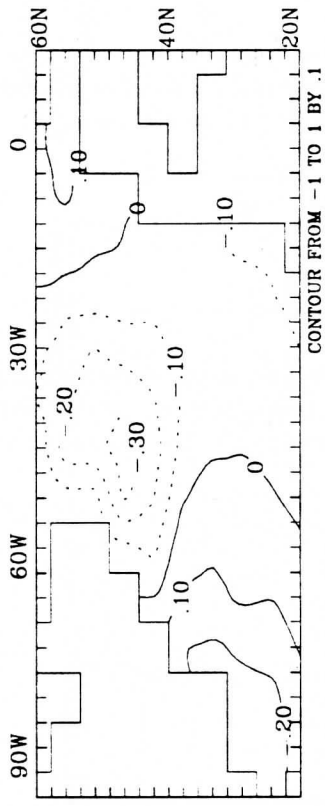
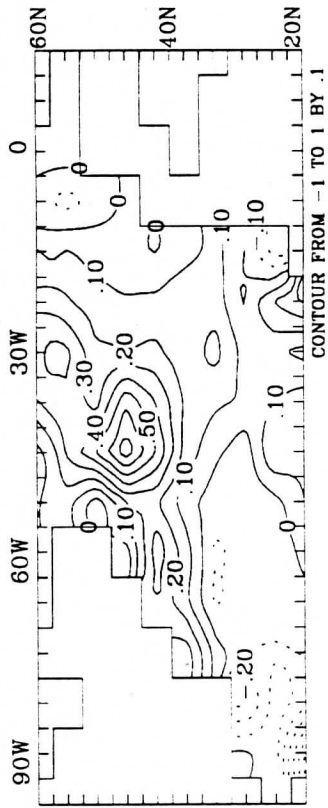


Figure 11.

A) Tom'



B) hmx'

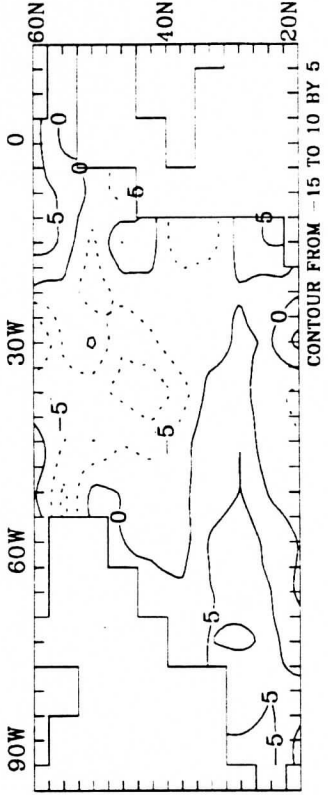
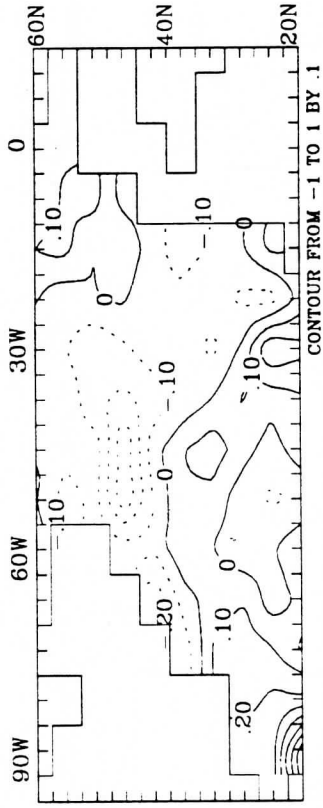
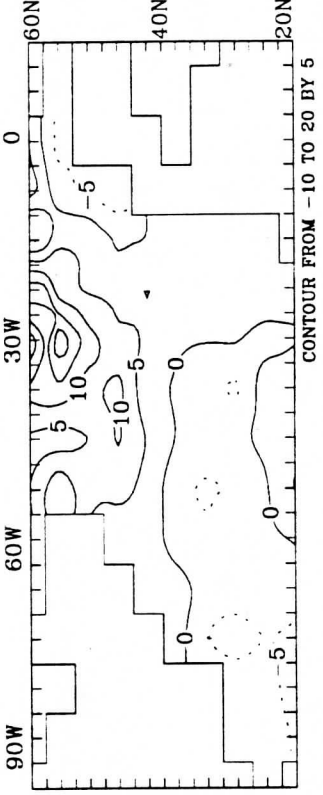


Figure 12

A) Tom'



B) hmx'



Simulated Ocean-Atmosphere Interaction in the North Pacific
from a GCM Coupled to a Constant Depth Mixed Layer

by

Robert G. Gallimore

Dept. of Atmospheric and Oceanic Sciences and the
IES-Center for Climatic Research
University of Wisconsin-Madison

Feb, 1994

Abstract

100-year seasonal climate simulations of both a coupled (interactive) and uncoupled (prescribed SSTs) ocean-atmosphere model are used to examine the life cycle and structure of the dominant wintertime SST anomalies and associated atmospheric response in the extratropical north Pacific. The study focuses on SST anomalies produced solely by ocean-atmosphere energy exchange.

The dominant (1st EOF) structure of anomalous SST, sensible plus latent heat flux and low tropospheric temperature is nearly identical; the pattern has a large negative component in the central Pacific (near 35N, 180W) flanked by positive centers in the western and eastern Pacific. The wintertime composite SST anomaly associated with the first EOF reaches about 1.0°C in the central Pacific for the warm (WCP) case and -1.5°C in the cold (CCP) case.

The growth and decay of the first EOF SST pattern is linked to the behavior of the model's dominant atmospheric teleconnection pattern. During the growth phase of the WCP (CCP) SST anomalies, anomalous highs (lows) occur over the western Pacific and over western North America and an anomalous low (high) is over the east-central Pacific. To rear of the anomalous low (high), a negative (positive) SST anomaly develops in response to anomalous cold (warm) air and positive (negative) heat flux loss from the ocean. The composited SST anomalies primarily develop in 1-2 months.

During the decay stage of the WCP SST anomaly, the atmospheric anomalies are essentially of opposite sign than during the growth stage and act to rapidly destroy the SST anomaly. In contrast, the atmospheric anomalies during the decay stage of the CCP SST anomaly are of the same sign but weaker than during the growth stage. For this case, the atmospheric anomaly structure helps maintain, through the process of ocean-atmosphere energy exchange, a more persistent SST anomaly than in the WCP composite case.

A set of prescribed SST anomaly experiments are used to show that the atmospheric anomalies present during the decay stage of the CCP SST anomalies are in part a consequence of ocean forcing of the atmosphere. The magnitude and position of the lower tropospheric anomalies forced by SST anomalies are similar to those obtained in idealized or linearized GCMs while the vertical structure (slightly baroclinic) is more akin to that found in full GCMs. There are some differences between the composite and prescribed SST anomaly results (e.g. in position of the atmospheric anomalies relative to the SST anomaly) which suggest that the anomalous response of the atmosphere to SST anomalies in a coupled ocean-atmosphere environment may not be the same as in a one-way forced system.

1. Introduction

The body of evidence from observation and modelling studies regarding the linkage between extratropical SST and atmospheric circulation anomalies is mixed. Recent observational studies using correlation analysis supports the contention that extratropical SST anomalies are forced by the atmosphere (Wallace and Jiang, 1987; Wallace et al, 1990). The observed correlations with atmospheric circulation anomalies leading the ocean temperature anomalies are greater than those for the ocean temperature anomalies leading the atmospheric circulation anomalies. Wallace and Jiang (1987) and Wallace et al (1990) further examined the question of atmospheric forcing of the ocean by correlating the dominant patterns of SST tendency against atmospheric 500 mb height anomalies. By this approach they were able to identify some atmospheric circulation patterns which may be important in forcing extratropical SST anomalies. These atmospheric circulation patterns were different, however, from the atmospheric patterns found in the simultaneous correlation with SST itself. Cayan (1992a) determined the dominant structures of anomalous latent and sensible heat fluxes over the ocean and their relationship with atmospheric circulation. Further analysis by Cayan (1992b) strongly suggested that these anomalous structures in the heat fluxes are important in driving SST anomalies in the extratropics.

While the observational results are more supportive of the atmosphere forcing the ocean than for the ocean forcing the atmosphere in extratropical latitudes, cause/effect relationships between oceanic and atmospheric variability cannot be unambiguously determined with present observations alone (Wallace and Jiang, 1987). A number of modelling studies also support the notion that the atmosphere can force significant SST variability in the extratropics. These results have come from simple one-way atmospheric forcing of the ocean experiments (e.g. Frankignoul and Hasselman, 1977; Haney, 1980; Alexander, 1990), from partially coupled ocean-atmosphere models (e.g. Luksch and von Storch, 1992) and more fully coupled models (e.g. Miller, 1992; Alexander, 1992a). In all of these experiments anomalous fluxes

of sensible and latent heat exchange between the ocean and atmosphere are important processes producing SST variability. The anomalous heat fluxes are associated with anomalous circulation features such as lower troposphere temperature, moisture and winds. The results of Miller (1992) and Alexander (1992a) suggest that the mechanisms of ocean advection and entrainment are also important in producing SST variability.

Evidence for an atmospheric response to extratropical ocean temperature anomalies can mostly be found in experiments whereby an atmospheric model is forced (one-way) by prescribed SST anomalies or diabatic anomalies that implicitly represent the effects of anomalous SST. The experiments use linear atmospheric models (e.g. Hoskins and Karoly, 1981; Ting, 1991), idealized GCMs using zonally symmetric conditions (e.g. Ting, 1991) and full GCMs using realistic geography (e.g. Palmer and Sun, 1985; Kushnir and Lau, 1992; Lau and Nath, 1990; Pitcher et al., 1988). In the linear model and idealized GCM experiments, an anomalous high (low) forms slightly downstream of a negative (positive) SST anomaly. The vertical structure is baroclinic.

In full GCM experiments using realistic land-ocean configuration and orography, the response is quite different with an anomalous equivalent barotropic low tending to form near a negative SST anomaly. The comparative picture for the atmospheric response to a positive SST anomaly in the full GCM experiments is less clear. Palmer and Sun (1985) found the response basically opposite that for the negative SST anomaly; namely, a positive height anomaly tends to occur over and downstream of the positive SST anomaly. In contrast, Kushnir and Lau (1992) and Pitcher et al. (1988) found the response to the positive SST anomaly more closely resembled that produced by the negative SST anomaly. The causes for these differences in the full GCM experiments appear to be in part attributable to the impact of SST anomalies on transient eddy processes (Kushnir and Lau, 1992).

A major problem with the strategy of prescribing SSTs in GCMs is that two way feedback interactions between the ocean and the atmosphere are not allowed (such as naturally occurs in the real world). As noted by Kushnir and Lau (1992) the simulated atmospheric anomalies may not be consistent with the imposed SST anomaly. A few recent studies have attempted to examine evidence for an extratropical atmospheric response to the ocean in coupled model experiments (for a discussion of some of the important processes effecting two-way atmosphere-ocean interaction see Frankignoul (1985)). Alexander (1992b) used a version of the NCAR Community Climate Model (CCMOB) coupled to a prognostic mixed layer ocean model to examine the extratropical atmosphere-ocean response during an El Niño cycle. Miller (1992) recently simulated large scale ocean-atmosphere interactions in the north Pacific with a two level quasi-geostrophic model coupled to a mixed layer ocean allowing advection. Both of these studies found evidence for an atmospheric response to the SST anomalies produced interactively within their models.

In this study, a coupled ocean-atmosphere model is used to examine cause/effect relationship between simulated SST and atmospheric circulation variability in the extratropical north Pacific during winter. The simulated SST anomalies are generated solely by variability in the ocean-atmosphere energy exchange. Other processes which are also important in the development of variability of extratropical SST (e.g. ocean current advection and entrainment) are excluded for this investigation.

The coupled model consists of a version of the low resolution atmospheric GCM (A model) described by Otto-Bliesner et al (1982) and Gallimore et al (1986), and the constant depth (50m) mixed layer ocean (CO) formulation, described by Gallimore and Houghton (1987, 1990). The coupled model differs from earlier versions in that a heat flux correction or adjustment (ADJ) is used to keep the simulated SST climatology close to the observed annual cycle values used in the A model. By having

similar mean state SST climates, the A and coupled (ADJACO) model experiments can be compared to assess the influence of the interactive ocean on simulated variability.

The variability results are obtained from 100-year seasonal simulations of the atmospheric (A) model with prescribed SST and the coupled (ADJACO) model. The dominant modes of SST and atmospheric variability are determined by empirical orthogonal function (EOF) analysis of the simulated monthly averaged output from the A and ADJACO model results. Based on the EOF analyses of the ADJACO model results, wintertime composites of the evolution of important model SST anomalies and associated atmospheric variables are produced. A set of atmospheric (A) model experiments using prescribed SST anomalies from the composite analysis are performed to help in the assessment of possible evidence for ocean forcing of the atmosphere in the coupled (ADJACO) model experiment.

A brief description of the models, experiments and basic relationships are provided in Sections 2-4. The spatial structure of the simulated mean state and variability in the models is briefly examined in Section 5. Following a discussion of the EOF analysis for SST and the latent plus sensible heat fluxes in Section 6, the analysis of composites and prescribed SST anomaly experiments are given in Section 7. Section 8 is devoted to summarizing the results.

2. Models

a. A model

The atmospheric model is a global, spectral, primitive equation model with triangular truncation at wave number 10. The vertical structure is represented by 5 equally spaced sigma levels. Parameterized physical processes are added to the model on its 11.6° by 11.25° latitude-longitude transform grid. A smoothed orography is incorporated spectrally into the model. The maximum heights of the Himalayan, Andes and Rocky mountains are 2900, 1100 and 900 m, respectively. Physical processes in the model include radiation, convection, large-scale

condensation and the surface fluxes of momentum, latent energy and sensible heat. A surface heat budget equation determines the temperature over land, snow, glacial ice, and sea ice. The annual cycle of sea surface temperature and the distribution of sea ice are specified from climatological data; these do not change from one year to the next in the A model simulation (see below). The latitude of equatorward limit of snow cover is specified by a sinusoidal variation. Over snow-free land, an annual average surface albedo is specified according to surface type, and the ground wetness (which is used to calculate the land evaporation) is a function of the land albedo. Cloudiness, long-wave emissivity and solar absorptivity are specified latitudinally and seasonally for the radiative calculations. A more detailed description of the A model can be found in Otto-Bliesner et al. (1982) and Gallimore et al. (1986).

b. ADJACO model

The atmospheric component of the ADJACO model is the same as for the A model. Over ocean areas, the ADJACO model computes sea surface temperatures using a constant depth 50m mixed layer ocean formulation patterned after that of Washington and Meehl (1984). The sea surface temperature tendency (and ocean heat storage) is determined solely from the net value of the sensible, latent and radiative heat fluxes at the ocean surface. The albedo of the ocean surface is calculated by a formula given in Robock (1980).

Sea ice is predicted when the sea surface temperature falls below 271.2 K. The thickness of sea ice is calculated using the 'zero order' model of Semtner (1976). The albedo for sea ice is the same as that used in the A model. Additional details of the sea ice and mixed layer ocean formulation are given in Gallimore and Houghton (1987) and Kutzbach and Gallimore (1988).

In contrast to earlier versions of the coupled model, the ADJACO model utilizes a surface heat flux correction in the SST predictive equation and a mass

adjustment; the mass adjustment removes a systematic positive tendency in global surface pressure which occurred in an earlier 100-year coupled model experiment (about 10mb/100 year - see Houghton et al., 1991). The heat flux correction is designed to produce near climatological SSTs in the monthly long term averages. The original coupled model (without correction) had systematic errors of up to 4-6°C in the western Pacific (Gallimore and Houghton, 1987).

The model employs coarser resolution and simpler physics than some of the current state of the art models (Washington and Parkinson, 1986). A number of important processes that contribute to climate variability are not represented in the ADJACO model. In the atmosphere, clouds are prescribed and although water vapor is a prognostic variable its effects on the model radiative calculations are prescribed (Otto-Bliesner et al, 1982). In addition the model version used here prescribes soil moisture and snow cover. The ocean component excludes the effects of salinity, diffusion and motion (e.g. ocean currents and upwelling) and does not allow energy exchange with ocean layers below the mixed layer. The lack of having ocean dynamics, however, may be more critical to realistic development of SST variability in the tropics than for the extratropics. A number of observational and modelling studies have shown that the net energy exchange across the ocean-atmosphere interface is an important factor in determining the variation of extratropical SSTs (Gill and Niiler, 1973; Frankignoul, 1985; Cayan, 1992b; Alexander, 1990, 1992a,b; Luksch and von Storch, 1992).

A major advantage in using a simpler atmosphere-ocean model is the capability of performing a set of comparative long multi-year simulations rather inexpensively. Long multi-year seasonal simulations (on the order of 100 years) are performed in order to capture a statistically meaningful record of model variability. The variability results from this relatively simple model should prove useful in helping to interpret results from more sophisticated higher resolution models.

3. Experiments and analysis domain

The variability results are obtained from two 100-year experiments - one performed with the ADJACO model and the other with the A model (model with prescribed climatological SSTs). The ADJACO model was integrated for 115 years at full (non-accelerated) seasonal coupling of the ocean and atmosphere with the last 100 years used for analysis of variability. In contrast to the earlier coupled model used by Houghton et al (1991), there were no noticeable trends in temperature over the 100 year experimental period. The details of the 100-year A model integration are given in Houghton et. al. (1991).

Grid point estimates of the interannual variability of SST and atmospheric variables are determined from the departures of the individual year monthly means from the 100-year monthly mean. The domain of interest is the Pacific Ocean basin from 11.6 S to 46.4 N (circled points in Fig. 1) with emphasis placed on assessing the SST variability for the northern extratropical part of the Pacific domain (north half of the Pacific area denoted by dark circles in Fig. 1). In analyzing the atmospheric circulation features associated with the SST variability over the north Pacific region, an extended domain of coverage is chosen (see Sections 6-7); this area extends from eastern Asia (123.75E) to western Europe (0°) and from 11.6N to 69.6N. In total, there are 73 grid points in the full Pacific area, 31 grid points in the northern Pacific area and 132 grid values in the extended area domain. With 1200 months, the departures for each variable in the three domains (full Pacific area, northern Pacific area and extended area) are represented by ordered matrices of 1200×73 , 1200×31 and 1200×132 values, respectively.

4. Basic relationships governing anomalous SST prediction

The basic equation determining the time rate of change of anomalous SST in the ADJACO model is given by

$$C_o \frac{\partial T_o'}{\partial t} = F_*' \quad (1)$$

where T_o is the SST, C_o is the heat capacity of the ocean mixed layer, F_* is the net surface energy flux and the symbol ($'$) denotes an individual year monthly mean deviation from the long term (100 yr) monthly mean which is denoted by a (-). The sensible and latent heat fluxes ($Q + LE$) are the principal terms in the surface energy exchange between the ocean and atmosphere that produce model SST variability, i.e.,

$$F_*' \approx -(Q + LE)' \quad (2)$$

The solar absorption into the upper ocean of the model does not vary from one year to the next since the processes affecting solar radiation (e.g. clouds, water vapor, ocean albedo, etc.) are prescribed from climatology. The parameterized net surface long-wave emission is determined solely by the variability of the surface temperature; the effects of clouds and water vapor are prescribed and hence do not contribute to variation in the downward longwave flux. As a result the variability of the net longwave flux, which acts only as a negative feedback on SST variability, is a second order process compared to the sensible and latent heat flux terms.

In the model, the latent and sensible heat fluxes are represented by bulk aerodynamic formulas. A linearization of these terms (for details see Houghton et al., (1991)) yields

$$(Q + LE)' = \bar{D}(T_o' - T_{900}') + D'(\bar{T}_o - \bar{T}_{900}) \quad (3)$$

where

$$D = \rho_* C_D C_p |\vec{V}_{900}| (1 + B^{-1}) \quad (4)$$

and C_p is the specific heat of air at constant pressure; ρ_* is the surface air density; C_D is the drag coefficient; $|\vec{V}_{900}|$ is the magnitude of the wind at 900 mb; T_{900} is the 900 mb air temperature and B is the Bowen Ratio.

According to (1)-(2), anomalous cooling (warming) of the ocean is produced by an anomalous positive (negative) sensible plus latent heat flux i.e. enhanced (reduced) energy loss from the ocean to the atmosphere. The linear approximation given by (3) emphasizes three processes that contribute to the evolution of an SST anomaly through ocean-atmosphere energy exchange;

- i) the $\bar{D}T_o'$ term requires a pre-existing SST anomaly. A positive (negative) anomalous SST promotes enhanced (reduced) heat flux loss from the ocean. Thus this term is a negative feedback process which acts to destroy the SST anomaly.
- ii) the $\bar{D}T_{900}'$ term represents anomalous temperature (and moisture) in the low troposphere. Anomalous cold (warm) air acts to enhance (lessen) the heat flux loss from the ocean thereby promoting development of a negative (positive) SST anomaly.
- iii) the $D'(\bar{T}_o - \bar{T}_{900})$ term represents the anomalous effects of the air-sea transfer coefficient which is primarily produced by anomalous wind speeds; an anomalously strong (weak) low tropospheric wind speed acts to enhance (lessen) the heat flux loss from the ocean thus leading to development of a negative (positive) SST anomaly.

5. Simulated Climate for Pacific region

Before proceeding to examine the structure of the dominant modes of SST and associated atmospheric variability, a brief assessment is made as to how well the models simulate the mean and standard deviation of SST and the latent and sensible heat fluxes for the Pacific region.

a. Mean state

The prescribed SST field used for the A model is based on climatological observations. The use of the flux correction scheme in the ADJACO model simulation produced an SST climatology generally within 1°C of the A model (Fig. 2). Because the differences in basic SST climatology between the A and ADJACO models are small, the role of the interactive ocean on variability can be isolated by comparison of the experiments.

Both models simulate reasonably realistic surface heat fluxes. For example, the models simulate nearly identical maxima in the evaporative rates (about 9mm/day) for the western Pacific during January (Fig. 3). These rates are very comparable to observed evaporative rates. A more detailed description of the basic A (and thus also ADJACO) model climatology is given in Gallimore et al, (1986).

b. Standard deviation

The basic variability of model SST for the Pacific region is assessed by analyzing the structure of the standard deviation of the monthly mean departures of SST from the 100-year monthly means (Fig. 4). The standard deviation of SST is greatest in middle latitudes (around 0.5 to 0.8°C) and least along the equator (around 0.3 - 0.4°C). Averaged over the middle latitude Pacific domain, the standard deviation of SST is greatest in spring (Apr) and least in fall (Sep) (Fig. 5-top).

The variability of model SST is similar in magnitude and structure to that generated in other integrations of mixed layer ocean-atmosphere GCMs (Hansen et al, 1988; Manabe, 1983; Meehl and Washington, 1985). As noted in Houghton et. al. (1991), the model underestimates SST variability over most areas of the ocean - particularly in the tropics and off the coasts of the northern continents (Fig. 4); this result is probably, in part, a consequence of the lack of ocean dynamics in the model.

The spatial distribution of the standard deviation of the individual January departures of the latent and sensible heat fluxes from the 100 year average for the A and ADJACO simulations are shown for the Pacific area in Figure 6.

Two features are noted:

i) The largest values of the standard deviation of the fluxes tend to occur where the mean fluxes are greatest; consistent with observations, maximum means and standard deviations of the sensible and latent heat fluxes occur in the western Pacific (Figs. 3,6).

ii) The models underestimate the interannual variability of the fluxes; this is particularly evident for the latent heat flux. In both models the maximum standard deviation of the latent and sensible heat fluxes is around 35 and 25 W/m², respectively. While the location of these maxima are close to the observed centers (Fig. 6), the magnitudes are only about 60% and 80% of the respective observed maxima.

The standard deviation of both the latent plus sensible heat flux and 900 mb temperature for the middle latitude north Pacific area is greatest in winter and least in summer (Fig. 5, middle and bottom); the seasonal behavior of the heat flux variability is consistent with observed results (Cayan, 1990). The extremes of variability for SST occurs about 60 days after the extremes of the latent plus sensible heat flux variability (Fig. 5); this phase lag is nearly identical to the

phase lag between the simulated heat storage and SST extrema (not shown - see Gallimore and Houghton, 1990).

There are modest differences in the variability of the latent plus sensible heat flux and 900 mb temperature between the ADJACO and A models (Fig. 5) which suggest an influence of the interactive ocean on model climate. Generally, the variability (standard deviation) of the latent plus sensible heat fluxes for the A model (noninteractive ocean case) is greater than for the ADJACO model (interactive ocean case) (Fig. 5, middle). In contrast, the variability results for 900 mb temperature are greater for the ADJACO model. The reasons for this difference in variability response between the models can be deduced by examining the effects of ocean-atmospheric energy exchange. Consider a positive heat flux anomaly ($(Q+LE)' > 0$) and an associated negative 900mb temperature anomaly ($T'_{900} < 0$); together these act via Eqs. (1-3) to force development of a negative SST anomaly ($T'_o < 0$) in the interactive ocean case. The negative SST anomaly in turn acts to reduce the magnitude of the positive heat flux anomaly from that which occurs in the absence of the interactive ocean ($T'_o = 0$), i.e. the magnitude of the heat flux anomaly (variability) is reduced for the interactive ocean case. A positive heat flux anomaly works to damp (negative feedback) the negative 900 mb temperature anomaly through anomalous heating of the lower troposphere. The reduction in positive heat flux anomaly for the non-interactive case lessens this heating effect for the low troposphere. Thus the negative atmospheric temperature anomaly in the interactive model is enhanced relative to the non-interactive model; this response is consistent with the greater variability for T'_{900} in the ADJACO versus A model (Fig. 5, bottom).

6. EOF analysis of SST, atmospheric temperature and latent plus sensible heat fluxes

Empirical orthogonal function (EOF) analysis is used to characterize the dominant spatial modes of variability of SST, the latent plus sensible heat fluxes and low tropospheric temperature (900 mb temperature) for the extratropical part of the Pacific domain (region from 23.2N to 46.4N, Fig. 1). These processes of ocean-atmosphere energy exchange are linked via eqs. (1-3). The analyses are performed on the individual year monthly mean departures (from the 100 year monthly means). The SST and the latent plus sensible heat flux departures are the same as were used to calculate the standard deviations shown in Figures 3 and 6. To assess the space consistency of results, EOF analyses of simulated departures are also made for the entire Pacific domain (11.6S to 46.4N).

The spatial pattern of the first EOF of SST has a large negative component in the central Pacific (minimum near 35N, 180W) flanked primarily by positive centers in the western and eastern Pacific (Fig. 7, top left). The second EOF is dominated by a central-eastern Pacific dipole structure (Fig. 7, top right). The extratropical patterns in these EOFs are also evident in the EOFs for the entire Pacific domain (11.6S-46.4N; Fig. 7, bottom panels). The first EOF pattern explains 19% (12%) of the extratropical (entire Pacific) domain variance compared to 10% (7%) variance explained for the second EOF. According to the criterion provided in North et al (1982), the first few EOFs derived from the 1200 months of SST departures are reasonable estimates of the true EOFs. This is further confirmed by the general consistency of results using the larger spatial domain.

Examples of actual SST anomalies (monthly mean SST for individual year minus 100 year monthly mean) that correspond to the pattern in the first EOF are shown in Fig. 8; for these years the magnitude of the time coefficient of the first EOF is greater than 3.5 (which represents a value of several standard deviations from the

mean value of zero for the time coefficient). The magnitude of the largest SST anomalies associated with this first EOF reach 2°C in the central Pacific.

The spatial structure of the first EOF of the ADJACO and A model sensible plus latent heat flux (Fig. 9, left panels) and 900 mb temperature (not shown) strongly resemble the pattern of the first SST EOF (Fig. 7). Quantitatively, the correspondence of the patterns is measured by spatially correlating the first EOF of one variable (say SST) against the first EOF of another variable (say latent plus sensible heat flux) both for the same experiment and between experiments (e.g. ADJACO SST vs A latent plus sensible heat flux). The resulting correlation coefficients (Table 1) are generally large (0.73 to 0.99). As with SST, the first EOF pattern for the A and ADJACO model latent plus sensible heat flux and 900 mb temperature are relatively robust—explaining 17–18% of the variance as compared to about 10–12% variance explained for the second EOF.

The patterns of the lower ordered EOFs (2–4) are also generally similar to one another. However because the spacings between the eigenvalues for the lower ordered EOFs are much less than the spacing between the first and second EOF, the order of the EOFs below the first changes depending on what variable is being considered (e.g. the second EOF of SST, and latent plus sensible heat flux (both models) and the third EOF of 900 mb temperature (both models) are quite similar).

The simulated SST and heat flux patterns in Figures 7 and 9 resemble observed features. The first EOF of model SST and latent plus sensible heat flux is structurally similar to the 5th SST and surface heat flux (mainly latent plus sensible) EOFs given in Frankignoul and Reynolds (1983) and the 3rd latent plus sensible heat flux EOF given in Cayan (1990). The model second EOF pattern shows some resemblance to the first EOF of SST and second heat flux EOF given in Frankignoul and Reynolds (1983) and the first latent plus sensible heat flux

given in Cayan (1990). A key feature of the observed results is the correspondence of the observed heat flux and SST EOFs. These results along with the more recent work of Cayan (1992b) indicates that ocean-atmosphere energy exchange is an important process in the occurrence of extratropical SST variability and makes this simple modelling study relevant to the investigation of extratropical ocean-atmosphere interaction.

The resemblance of the second EOF of model SST to the first EOF of observed SST in the extratropical North Pacific is of interest in that both show a dominant central-eastern Pacific dipole structure. In observations, this type of structure has been linked to the tropical SST anomalies in the eastern Pacific associated with El Niño events (e.g. Weare et al., 1976; Kawamura, 1984). Recent modelling studies (e.g. Alexander, 1990; 1992a,b) suggest that this tropical SST variability forces (at least part) of extratropical north Pacific dipole SST anomaly pattern through atmospheric tropical-middle latitude interaction. In the ADJACO model simulation, the SST anomalies in the central and eastern Pacific are not associated with any significant tropical SST variability (Fig. 7) but are (as will be discussed below) solely a consequence of the dominant modes of simulated atmospheric variability in the extratropics; the model lacks the necessary ocean dynamics to produce realistic tropical SST variability.

7. Composite Analysis

The linkage between the dominant structure of model SST anomalies and atmospheric circulation features is examined using composite analysis. Mathematically, the spatial vector of M values of the SST departures (from the 100-year mean) at time $j\Delta t$ ($0 \leq j \leq N=1200$) is expressed as a linear sum of M

orthogonal eigenvectors

$$\tilde{T}'_j = \sum_{i=1}^M C_{ij} \tilde{e}_i \quad (5)$$

where \tilde{e}_i is the i th-spatial eigenvector, C_{ij} is the corresponding time coefficient at time $j\Delta t$ and the symbol (\sim) denotes a spatial vector of M values, i.e.

$$\tilde{T}' = \begin{pmatrix} T'_1 \\ \vdots \\ T'_M \end{pmatrix}, \quad \tilde{e}_i = \begin{pmatrix} e_{1i} \\ \vdots \\ e_{Mi} \end{pmatrix} \quad (6)$$

The time coefficients C_{ij} essentially convey the amount of loading or contribution to the overall field at a particular time by the i th eigenvector. For reference the distributions of \tilde{e}_1 and \tilde{e}_2 are given in Figure 7.

The composite cases are found by selecting the late fall to middle winter months (j values for November, December, January) out of the $N = 1200$ months when the structure of SST departures has its strongest expression in the first EOF pattern, i.e. when the magnitude of the time coefficient of the first EOF (C_{1j}) achieves a maximum that exceeds a chosen critical limit. In this study, a critical value of 3 is selected which corresponds to slightly more than two standard deviations from the mean value of 0 for the time coefficient. One bin of months is for maximum coefficients exceeding +3.0 and a second bin is for months with minimum coefficients less than -3.0. Composites are formed by averaging the actual SST anomalies for the months in each bin.

A total of 8 cases of SST anomalies comprise the first composite (cases where the maximum coefficient exceeds 3.0) and 4 cases of SST anomalies comprise the second composite (cases where the minimum time coefficient is less than -3.0). Examples of specific cases of SST anomalies that went into making up the composites are shown in Fig. 8.

The temporal evolution of the SST anomalies is assessed by forming composite averages for the 4 months preceding and 4 months following the month when the time coefficient is at its extreme value. The evolution of the composite SST anomaly is thus followed for a period of 9 months from fall through spring with the midpoint of the 9 month sequence representing the month (month 5) when the SST anomaly associated with the first EOF is at a maximum.

The time evolution of the composite SST anomalies over the middle 5 months of the 9 month sequence (months 3-7) is shown Fig. 10. The major features of the SST composites are:

- 1) The structure of north Pacific SST anomalies are nearly identical to the 1st EOF pattern (Fig. 7). This is not unexpected since the composites are based on the extrema of the time coefficient of the 1st SST EOF and the contributions to the SST field by the other EOF components are small (not shown).
- 2) The first composite (positive time coefficient) is dominated by a negative SST anomaly in the central Pacific (CCP case) of less than -1.5°C (Month 5, right panel Fig. 10); the second composite (negative time coefficient) has a positive central Pacific SST anomaly (WCP case) around 1°C (left panel Fig. 10). The largest SST anomalies for individual cases that went into forming the composites exceed 2°C in magnitude (Fig. 8). The central Pacific anomaly is flanked by weaker opposite signed anomalies in the eastern and western Pacific.
- 3) The SST anomalies for the CCP case develop more rapidly (over months 3-4) than they decay (over months 6-7). In the WCP case the anomalies decay at about the same rate as they grow with the result that they are less persistent than for the CCP case. In general the SST anomalies show little tendency to shift position over their life history.

a. Atmospheric structure during growth and decay stages

The relationship between the composite SST anomalies (Fig. 10) and model atmospheric circulation structures are examined over the same sequence of 9 months used in forming the SST composites. The structure of these variables (composited anomalies for the sensible plus latent heat flux (Q+LE), atmospheric temperature at 900 and 700 mb (T_{900} and T_{700}), sea level pressure (PMSL) and 500 mb heights (Z_{500})) are determined for the growth stage (average of months 2-4) and decay stage (average of months 6-8) of SST anomaly development.

1) GROWTH STAGE

The structure of the model sensible plus latent heat flux and atmospheric temperature anomalies are consistent with the growth of the SST anomalies in the composites. The location of the anomalous centers for SST, T_{900} , T_{700} and Q+LE all generally coincide and closely resemble their 1st EOF patterns (Fig. 11, top 4 panels, vs. Figs. 7 and 9). Generally where a positive (negative) SST is developing (e.g. in the central Pacific), a negative (positive) anomaly in Q+LE and associated positive (negative) T_{900} anomaly is present; the sensible plus latent flux anomalies are mainly produced by the atmospheric temperature anomalies during the SST growth phase.

The associated model sea level pressure anomalies are located between the SST, T_{900} and Q+LE anomalies; the PMSL anomaly structure for the WCP (CCP) case consists of anomalous lows (highs) over the western Pacific and western North America and an anomalous ridge (trough) in the east central Pacific. The relationship between the PMSL, Q+LE and T_{900} structures strongly suggests that anomalous warm and cold air advection is important to the development of SST anomalies in the model. For example, the northwesterly flow of air to the rear of the anomalous trough in the east-central Pacific (Fig. 11; 5th right panel)

in the CCP case is linked with temperatures at 900 mb (Fig. 11; 3rd right panel) that are 1-2°C lower near 180 W than the 100-year mean. This anomalous cold air enhances the heat loss by sensible plus latent heat by 20-30 W/m² (Fig. 11; 2nd right panel) and leads to formation of the negative SST anomaly near 180 W (Fig. 11; top right).

The corresponding 500 mb height anomalies are located a little west (about 1 model grid point) of the position of the sea level pressure anomalies (Fig. 11; 5th and 6th panels); this tilt relationship between the surface and 500 mb level is consistent with the structure of the atmospheric temperature anomalies (Fig. 11, 3rd and 4th panels). The structure of the height anomalies in Fig. 11 (bottom) is nearly the same as the pattern of the first EOF of the model 500mb heights, i.e. the dominate pattern of 500 mb height variability in both the A and ADJACO models (Fig. 12); about 12% of the variance of 500 mb heights for the Pacific-North American region is explained by this first EOF.

The finding that the dominate structure of atmospheric variability is linked with the development of the dominant SST variability in the model is consistent with observational results. For example, Wallace et. al. (1990) have shown a correspondence between an important 500 mb height anomaly pattern over the Pacific-North American region (the so-called PNA pattern identified by Wallace and Gutzler (1981)) and the dominant pattern of extratropical SST anomalies in the North Pacific (which consists of a central-eastern Pacific dipole structure). It is interesting to note that the model teleconnection pattern bears some resemblance to the observed PNA pattern from the central Pacific to North America. However, the model pattern (Fig. 12) should not be viewed as a PNA pattern since the observed PNA pattern does not have anomaly structures in the Western Pacific like that found in the simulated results.

2) DECAY STAGE

The atmospheric anomalies for T_{900} , Z_{500} and $Q+LE$ during the decay stage (as reflected in the 3 month averages following the month when the composite SST anomalies are greatest) are structurally similar to those present during the development stage (Figs. 11 and 13). For both the WCP and CCP cases, the latent plus sensible heat flux anomalies during the decay stage are in the same location as the heat flux anomalies during the growth phase but with opposite sign; the heat flux anomalies for the decay stage have the same sign as the anomalous SST and are now acting to destroy the SST anomaly. For example, over the region of the negative SST anomaly in the central Pacific (180 W, 30-40 N) in the CCP case, the heat flux anomaly is over $20W/m^2$ during the growth stage and around $-10W/m^2$ during the decay stage. A contributing factor as to why the heat flux and SST anomalies are of same sign is the negative feedback term between SST and the heat flux (the \overline{DT}_o' term in (3)); a negative (positive) SST anomaly acts to reduce (enhance) the heat flux i.e. produce a negative (positive) heat flux anomaly.

For the WCP case, the anomalies for T_{900} and Z_{500} are also structurally similar but of nearly opposite sign to those during the SST growth stage (Fig. 13, 3rd and 4th left panels). For example negative T_{900} and Z_{500} anomalies reside near 170W - 180W during the decay stage whereas these anomalies are positive in this region during the growth stage. The negative (positive) T_{900} anomaly, acting through the \overline{DT}_{900}' term in (3), works to enhance (reduce) the heat flux loss in the central (eastern and western) Pacific. This process in combination with the negative SST feedback term (\overline{DT}_o' in (3)) promotes rapid decay of the SST anomalies in those regions.

For the CCP case, the T_{900} and Z_{500} anomalies resemble weakened versions of the anomaly structures (same sign) during the growth phase. During the growth stage, a negative T_{900} anomaly (between -1.0°C and -1.5°C) occurs in the central Pacific and positive T_{900} anomalies (around 1°C) occur in the eastern and western Pacific. During the decay stage these anomalies are still basically present in these regions but their magnitudes are much smaller (around 0.5°C or less). The negative (positive) T_{900} anomaly helps to enhance (reduce) the heat flux loss in the central (eastern and western Pacific); in this situation the atmospheric temperature anomalies help maintain the SST anomalies (negative in the central Pacific and positive in the eastern and western Pacific) against the negative SST feedback that is acting to destroy the SST anomaly. This in part explains why the SST anomalies in the CCP case decay more slowly than in the WCP case.

b. Evolution of composited time coefficients

The results of the previous sections indicate that the first EOF of SST and components of atmospheric circulation are structurally consistent over the life cycle of the SST anomaly. Through an analysis of the relationship between composited time coefficients for these first EOF components additional insight is made into the life cycle of the composited SST anomalies and associated atmospheric circulation structures. The connection between the composited time coefficients for SST, $Q+LE$ and T_{900} is determined from a simplified version of (1-3) that neglects the term involving the anomalous variation of the transfer coefficient (D'), i.e.,

$$C_o \frac{\partial T'_o}{\partial t} = -(Q+LE)' \approx -\bar{D}(T'_o - T'_{900}) \quad (7)$$

Based on (5), the composited variables T_o' , $(Q+LE)'$ and T_{900}' are assumed to be described by the continuous functions

$$T_o'(x, t) = C_{T_o}(t) e_1(x) + \delta'_{T_o}(x, t)$$

$$(Q+LE)'(x, t) = C_{QLE}(t) e_1(x) + \delta'_{QLE}(x, t) \quad (8)$$

$$T_{900}'(x, t) = C_{T_{900}}(t) e_1(x) + \delta'_{T_{900}}(x, t)$$

where the quantities C_{T_o} , C_{QLE} and $C_{T_{900}}$ are the composite first EOF time coefficients for the respective variables T_o , $Q+LE$ and T_{900} ; x is the spatial coordinate of the field variables; and the functions δ'_{T_o} , δ'_{QLE} and $\delta'_{T_{900}}$ are the respective summations of the higher order EOFs (greater than one) that contribute to the total fields for T_o' , $Q+LE'$ and T_{900}' . The assumption that the first spatial EOF (e_1) is the same for all three variables in (8) is based on the close similarity of the first EOFs for these simulated fields from the ADJACO and A model experiments (see earlier discussion of the results of Figs. 7 and 9). In addition the spatial patterns for the lower ordered EOFs (2-4) are also very similar. Based on these results, a substitution of (8) into (7), a multiplication of the resulting equation by $e_1(x)$ and use of the orthogonality condition for the domain area (A),

$$\int_A e_1(x) \delta'(x, t) dx = 0, \quad (9)$$

the following approximate equation governing the relationship between the first EOF time coefficients is obtained,

$$C_o \frac{\partial}{\partial t} C_{T_o} = -C_{QLE} = -\bar{D}C_{T_o} + \bar{D}C_{T900} \quad (10)$$

The relationship in (10) is used to assess the temporal consistency of the composited time coefficients for the first EOF of SST, Q+LE and T900 from the ADJACO model experiment (Fig. 14). The composited time coefficient for the first EOF of SST (C_{T_o}) is positive for the CCP case (Fig. 14; top right) and negative for the WCP case (Fig. 14; top left); this coefficient when multiplied by the spatial EOF shown in Fig. 7 (top left) yields the contribution of the first EOF to the total SST anomaly pattern shown in Fig. 10. The following features of temporal behavior of C_{T_o} for the CCP and WCP composites are consistent with the temporal behavior of the spatial SST composites shown in Fig. 10:

i) The magnitude of C_{T_o} reaches a maximum at month 5; the maximum (minimum) value of C_{T_o} for the CCP (WCP) composite case is 4.0 (-3.5).

ii) In both composite cases the most rapid growth for C_{T_o} occurs in the 2 month period (months 3-4) preceding when the maximum occurs. During the decay phase (months 6-9), the C_{T_o} coefficient for the WCP case decays at a rate comparable in magnitude to the overall growth rate. In contrast the C_{T_o} coefficient for the CCP case decays much more slowly than it grows.

The temporal variation of the time coefficient for the latent plus sensible heat flux (C_{QLE}) is opposite the sign of the time tendency of the SST time coefficient ($\frac{\partial}{\partial t} C_{T_o}$); this result is consistent with (10). During the growth stage (months 1-5), when the time rate of change of C_{T_o} is positive (negative) for the CCP (WCP) case, C_{QLE} is negative (positive). During the decay stage (months 6-9)

the relationship between the time coefficients. For the CCP case the estimated \bar{D} value is $24 \text{ Jm}^{-2} \text{ K}^{-1} \text{ sec}^{-1}$ whereas the value for the WCP case is $16 \text{ Jm}^{-2} \text{ K}^{-1} \text{ sec}^{-1}$. The corresponding correlation coefficients are 0.91 and 0.87, respectively. These estimates for the mean transfer coefficient translate into a 900 mb mean wind magnitude ($|\vec{V}_{900}|$) of about $5\text{--}8 \text{ m sec}^{-1}$ averaged over the extratropical Pacific domain (the Bowen Ratio is on the order of 0.5).

c. Evidence for an atmospheric response to the SST anomalies

The results presented so far do not readily reveal a signal of ocean forcing of the atmosphere. During the growth phase of the SST anomalies (months 1-4) for both the WCP and CCP cases the dominant signal is of atmospheric anomalies forcing development of anomalous SST. In the subsequent months of the WCP case (with only 4 samples), the magnitude of the SST anomalies reach about 1°C at maximum (month 5) and then decay rather rapidly in response to atmospheric anomalies opposite those present during the SST growth phase. The most likely scenario for this composite case is that natural (model) atmospheric variability is forcing the WCP SST anomaly over its life cycle with little evidence for ocean forcing of the atmosphere.

The CCP case with more samples (8) presents a different situation. In this case the SST anomaly (in the central Pacific) reaches a robust -1.5°C (month 5) and then decays rather slowly; the average of the anomaly is around -1.1°C over the subsequent months. The structure of the atmospheric anomalies over the period of slow decay of this SST anomaly is compatible with a possible response to the ocean. For example, residing near the negative (positive) SST anomaly in the central (eastern and western) Pacific are negative (positive) atmospheric 900 mb temperature and 500 mb height anomalies (Fig. 13; right panels). The presence of a negative 500 mb height anomaly near the negative SST anomaly is consistent with the findings

the sign of C_{QLE} and $\partial C_{TO}/\partial t$ reverses from that of the growth stage. The change in sign for C_{QLE} reflects the change in sign of the heat flux anomaly $(Q+LE)'$ between the growth and decay stage (Figs. 11 and 13).

An estimate of the change in C_{TO} , ΔC_{TO} , between the beginning and end of the growth and decay stages (between months 1 and 5 for growth and months 5 and 9 for decay) is obtained from (10) using the 3 month average of C_{QLE} over months 2-4 and over months 6-8, respectively. Generally, the estimated value of ΔC_{TO} compares favorably with the actual values obtained from Fig. 14 (Table 2). In the calculation the estimated ΔC_{TO} for the CCP case indicates a slower decay rate than for the WCP case which is in agreement with the actual time behavior of C_{TO} (Table 2) and corresponding SST anomaly (Fig. 10).

The temporal behavior of the time coefficient for the 900 mb temperature (C_{T900}) is also consistent with the time behavior of C_{QLE} and C_{TO} and with the previously discussed time behavior of atmospheric temperature structures during both the growth and decay stages (Figs. 11 and 13). During the growth stage for the WCP (CCP) case, a negative (positive) C_{T900} is coupled with a positive (negative) C_{QLE} . During the decay stage for the WCP case the C_{T900} coefficient reverses sign thereby contributing to the reversal of sign of the C_{QLE} coefficient; this response supports the rapid decay of the C_{TO} coefficient (SST anomaly). For the CCP case, however, the C_{T900} coefficient is generally of the same sign but weaker than during the growth stage. For this case, the C_{T900} coefficient acts to slow the decay of the C_{TO} coefficient.

A linear regression analysis of the values of $C_{TO} - C_{T900}$ versus C_{QLE} can be used to provide a statistical estimate of \bar{D} in (10) and a measure of the strength of

of GCM experiments using prescribed negative SST anomalies of comparable or larger magnitude (Lau and Nath, 1990; Palmer and Sun, 1985; Pitcher et al., 1988; Kushnir and Lau, 1992). However, the simulated anomaly at 500 mb in the ADJACO model (around -5 to -10m) is much weaker than those calculated in these previous GCM experiments.

In an effort to assess further the possibility that the ocean is forcing the atmosphere in the coupled model experiment, a set of prescribed (one-way forced) SST anomaly experiments are performed with the atmospheric (A) model. The prescribed anomalous SST consists of the composited 3-month averaged SST anomalies from the decay stage of the CCP case (months 6-8) for the extratropical North Pacific (11.6N - 46.4N) (Fig. 13; top right). Starting from December 1st of Years 8-31 of the 100-year A model experiment, 24 4-month runs are made using the prescribed anomalous SST forcing. The results of each run are averaged for the last 3 months of integration. Ensemble means of the 24 runs are then made after subtracting the corresponding 3 month averages from the control simulation without the SST anomaly (100-year A model experiment). The atmospheric anomalies from the prescribed CCP SST anomaly experiments (Fig. 15, right panels) are compared to the atmospheric anomalies composited during the decay stage of the CCP SST case (Fig. 15, left panels); the top three panels represent anomalous components of atmospheric circulation (900 mb temperature, T_{900} ; sea level pressure, P_{MSL} ; 500 mb heights, Z_{500}) while the bottom two panels represent anomalous components of the hydrologic cycle (evaporation, E; precipitation, P). The comparative results are discussed only for the immediate region encompassing the prescribed SST anomaly composite (150E-120W, 15N-60N).

In the prescribed SST anomaly experiments, a negative (positive) T_{900} anomaly is positioned over and just downstream of a negative (positive) CCP SST anomaly (Fig. 13, top right; Fig. 15, top right). For example in the central Pacific the

core of the negative T_{900} anomaly (about -1.2°C) is about 10° east of the position of the prescribed negative SST anomaly. At the surface, anomalous highs (lows) are positioned over to slightly west of the negative (positive) SST anomalies and thus a bit upstream of the corresponding T_{900} anomalies. As a consequence, the 500 mb height (Z_{500}) anomalies are shifted (or tilted) slightly west (about $10-20^{\circ}$) of the sea level pressure (P_{MSL}) anomalies. Overall the anomaly structure is slightly baroclinic. The negative T_{900} and positive P_{MSL} anomalies located near the negative SST anomaly in the central Pacific are the only circulation features that are statistically significant at the 95% level.

The T_{900} , P_{MSL} and Z_{500} anomalies in the prescribed SST anomaly experiments generally correspond with those in the CCP SST composites during the decay stage (Fig. 15; top three panels); the size of the anomalies are quite comparable. One major difference is that the circulation anomalies in prescribed SST experiments are located about $10-20^{\circ}$ downstream of the corresponding centers in the composites.

The comparative hydrologic response shows both similarities (evaporation) and significant differences (precipitation). The evaporative anomalies in the prescribed SST anomaly experiments are positioned a bit upstream (west) of their corresponding position in the composites. Anomaly magnitudes are very comparable. The differences in position of the evaporation anomalies however has important consequences for SST anomaly development. In the composites the heat flux anomalies are located almost directly over the SST anomaly; the magnitude and sign of the anomalies are consistent with the in situ decay of the SST anomaly (e.g., the negative evaporative anomaly over the negative SST anomaly in the central Pacific). In the prescribed SST anomaly experiment the anomalous negative (positive) evaporative centers are located a little upstream of the negative (positive) SST anomalies. This configuration would lead to a slow eastward propagation of the SST

anomaly if two-way ocean-atmosphere coupling was allowed. The SST anomaly would thus shift into a position with respect to the atmospheric circulation anomalies that more closely conforms with the coupled model result.

The anomalous precipitation patterns (Fig. 15, bottom panels) show little correspondence. In the composites there is generally decreased (increased) rainfall along (south of) the model storm track (not shown); in the prescribed SST anomaly experiments, decreased (increased) rainfall occurs close to the negative (positive) SST anomaly and somewhat downstream of the negative (positive) evaporative anomalies. In contrast to the evaporative anomalies the precipitation anomalies in the prescribed SST anomaly experiments (except for those in the western Pacific) are generally not statistically significant at the 95% level.

In summary, there are similarities in the structures of the atmospheric anomalies in the CCP composites and prescribed SST anomaly experiments (e.g. the sign and magnitude of the atmospheric anomaly associated with an SST anomaly) which are suggestive of an atmospheric response to anomalous SST in the coupled model. However, there are also enough differences in the results (particularly regarding the systematic differences in location of anomalous features with respect to an SST anomaly) to suggest the possibility that the atmospheric response to SST anomalies in the one-way coupled environment (prescribed SST anomaly) may differ somewhat from the response in the two-way coupled environment. Other, more remote, differences in lower boundary conditions may also be influencing the results for the extratropical Pacific region. For example, there are no differences in sea ice coverage or thickness between the prescribed SST anomaly and control A model experiments whereas there are small differences in sea ice between the ADJACO (coupled) model composite and the 100-year mean. It is unlikely that the remote differences in these boundary effects are dominating the results for the local region of the composite SST anomaly. One possible way of removing the influence of remote surface boundary effects would be to perform (for future study) long multi-year integrations with

the interactive ocean attached to the atmospheric model only for the extratropical north Pacific region; elsewhere SST and sea ice are prescribed as in the control A model experiment.

d. Brief comparison of prescribed SST anomaly experiments to other studies

The anomalous atmospheric response to the prescribed SST anomalies has elements of both previous full GCM experiments using realistic geography (e.g. Kushnir and Lau, 1992) and idealized GCM and linear model studies (e.g. Ting, 1991). The general magnitude of the anomalous response conforms to the linear theory results for shallow heating (including thermal transients); the response to the 10°C SST anomaly in Ting's (1991) study is about one order of magnitude greater than the response in this study to a 1°C SST anomaly. Consistent with the linear theory, an anomalous surface high (low) tends to form close to a negative (positive) SST anomaly, although the sea level pressure anomalies in the prescribed SST anomaly experiments are located a bit upstream of those in Ting's results. The structure of the low tropospheric temperature, evaporative and precipitation anomalies are also quite similar to the linear results.

The vertical structure of the anomalous atmospheric response is weakly baroclinic in the prescribed SST anomaly experiments and thus more nearly approximates the vertical structure in the full GCM experiments (equivalent barotropic) than the structure in the linear theory (highly baroclinic). The work of both Kushnir and Lau (1992) and Ting (1991) suggests that the role of momentum transients is important in determining the vertical structure of the anomalous atmospheric response to SST. In the idealized GCM (no land-ocean differences) the interaction between the model storm tracks and the wave trains forced by the SST anomalies are weak in comparison to the interactions that take place in the full GCM's with realistic land-ocean configuration. Perhaps, realistic earth geography

allows for preferred regions of wave train-storm track interactions which produce a large anomalous equivalent barotropic time mean response to momentum transient effects. In the low resolution model of this study realistic geography is included but the strength of the momentum transients is much weaker than found in the observations (Otto-Bliesner, 1984) and in the higher resolution model studies (e.g. Kushnir and Lau, 1992). The effects of momentum transients in the low resolution model experiments probably falls somewhere in between the effects in the idealized and realistic GCM experiments. While this interpretation can only be confirmed by a detailed analysis of the transient forcing in the experiments, the required analysis is beyond the desired scope of the present study.

8. Conclusions

In this study, results from a 100 year seasonal climate simulation of a coupled ocean-atmosphere model and from a 100-year parallel run with an uncoupled model (prescribed SSTs) are used to assess the structure of the dominant wintertime SST anomalies and associated atmospheric response in the extratropical north Pacific. The coupled model is a low resolution atmospheric, general circulation model attached to a constant 50m depth mixed layer ocean. The variability in net surface energy exchange between the ocean and the atmosphere is the sole process generating SST anomalies in the model. The model simulates a reasonable mean SST and surface energy flux climatology for the north Pacific ocean area, but underestimates the observed variability of SST and the surface heat fluxes in most areas of the Pacific region.

The principal pattern of SST variability is determined by EOF analysis. The first SST EOF has a large negative component in the central Pacific (minimum near 35N, 180W) flanked by positive centers in the western and eastern Pacific. The

second EOF is dominated by a central-eastern Pacific dipole structure. The first EOF pattern is quite robust explaining 19% of the variance compared to 10% explained by the second EOF. The dominant structure of anomalous sensible plus latent heat flux and low tropospheric temperature in both the coupled and uncoupled models are nearly identical to the dominant SST pattern. Observations also show a correspondence between important patterns of SST and ocean-atmosphere energy exchange in the extratropics (e.g. Cayan, 1992b) which indicates that the coupled model results are relevant to the study of ocean-atmosphere variability.

Composite analysis is used to assess the relationship between model SST anomalies and atmospheric circulation features. Composites are obtained by averaging the cases of wintertime SST anomalies for which the time coefficient of the first EOF exceeded in magnitude about 2 standard deviations. The first SST anomaly composite, denoted WCP for warm central-cold eastern and western Pacific SST anomaly, is derived from 4 winter cases; the second SST anomaly composite, denoted CCP for cold central-warm eastern and western Pacific SST anomaly, is derived from 8 winter cases. The composite SST anomaly in the central Pacific is between 0.5°C and 1.0°C for the WCP case and between -1.0°C and -1.5°C for the CCP case.

The growth and decay of the dominant SST anomaly pattern is linked to the time behavior of the dominant model atmospheric teleconnection pattern. During the growth phase of the WCP (CCP) SST anomalies, anomalous highs (lows) reside over the western Pacific and western North America and an anomalous trough (ridge) is in the east-central Pacific. Anomalous cold (warm) air to the near of the anomalous low (high) enhances (reduces) the sensible plus latent heat flux loss over the ocean and leads to development of a negative (positive) SST anomaly in the model. The SST anomalies in both composites nearly develop to full amplitude over a period of about 1-2 months.

The SST anomalies in the WCP case decay at a rate that is comparable in magnitude to the growth rate; for the CCP case, the SST anomalies decay much more

slowly, retaining a significant fraction of their maximum size even after 4 months. In the WCP case the atmospheric anomalies during the decay stage are nearly reverse those present during the growth stage. An analysis of the relationship between the first EOF time coefficients of SST and associated atmospheric components verifies that this reversal in atmospheric structure accounts for most of the rapid decay of the WCP SST anomalies. For this case there is no clear evidence of an atmospheric response to SST but rather in the words of Wallace and Jiang (1987), the growth phase atmospheric anomalies are "followed by equally strong atmospheric circulation anomalies of the opposite sign which" subsequently destroys the SST anomalies.

For the CCP case, atmospheric anomalies during the decay stage are of the same sign and structure but substantially weaker than during the growth stage. Positive (negative) atmospheric temperatures generally reside over positive (negative) SST departures. This configuration of atmospheric anomalies help to maintain the SST anomalies against the decay produced by the negative SST-heat flux feedback and explains why these anomalies decay much more slowly than they do in the WCP SST case. Further support of this conclusion is quantitatively given by an analysis of the time coefficients for the first EOFs of SST and atmospheric structures.

A set of prescribed SST anomaly experiments provides some evidence that the atmosphere is in part responding to the ocean during the slow decay of the CCP SST composite. Twenty four 4 month integrations of the uncoupled model are performed using the CCP SST anomalies in the northern Pacific during the decay stage. A comparison of the ensemble 3-month averages of the atmospheric anomalies from these experiments with the composite (two-way coupled model anomalies) during the decay stage reveals very similar structures in 900 mb temperature, sea level pressure, 500 mb heights and evaporation. The main difference is in location of the anomalous features; the anomalies for the 900 mb temperature, 500 mb height and sea level pressure are 10-20° downstream of their position in the composite case while the

evaporation anomalies are bit upstream of their corresponding position in the composite. The position of the evaporative anomaly with respect to the SST anomaly in the prescribed SST anomaly experiments would lead to an eastward shift of the SST anomaly over time if two-way interaction was allowed. The anomalous structure of precipitation is quite different between the two experiments; in the composite, rainfall decreases (increases) along (south of) the north Pacific storm track, whereas it tends to decrease (increase) near the position of the negative (positive) SST anomaly in the prescribed SST anomaly experiments. The results suggest that the atmospheric response to anomalous SST in the coupled ocean-atmosphere environment may differ somewhat from that generated in the one-way forced (prescribed SST) system.

The atmospheric response to the prescribed SST anomalies in the uncoupled model contain aspects of the responses of linear models and idealized GCMs using all ocean conditions (Ting, 1991) and the responses of GCMs using realistic geography (e.g. Kushnir and Lau, 1992). For example, the magnitude, sign and position of the lower tropospheric anomalies (e.g. evaporation, precipitation, 900 mb temperature and sea level pressure) with respect to the SST anomaly conform to the results of linear theory (with shallow heating). However, the vertical structure (between the surface and 500mb) is weakly baroclinic and thus more compatible to GCM models using realistic geography (equivalent barotropic). Although the present model utilizes observed geography, its low resolution probably does not allow for adequate simulation of the thermally forced wave-transient interaction found in the higher resolution, more realistic GCMs. The necessary calculations of the thermal and momentum transients have not been performed to further elucidate on the reasons why the model simulation does not produce a realistic structural response to SST anomalies. This additional analysis was beyond the desired scope of the present study, but should be carried out in future studies (see below).

Future work should consider long seasonal integrations of coupled ocean-atmosphere models with greater resolution and more sophisticated representation of physical processes than are used in this study. A higher resolution atmospheric model with an interactive cloud parameterization would allow for more realistic simulation of transient eddy processes. A detailed comparison of integrations performed using an improved atmospheric model with the experiments of this study should provide a better understanding of the relationship between anomalous SST, storm tracks and associated time mean atmospheric anomalies. For example, the comparative results should help in our understanding of the possible role of momentum transients in the time mean response to interactive SST anomalies.

Finally the ocean component in future studies should include important processes which can effect the structure and evolution of SST anomalies that were not included in this study (e.g. advection, entrainment, upwelling). In this study the process of ocean-atmosphere energy exchange alone produces relatively persistent (3-4 month duration) large scale SST anomalies on the order of 1-2°C. Recent studies have shown that the mechanisms of ocean advection and entrainment are also important to the development and persistence of anomalous SST in the extratropics (Miller, 1992; Alexander, 1990).

Acknowledgements. This research was supported by National Science Foundation Grant ATM-8913261. Numerical calculations were performed at the Scientific Computing Division of the National Center for Atmospheric Research, which is supported by the National Science Foundation. The author wishes to acknowledge Dr. David Houghton for his comments on the paper, Marilyn Wolff for technical preparation of the manuscript, and Linda Keller for finalizing the figures.

References

- Alexander, M.A., 1990: Simulation of the response of the north Pacific Ocean to the anomalous atmospheric circulation associated with El Niño. Climate Dynamics, 5, 53-65.
- Alexander, M.A., 1992a: Midlatitude atmosphere-ocean interaction during El Niño. Part I: The North Pacific Ocean. J. Climate, 5, 949-958.
- Alexander, M.A., 1992b: Midlatitude atmosphere-ocean interaction during El Niño. Part II: The Northern Hemisphere Atmosphere. J. Climate, 5, 959-972.
- Cayan, D.R., 1990: Variability of latent and sensible heat fluxes over the oceans. Ph.D. Thesis, Univ. of California-San Diego, 199 pp.
- Cayan, D.R., 1992a: Latent and sensible heat flux anomalies over the northern oceans: The connection to monthly atmospheric circulation. J. Climate, 5, 354-369.
- Cayan, D.R., 1992b: Latent and sensible heat flux anomalies over the northern oceans: Driving the sea surface temperature. J. Phys. Oceanogr., 22, 859-881.
- Frankignoul, C., 1985: Sea surface temperature anomalies, planetary waves, and air-sea feedbacks in the middle latitudes. Rev. Geophys., 23, 357-390.
- Frankignoul, C., and K. Hasselmann, 1977: Stochastic climate models. II: Application to sea-surface temperature variability and thermocline variability. Tellus, 29, 284-305.
- Frankignoul, C., and R. W. Reynolds, 1983: Testing a dynamical model for mid-latitude sea surface temperature anomalies. J. Phys. Oceanogr., 13, 1131-1145.
- Gallimore, R. G., and D. D. Houghton, 1987: Approximation of ocean heat storage by ocean-atmosphere energy exchange: Implications for seasonal cycle mixed layer ocean formulations. J. Phys. Oceanogr., 17, 1214-1231.
- Gallimore, R. G., and D. D. Houghton, 1990: Simulation of ocean temperature and heat storage from a GCM coupled to a variable depth upper ocean. J. Phys. Oceanogr., 20, 1312-1332.
- Gallimore, R. G., B. L. Otto-Bliesner and J. E. Kutzbach, 1986: The effects of improved parameterizations for orography, snow cover, surface fluxes and condensational processes on the climate of a low resolution GCM. J. Atmos. Sci., 43, 1961-1983.
- Gill, A. E., and P. P. Niiler, 1973: The theory of the seasonal variability in the ocean. Deep-Sea Res., 20, 141-177.
- Haney, R. L., 1980: A numerical case study of the development of large-scale anomalies in the central North Pacific Ocean. J. Phys. Oceanogr., 10, 541-556.
- Hansen, J., I. Fung, A. Lacis, D. Rind, S. Lebedeff, R. Rudy, G. Russell and P. Stone, 1988: Global climate changes as forecast by Goddard Institute for Space Studies three dimensional model. J. Geophys. Res., 93, 9341-9364.

- Hoskins, B. J., and D. J. Karoly, 1981: The steady linear response of a spherical atmosphere to thermal and orographic forcing. J. Atmos. Sci., 38, 1179-1196.
- Houghton, D. D., R. G. Gallimore and L. M. Keller, 1991: Stability and variability in a coupled ocean-atmosphere climate model: Results of 100-year simulations. J. Climate, 4, 557-577.
- Kawamura, R., 1984: Relation between atmospheric circulation and dominant sea surface temperature anomaly patterns in the north Pacific during the northern winter. J. Meteor. Soc. Japan, 62, 910-916.
- Kushnir, Y., and N.-C. Lau, 1992: A general circulation model study of the stationary and transient response to midlatitude SST anomalies. J. Climate, 5, 271-283.
- Kutzbach, J. E., and R. G. Gallimore, 1988: Sensitivity of a coupled atmosphere/mixed layer ocean model to changes in orbital forcing at 9000 years B. P. J. Geophys. Res., 93, 803-821.
- Lau, N.-C. and M. J. Nath, 1990: A general circulation model study of the atmospheric response to extratropical SST anomalies observed in 1950-1979. J. Climate, 3, 965-989.
- Luksch, U., and H. von Storch, 1992: Modeling the low-frequency sea surface temperature variability in the North Pacific. J. Climate, 5, 893-906.
- Manabe, S., 1983: Oceanic influence on climate—studies with mathematical models of the joint-atmosphere system. Large-Scale Oceanographic Experiments in the WCRP, Vol. 2, WCRP Publ. Serv. No. 1, WMD, 27 pp.
- Meehl, G. A., and W. M. Washington, 1985: Sea surface temperatures computed by a simple ocean mixed layer coupled to an atmospheric GCM. J. Phys. Oceanogr., 15, 92-104.
- Miller, A. J., 1992: Large-scale ocean-atmosphere interactions in a simplified coupled model of the midlatitude wintertime circulation. J. Atmos. Sci., 49, 273-286.
- North, G. R., T. L. Bell, R. F. Cahalan and F. J. Moeng, 1982: Sampling errors in the estimation of empirical orthogonal functions. Mon. Wea. Rev., 110, 699-706.
- Otto-Bliesner, B. L., 1984: A global low-order spectral general circulation model. Part II: Diagnosis of the seasonal energetics. J. Atmos. Sci., 41, 508-523.
- Otto-Bliesner, B. L., G. W. Branstator and D. D. Houghton, 1982: A global low-order spectral general circulation model. Part I. Formulation and seasonal climatology. J. Atmos. Sci., 41, 508-523.
- Palmer, T. N., and Sun Zhaobo, 1985: A modelling and observational study of the relationship between sea surface temperature in the north-west Atlantic and the atmospheric general circulation. Quart. J. Roy. Met. Soc., 111, 947-975.
- Pitcher, E. J., M. L. Blackmon, G. T. Bates and S. Muñoz, 1988: The effect of north Pacific sea surface temperature anomalies on the January climate of a general circulation model. J. Atmos. Sci., 45, 173-188.

- Robock, A., 1980: The seasonal cycle of snow cover, sea ice, and surface albedo. Mon. Wea. Rev., 108, 267-285.
- Schlesinger, M. E., and W. L. Gates, 1980: The January and July performance of the OSU two-level atmospheric general circulation model. J. Atmos. Sci., 37, 1914-1943.
- Semtner, A. J., Jr., 1976: A model for thermodynamical growth of sea ice in numerical investigations of climate. J. Phys. Oceanogr., 6, 379-389.
- Shea, D. J., 1986: Climatological Atlas: 1950-1979, NCAR Tech. Note (NCAR/TN-209 + STR), Atmospheric Analysis and Prediction Divisions, National Center for Atmospheric Research, Boulder, Colorado, 35 pp.
- Ting, M., 1991: The stationary wave response to a midlatitude SST anomaly in an idealized GCM. J. Atmos. Sci., 48, 1249-1275.
- Wallace, J. M., and D. S. Gutzler, 1981: Teleconnections in the geopotential height field during the Northern Hemisphere winter. Mon. Wea. Rev., 109, 784-812.
- Wallace, J. M., and Q. Jiang, 1987: On the observed structure of the interannual variability of the atmosphere/ocean climate system. Atmospheric and Oceanic Variability, H. Gattle, Ed., Roy. Meteor. Soc., Bracknell, Berkshire, 17-43.
- Wallace, J. M., C. Smith and Q. Jiang, 1990: Spatial patterns of atmosphere-ocean interaction in the northern winter. J. Climate, 3, 990-998.
- Washington, W. M., and G. A. Meehl, 1984: Seasonal cycle experiments on the climate sensitivity due to a doubling of CO₂ with an atmospheric general circulation model coupled to a mixed layer ocean model. J. Geophys. Res., 89, 9475-9503.
- Washington, W. M., and C. L. Parkinson, 1986: An Introduction to Three-Dimensional Climate Modelling. University Science Books, 422 pp.
- Weare, B., A. Navato and R. E. Newell, 1976: Empirical orthogonal analysis of Pacific Ocean sea surface temperatures. J. Phys. Oceanogr., 6, 671-678.

Table 1

Correlation between the spatial patterns of the first EOF for the variables (SST, latent plus sensible heat (Q + LE) and 900 mb temperature (T_{900})) from the A and ADJACO model experiments.

<u>ADJACO vs ADJACO</u>		Correlation Value
Q+LE	SST	0.89
Q+LE	T_{900}	0.84
T_{900}	SST	0.73
<u>A vs A</u>		
Q+LE	T_{900}	0.88
<u>ADJACO A</u>		
Q+LE	Q+LE	0.96
SST	Q+LE	0.77
T_{900}	T_{900}	0.99

Table 2

Estimated and actual values of the change in the time coefficient for SST between the beginning and end of the growth and decay stages for the WCP and CCP cases. The estimated value is obtained from (10) using the 3 month averages (months 2-4 for growth and months 6-8 for decay) of the C_{OLE} values.

	WCP	
	Growth	Decay
$\Delta C_{T0}(\text{est})$	-3.0	-3.7
$\Delta C_{T0}(\text{act})$	-3.3	-3.0

	CCP	
	Growth	Decay
$\Delta C_{T0}(\text{est})$	3.7	1.4
$\Delta C_{T0}(\text{act})$	3.4	2.0

Figure Legends

- Fig. 1. Extended Pacific area with grid coverage of full Pacific Ocean domain (solid plus open circles) and extratropical north Pacific domain (solid circles) used for analysis in model study.
- Fig. 2. Distribution of the difference between ADJACO 100 year January mean SST and observed (10^{-1}°C).
- Fig. 3. The distribution of the 100 year January mean evaporation (mm/day) from the A model (top) and ADJACO model (middle) for the Pacific Ocean area. The observed distribution of January mean evaporation (mm/day, bottom) is taken from Schlesinger and Gates (1980).
- Fig. 4. Distribution for the Pacific Ocean area of the standard deviation of the departures of January SST (10^{-1}°C) from the 100-year January mean for the ADJACO model experiment (top). The observed distribution of the standard deviation of January SST (10^{-2}°C , bottom) is taken from Shea (1986). The observed results are based on 30 years of data; stippling indicates data sparse areas.
- Fig. 5. The annual cycle of the area average standard deviation of monthly mean SST (top; °C), net surface heat flux (middle; W/m^2), and atmospheric temperature at 900mb (bottom; °C) over the extratropical north Pacific from the ADJACO model (solid curves) and A model (dashed curves).
- Fig. 6. Distribution for the Pacific Ocean area of the standard deviation of the departures of January latent heat flux (left, W/m^2) and sensible heat flux (right; W/m^2) from the 100-year January means for the A model experiment (top) and ADJACO model experiment (middle). The observed distribution for these heat fluxes (bottom, W/m^2) are from Cayan (1990).
- Fig. 7. The distribution of the first (left) and second (right) EOF of Pacific SSTs (10^{-1}°C) from the 100 year ADJACO model experiment for the extratropical Pacific domain (top) and full Pacific domain (bottom). Variance explained is denoted in upper right part of each panel.
- Fig. 8. The distribution of the departure of November SST for Year 72 (top), November SST for Year 42 (middle), and November SST for Year 75 (bottom) from the respective 100-year November mean. Temperatures are in units of 10^{-1}°C .
- Fig. 9. The distribution of the first (left) and second (right) EOF of sensible plus latent heat flux at the surface (W/m^2) for the extratropical Pacific domain from the ADJACO model (top) and A model (bottom). Variance explained is denoted in upper right part of each panel.
- Fig. 10. Composite anomalies of SST (10^{-1}°C) during growth (months 3-4), maximum (month 5) and decay (months 6-7) phases of the WCP (left panels) and CCP (right panels) SST cases.
- Fig. 11. Composite for SST anomaly at maximum (top panels, 10^{-1}°C) and 3 month average anomalies of selected variables (panels 2-6) during growth stage of the WCP (left panels) and CCP (right panels) SST cases. Variables shown are the sensible plus latent heat flux ($Q+LE$, 10W/m^2); 900mb temperature (T_{900} , 10^{-1}°C); 700mb temperature (T_{700} , 10^{-1}°C); sea level pressure (P_{MSL} , mb) and 500 mb height (Z_{500} , 10^1m).

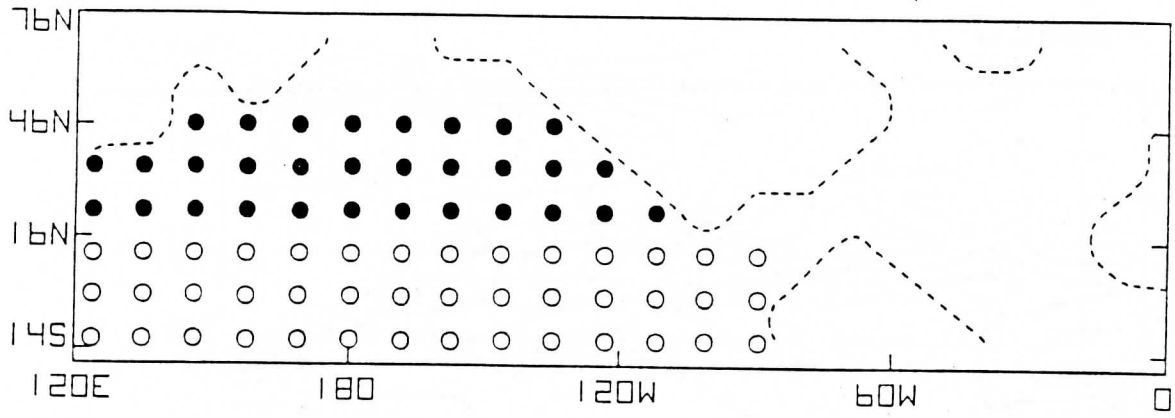
Fig. 12. The distribution of the first EOF of 500mb heights for the extended Pacific area from the ADJACO (top) and A(bottom) models. Variance explained is denoted in upper right part of each panel.

Fig. 13. Composite 3 month average anomalies for selected variables during decay stage of the WCP (left panels) and CCP (right panels) SST cases. Variables shown are sea surface temperature (SST, 10^{-1}°C , 1st panel); sensible plus latent heat flux ($Q+LE$, 10W/m^2 , 2nd panel); 900 mb temperature (T_{900} , 10^{-1}°C , 3rd panel) and 500mb height (Z_{500} , 10m, 4th panel).

Fig. 14. Time plot of composite time coefficient for the first EOF of SST (C_{T0} , °C , top panels), sensible plus latent heat flux (C_{QLE} , W/m^2 , middle panels) and 900 mb temperature ($C_{T_{900}}$, °C , bottom panels) for the WCP (left) and CCP (right) SST cases. Note: SST anomalies reach maximum magnitude at month 5.

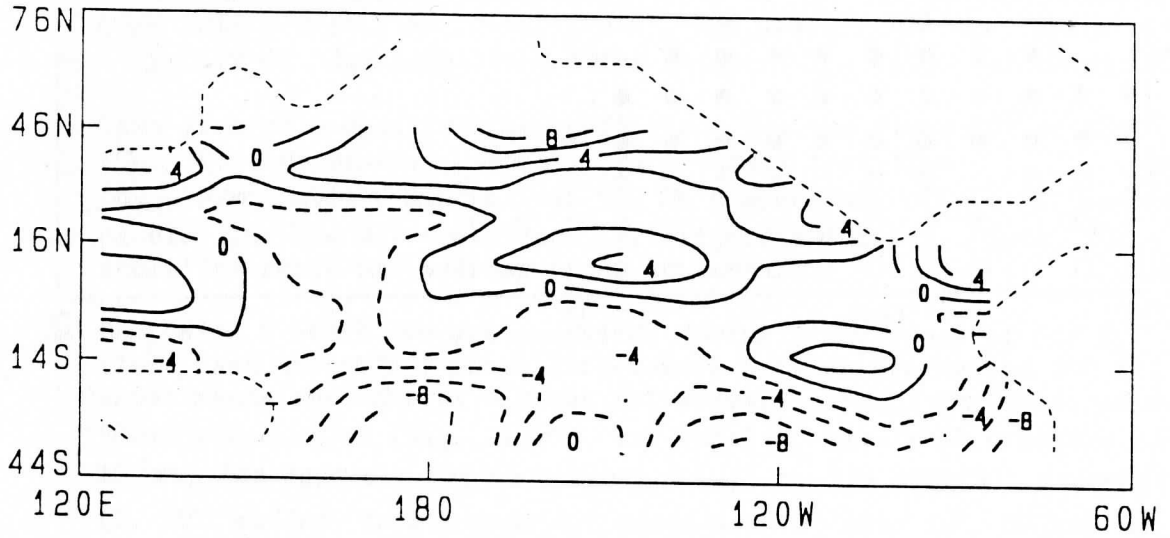
Fig. 15. Composite 3 month average anomalies during decay stage of CCP SST case (left) and ensemble 3 month differences between prescribed CCP SST anomaly experiments and control without SST anomaly (right) for selected variables: 900mb temperature (T_{900} , 10^{-1}°C , 1st panels); sea level pressure (P_{MSL} , 10^{-1}mb , 2nd panels); 500 mb heights (Z_{500} , m, 3rd panels); evaporation rate (E , 10^{-1}mm/day , fourth panels); precipitation rate (\dot{P} , 10^{-1}mm/day , fifth panels). Regions bounded by thick curved lines denote areas with statistically significant differences at the 95% level in the prescribed CCP SST anomaly experiments (right panels).

ANALYSIS DOMAINS



JANUARY
SST

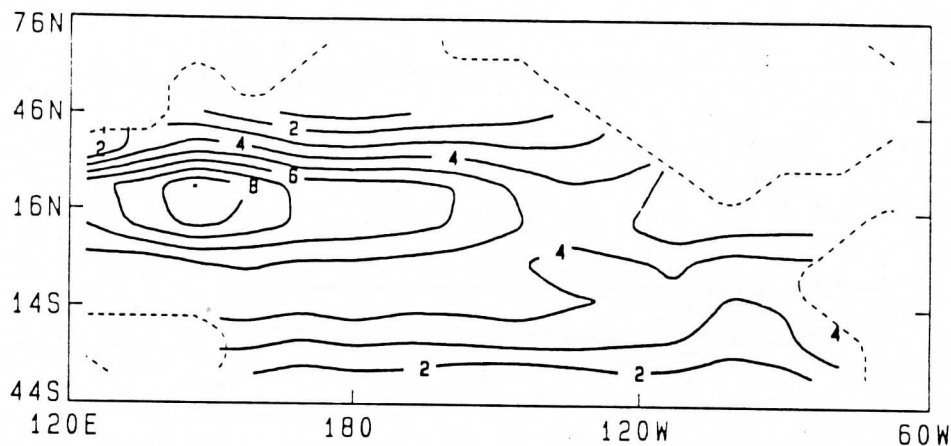
ADJACO-A



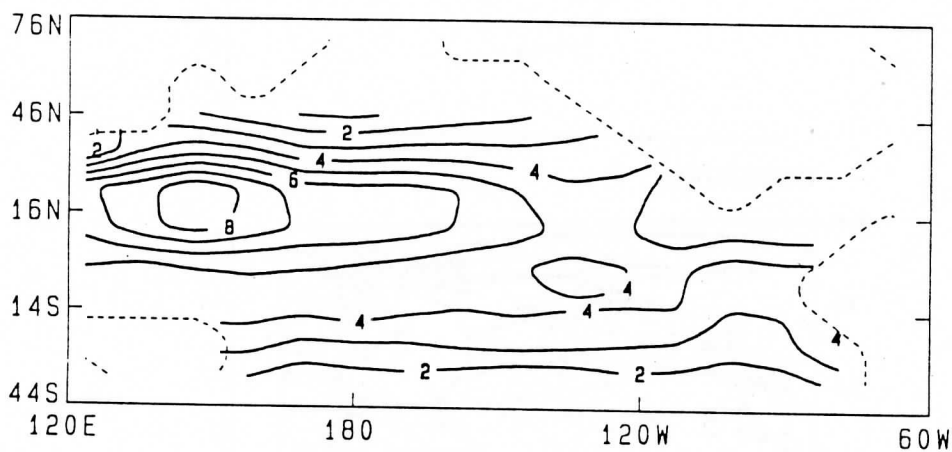
JANUARY
EVAPORATION

Fig 3

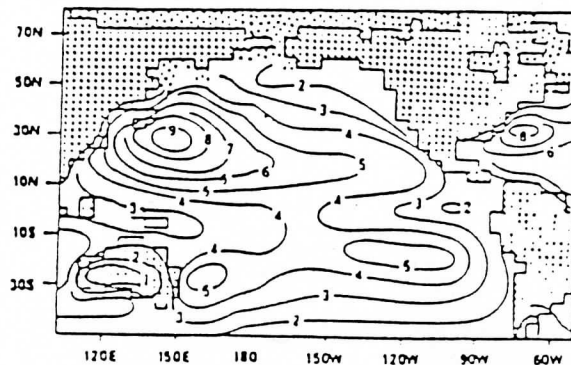
A MODEL



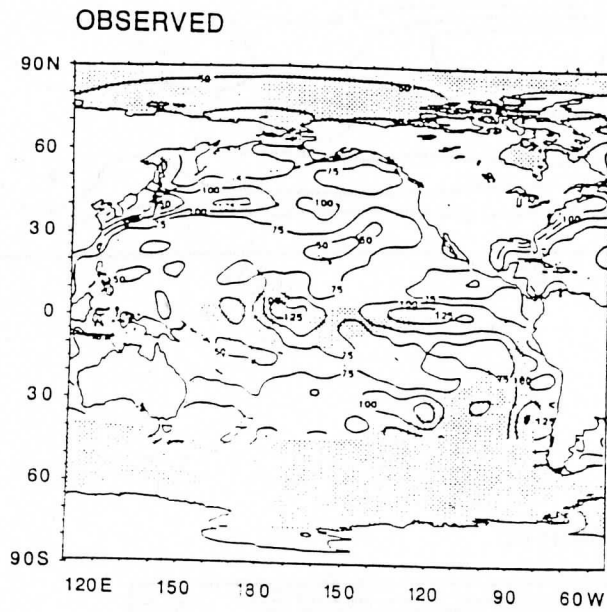
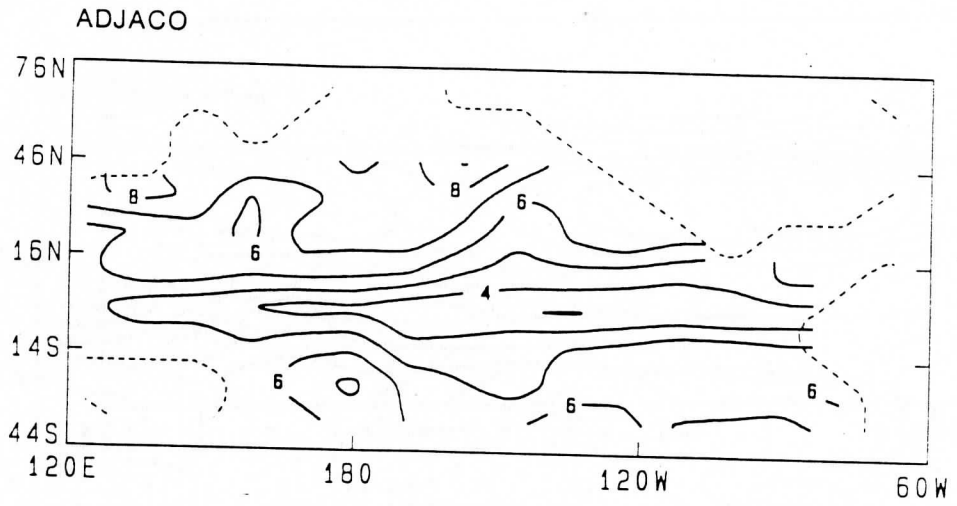
ADJACO MODEL

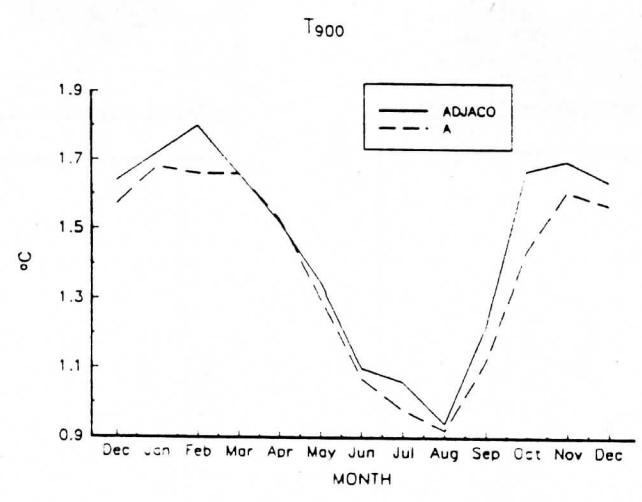
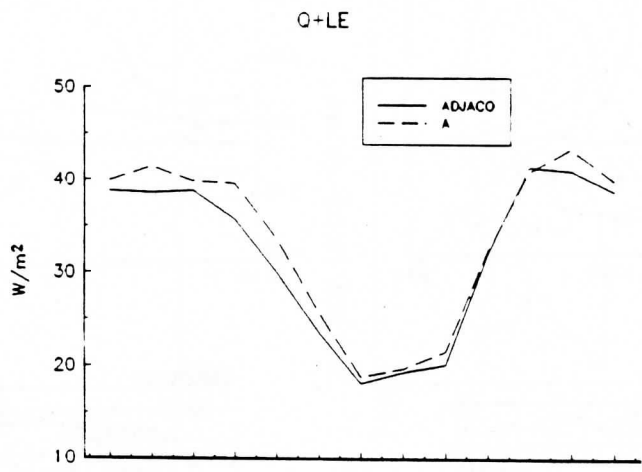
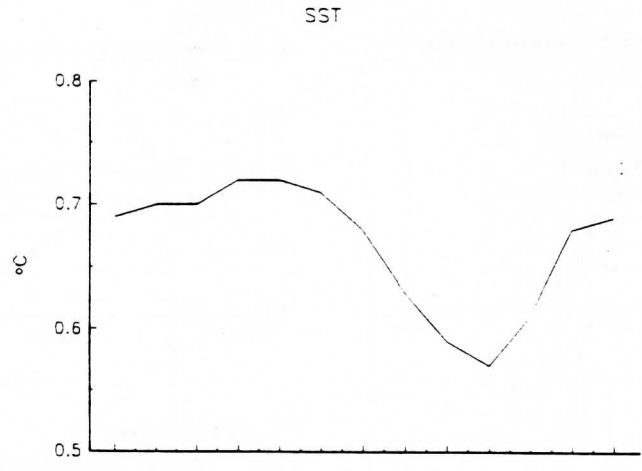


OBSERVED

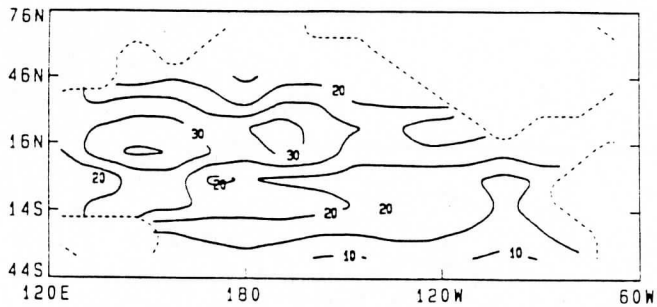


JANUARY SST STD

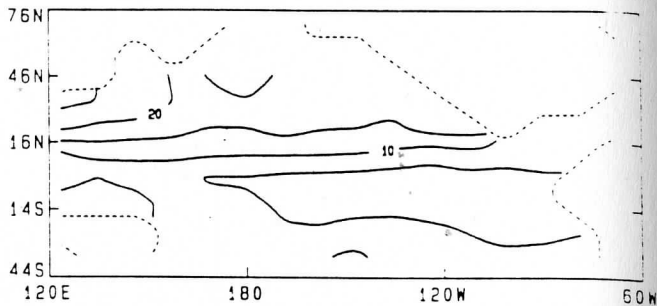




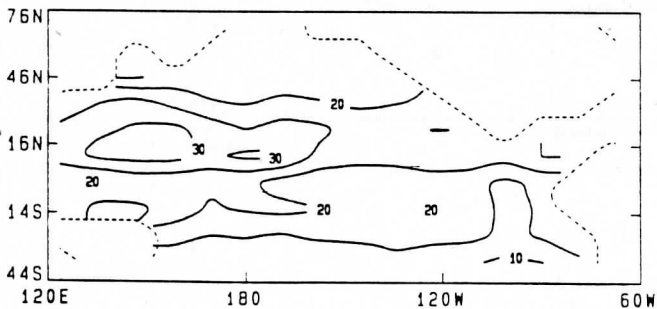
A MODEL



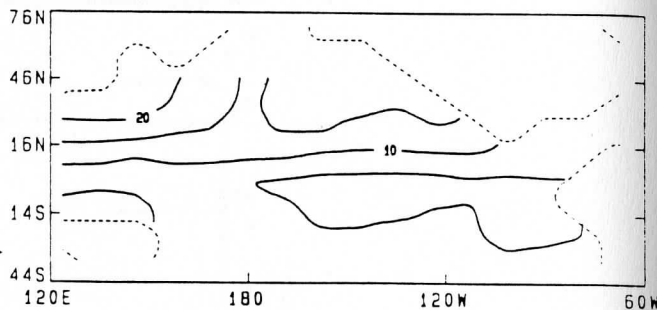
A MODEL



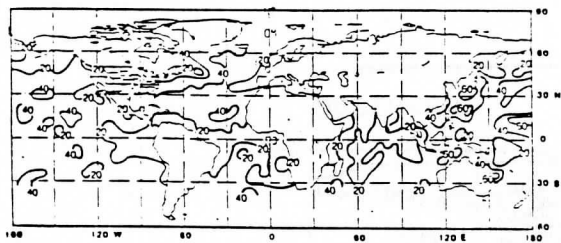
ADJACO MODEL



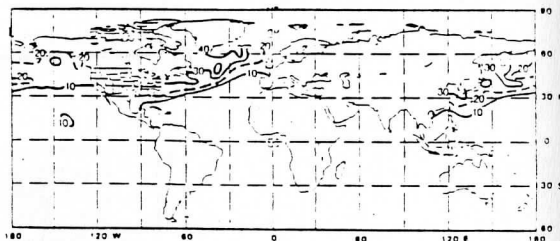
ADJACO MODEL



OBSERVED

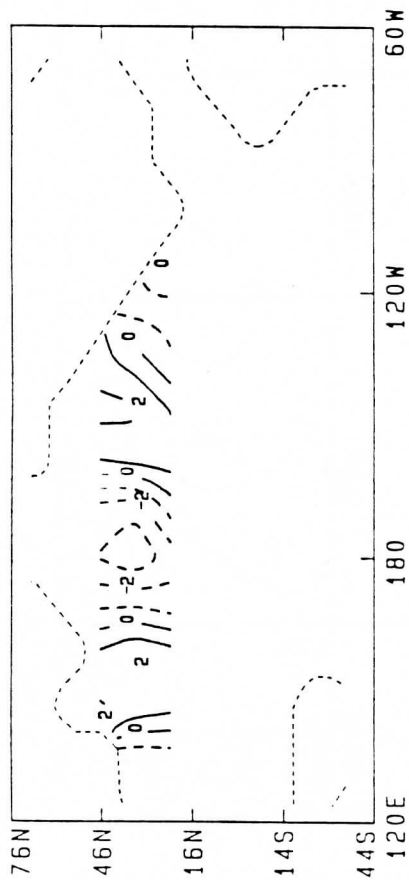


OBSERVED



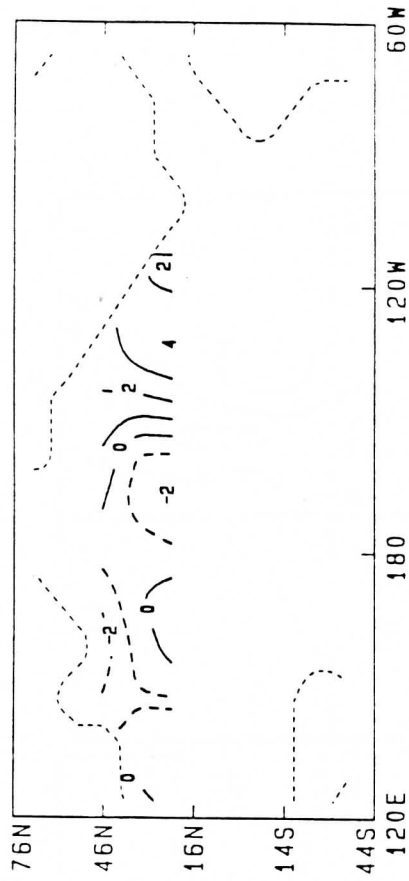
1st EOF (23.2N-46.4N)

19%



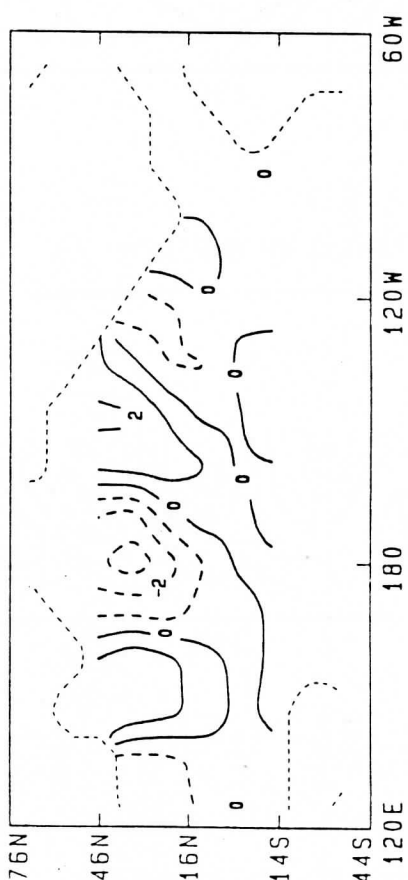
2nd EOF (23.2N-46.4N)

10%



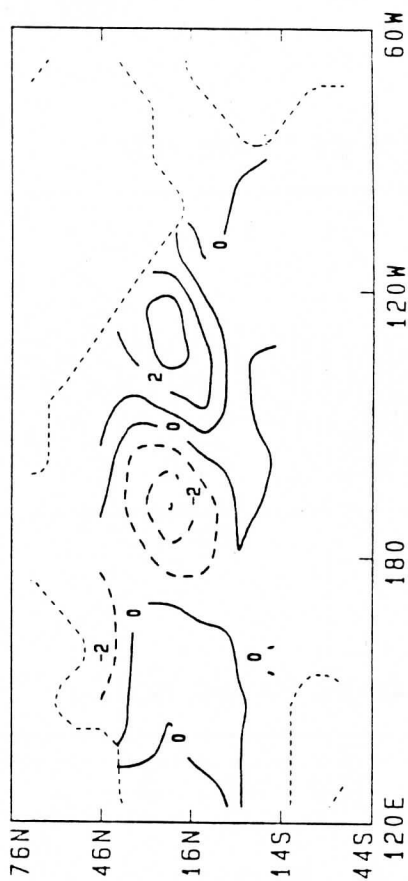
1st EOF (11.6S-46.4N)

12%



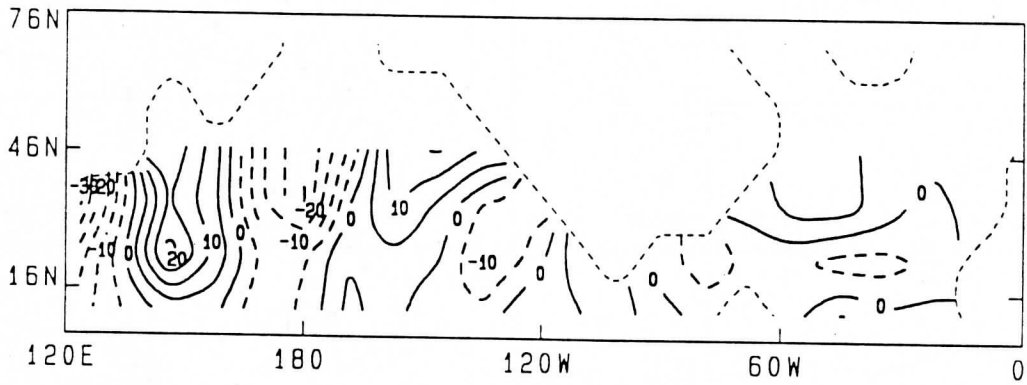
2nd EOF (11.6S-46.4N)

7%

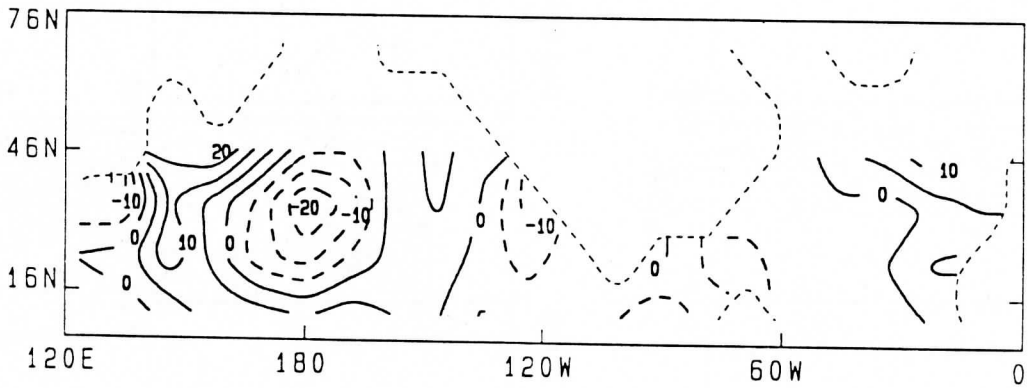


SST ANOMALY

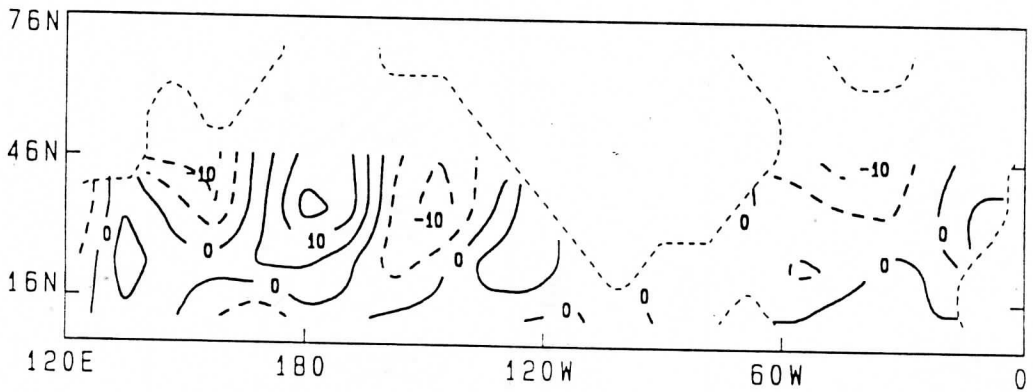
YR 72-100 YR AVE, NOV

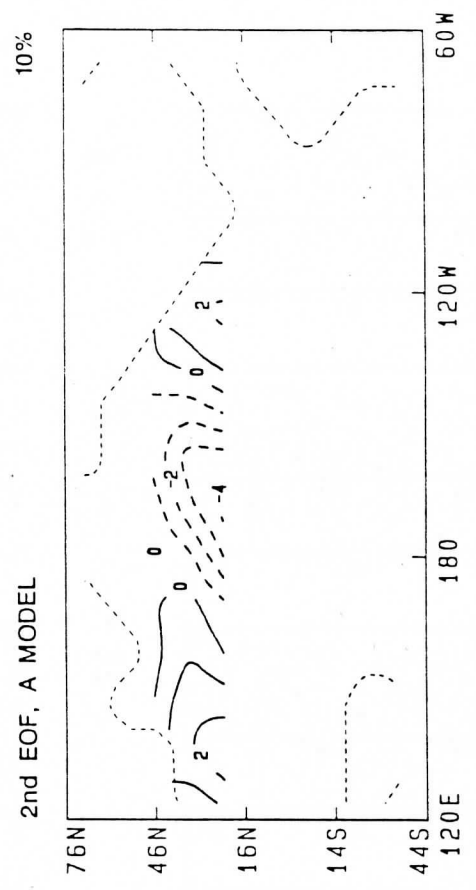
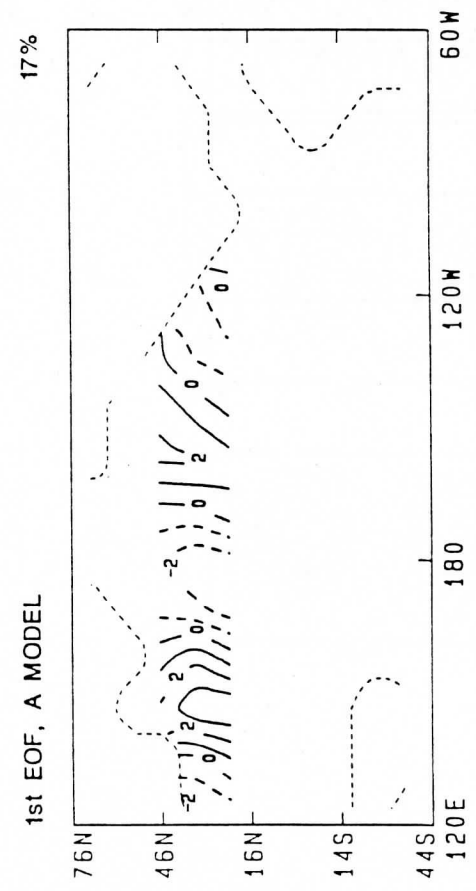
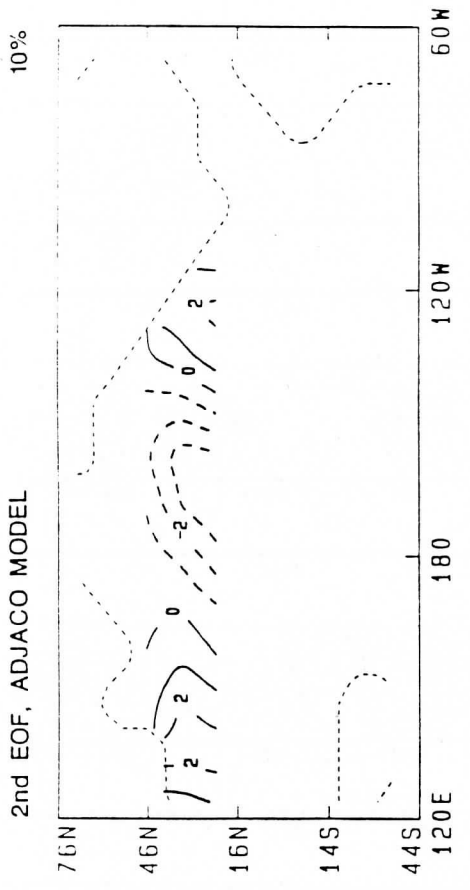
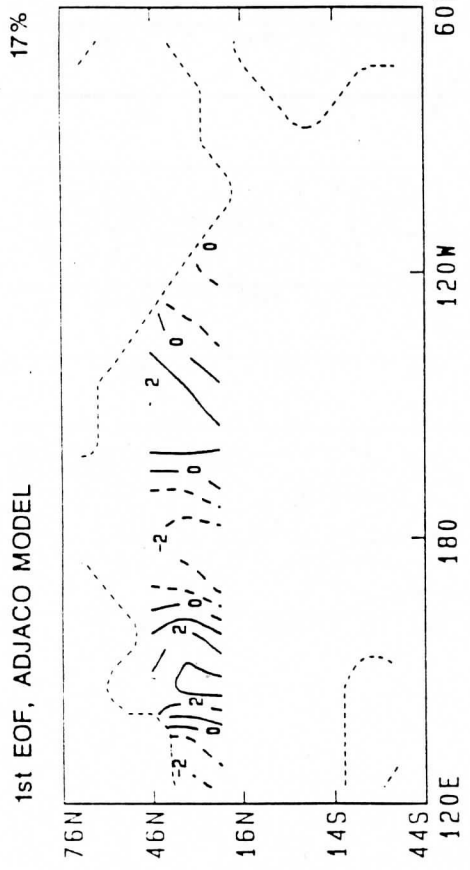


YR 42-100 YR AVE, NOV



YR 75-100 YR AVE, NOV

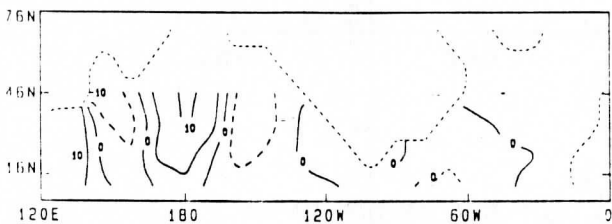
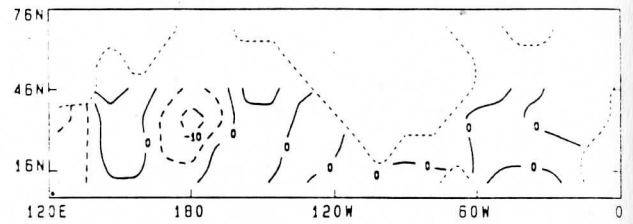
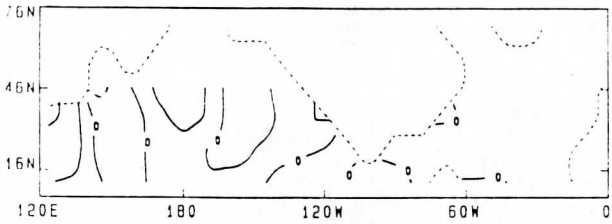
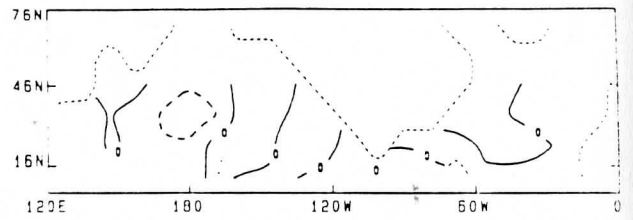
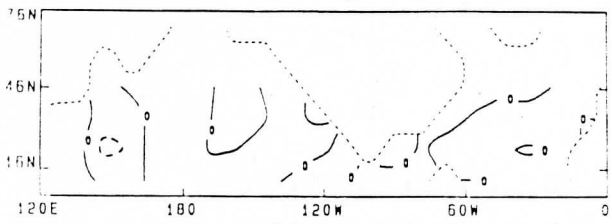




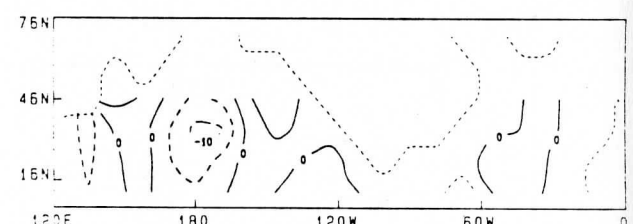
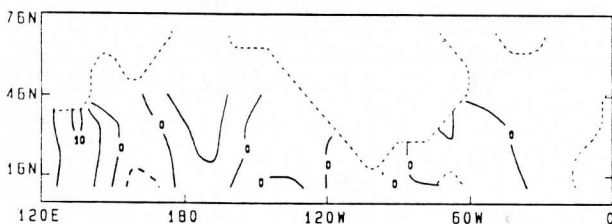
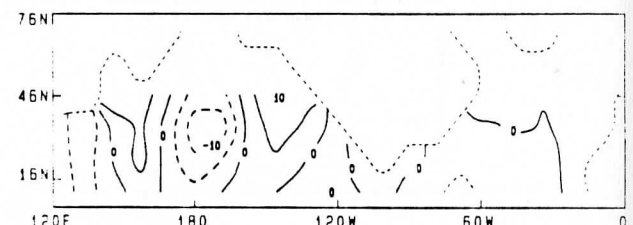
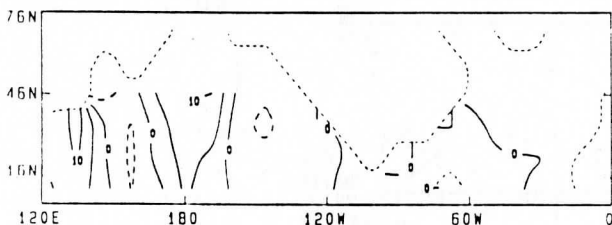
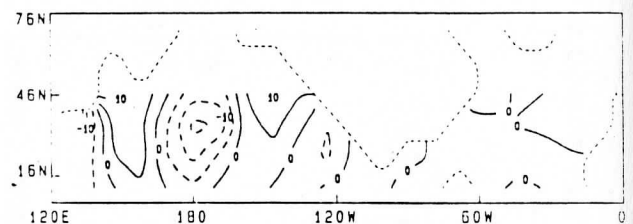
WCP SST

CCP SST

MONTH



5
SST
MAX



WCP

CCP

SST
AT
MAX

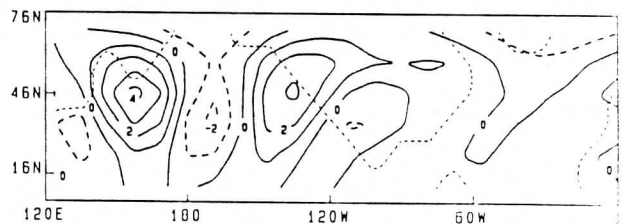
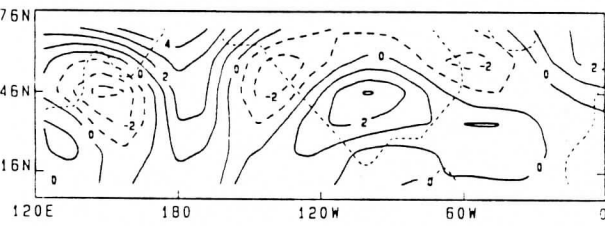
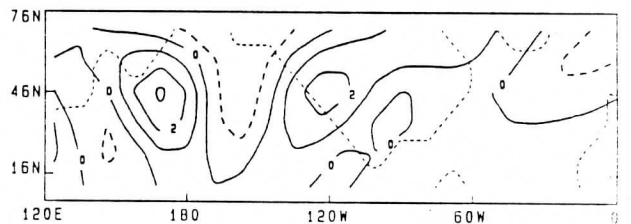
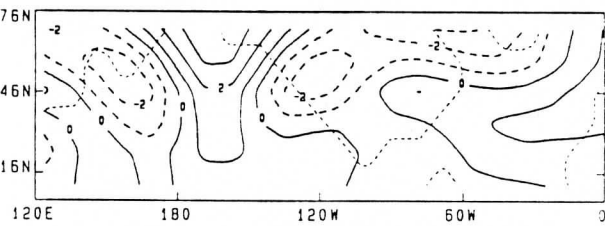
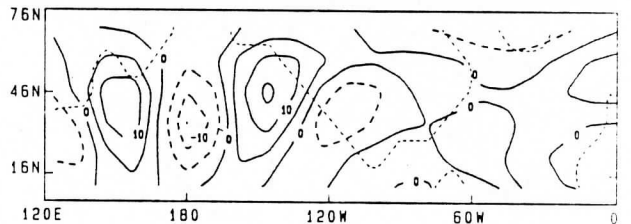
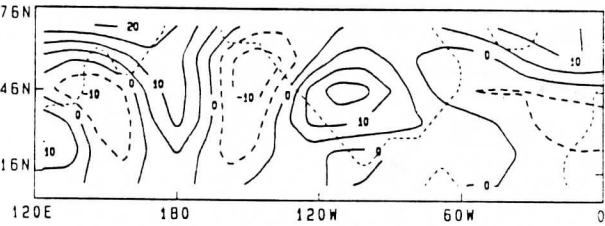
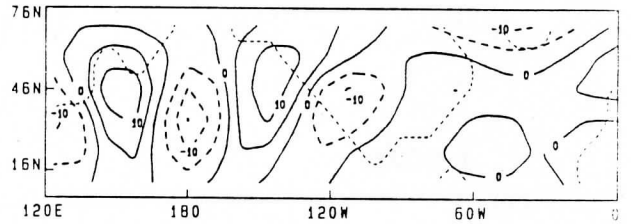
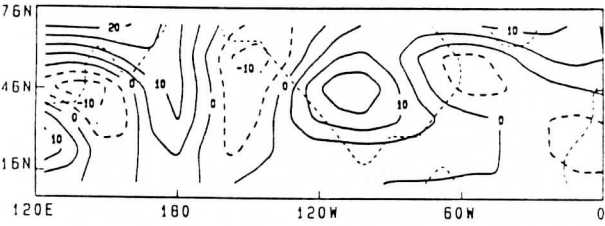
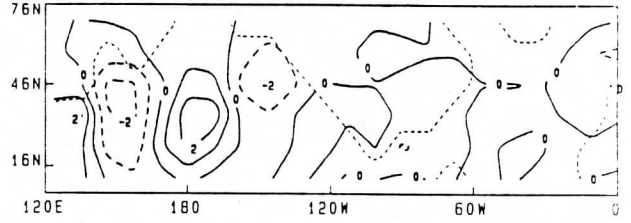
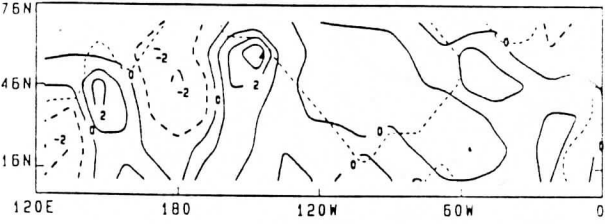
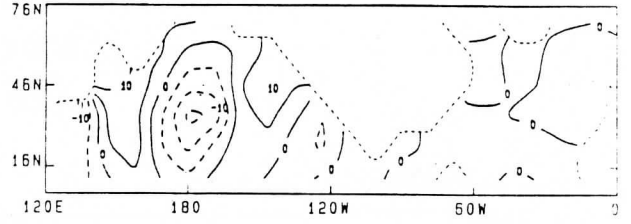
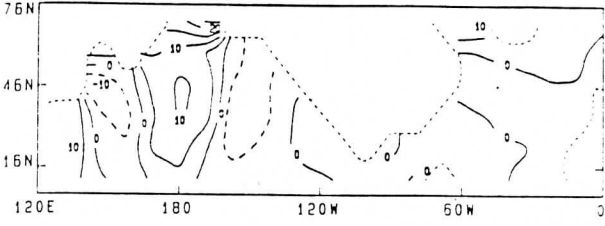
Q
+
LE

T₉₀₀

T₇₀₀

P_{MSL}

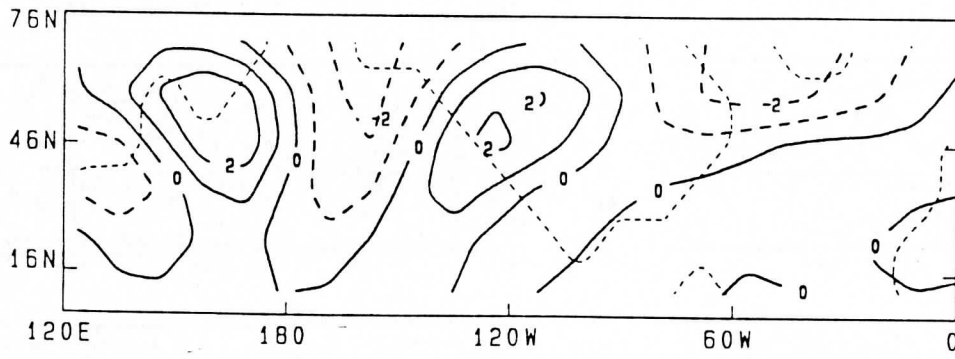
Z₅₀₀



EOF1
Z₅₀₀

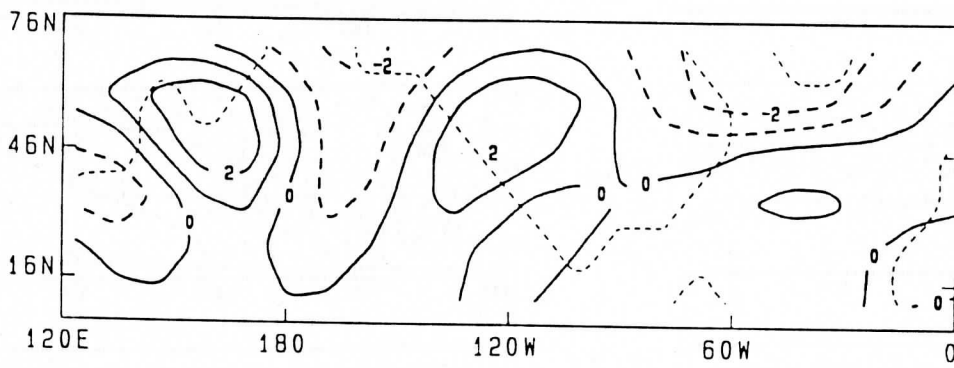
ADJACO

9.2%

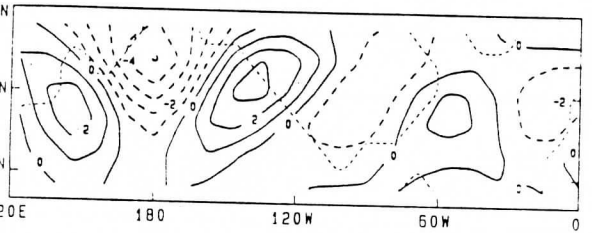
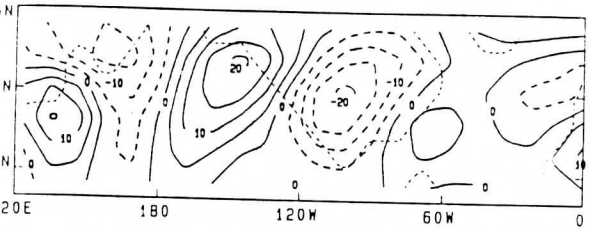
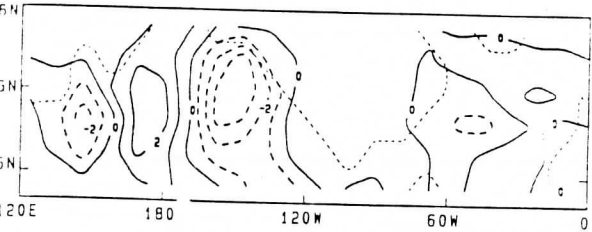
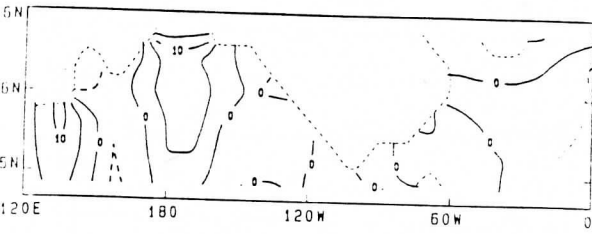


A MODEL

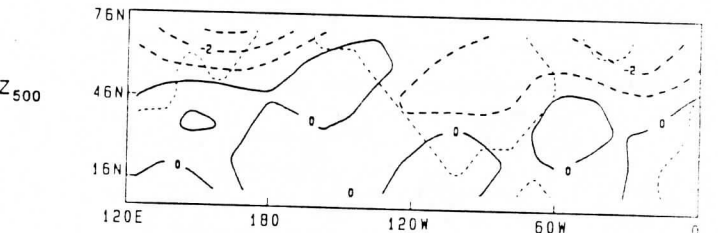
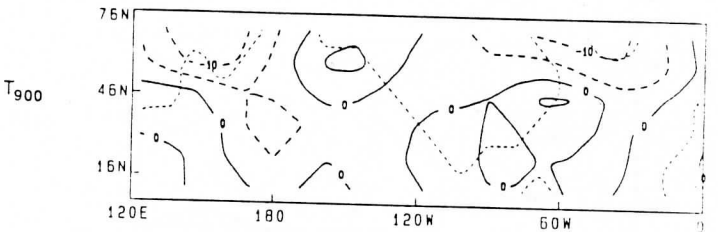
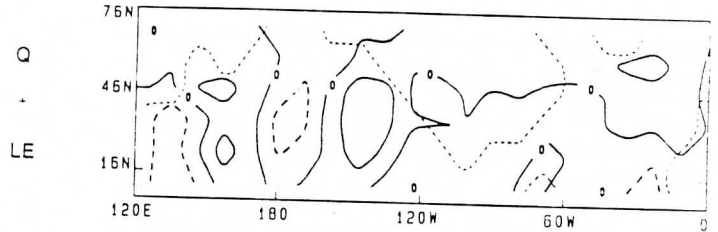
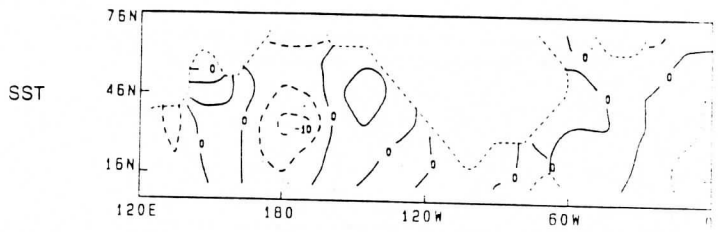
11.1%



WCP

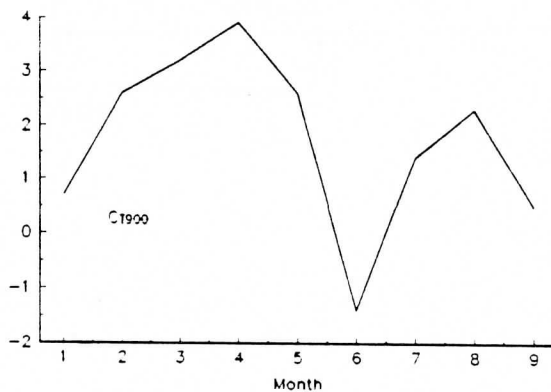
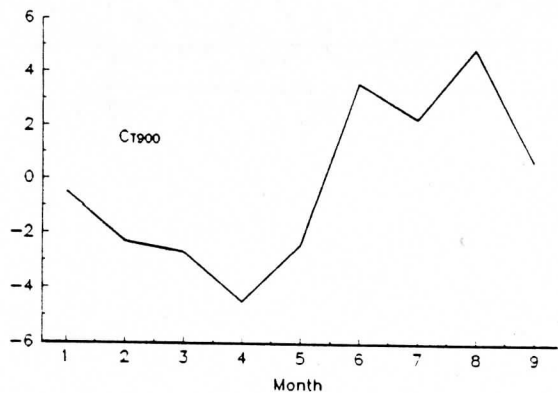
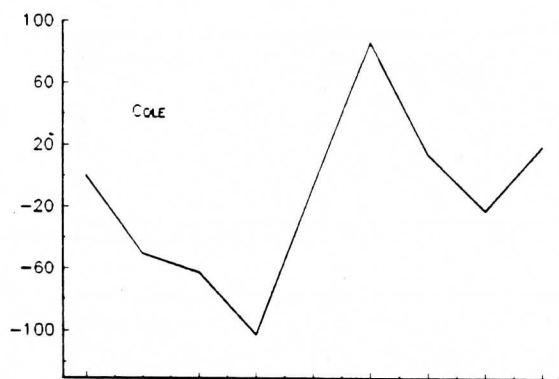
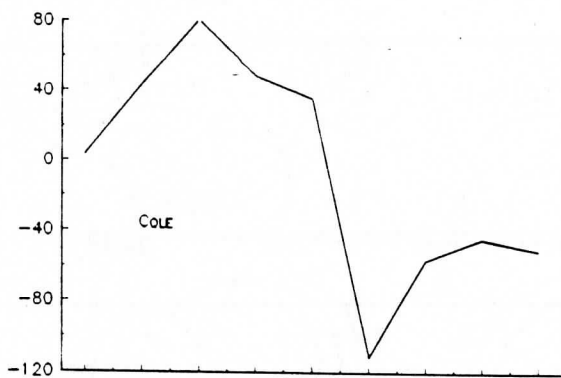
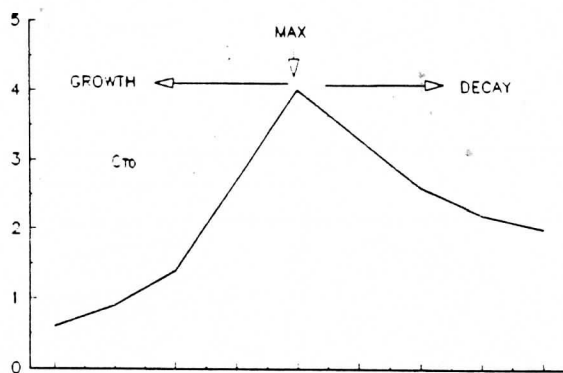
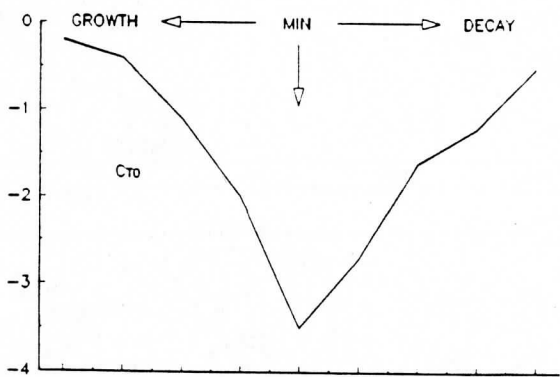


CCP



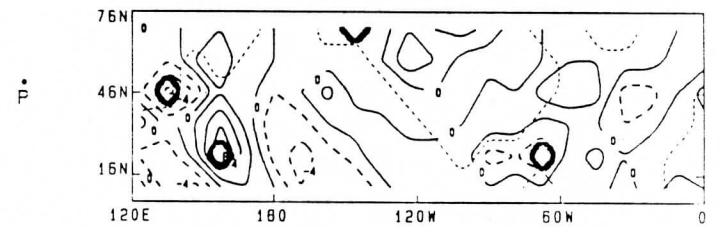
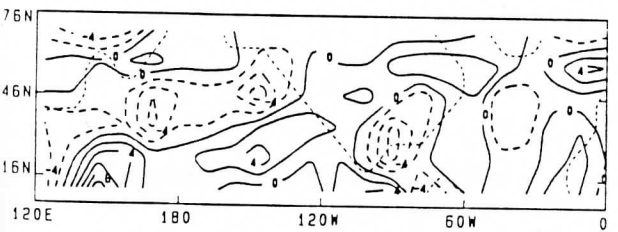
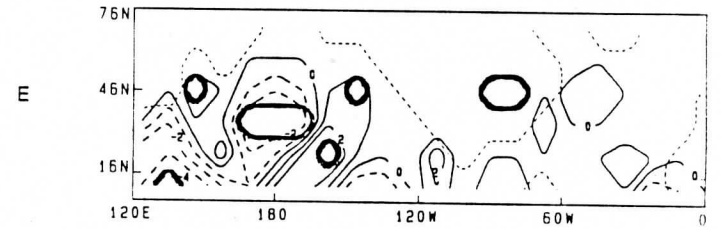
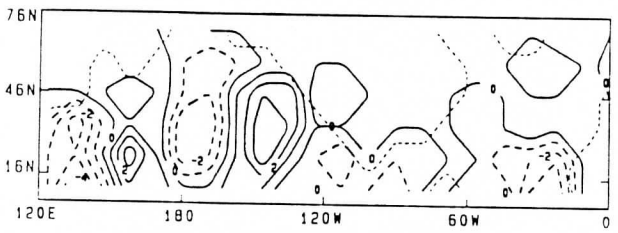
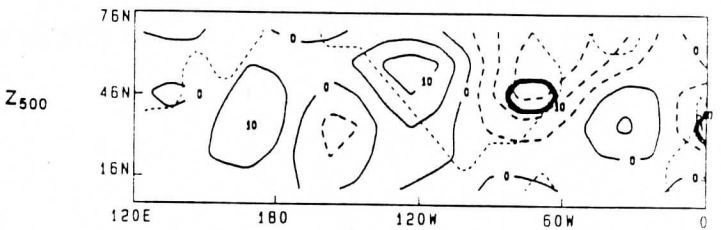
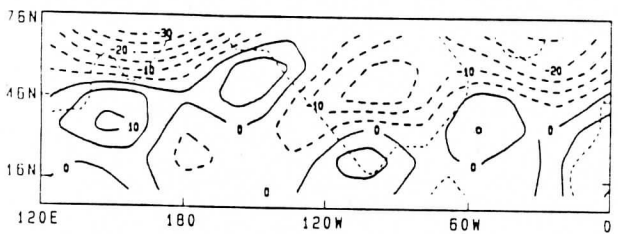
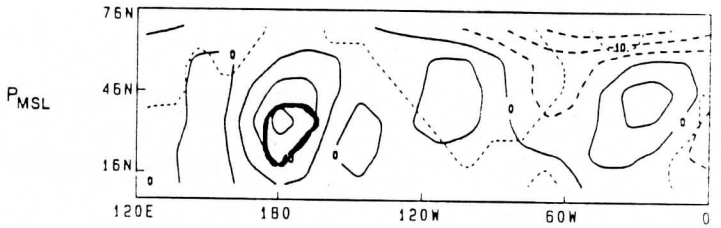
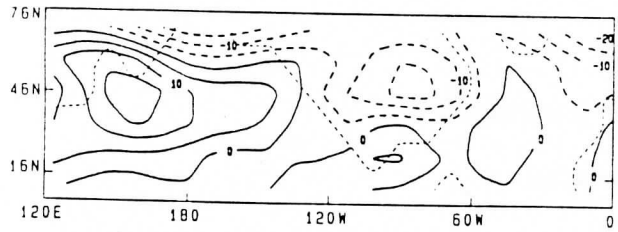
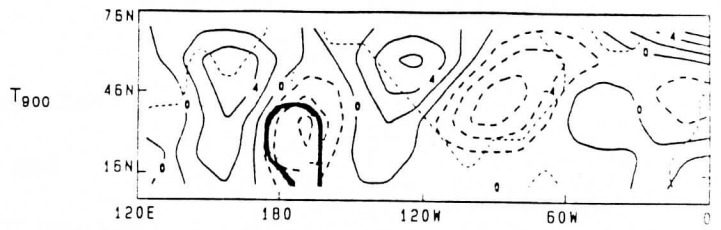
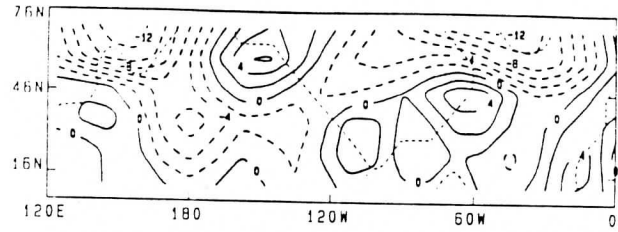
WCP

CCP



ADJACO CCP COMPOSITE
DECAY STAGE

PRESCRIBED CCP SST ANOM EXP
(MINUS CONTROL)



The Impact of Indian Ocean SST on the Large Scale Asian Summer Monsoon and the Hydrological Cycle

Yunlai Zhu

and

David D. Houghton

Department of Atmospheric and Oceanic Sciences

University of Wisconsin-Madison

June 10, 1994

Submitted to Journal of Climate

Corresponding Author Address

David D. Houghton

Department of Atmospheric and Oceanic Sciences

University of Wisconsin-Madison

1225 West Dayton Street

Madison, WI 53706

ABSTRACT

Relationships among the large-scale hydrological cycle, Asian summer monsoon and sea surface temperature (SST) anomalies in the Indian Ocean are investigated in a series of numerical experiments. Ensembles of integrations with the NCAR community climate model, CCM1, focusing on the summer months (June, July, August) provide the basic information for analysis. Impacts of SST anomalies in the southern Indian Ocean are evaluated by intercomparison of experiments with and without these anomalies. Systematic changes in the hydrological cycle and monsoon circulation are demonstrated and summarized in the context of a three-dimensional framework for the component processes of the Asian summer monsoon system. In the negative SST anomaly case, both the hydrological cycle and circulation processes are enhanced by virtue of their close relationship and especially the inherent coupling between the large-scale water vapor transport and the low-level monsoon flow. The overall intensity of the monsoon, in this case, is much enhanced resulting in a strong monsoon scenario. In the positive SST anomaly case, the model response is essentially opposite to that of the negative case. These strong/weak monsoon scenarios are very similar to those observed interannual variations of the Asian summer monsoon. Evidence also shows that the changes in surface heat fluxes induced by the presence of the prescribed SST anomaly would in turn lead to the dissipation of that anomaly in several months if the SST were allowed to change as in an coupled atmosphere-ocean system. Implications of these results are discussed.

1. INTRODUCTION

Observational studies have indicated that the variations of the Asian summer monsoon circulation and rainfall are closely related to the variations of the Indian Ocean sea surface temperature. For instance, Joseph and Pillai (1987) suggested a relationship between interannual changes in both Indian monsoon rainfall and sea-surface temperature (SST) anomalies over the Indian Ocean. Based on their 13-year records, both anomalies had a tendency for alternating signs approximately every 2-3 years. The composite SST anomaly compiled by Meehl (1987) for the month of July showed that there exists a broad scale negative (positive) SST anomaly in the southern Indian Ocean during strong (weak) monsoon years. These anomalies are even more pronounced for the composites containing only years of cold (warm) ENSO events or very strong (weak) monsoons characterized by abundant (deficient) monsoon rainfall (Meehl, 1987). Cadet and Diehl (1984) presented two contrasting examples of individual year (1956, 1972) anomalies of SST and sea level pressure which agreed with Meehl's results. Note that Meehl (1987) classified 1956 as a strong Asian monsoon year in an anti-El Nino (cold) events category and 1972 as a weak monsoon year associated with a strong El Nino (warm) event.

Observations also show interconnections between the monsoon circulation and rainfall and other components of the hydrological cycle. Findlater (1969) found a correlation between the rainfall over the west coast of India and the low-level equatorial winds over Kenya. Krishnamurti et al. (1976) also indicated that cross-equatorial winds are stronger during a good (strong) monsoon than a poor (weak) monsoon. Cadet and Diehl (1984) and Cadet (1983) revealed that during the summer monsoon, the cross-equatorial water vapor flux is closely related to variations of the low-level winds over the Indian Ocean and the rainfall over India. Cadet and Reverdin (1981) showed that about 70% of the water vapor crossing the west coast of India originated from the Southern Indian Ocean. Similar results were also obtained by Hastenrath and Lamb (1980). The analysis of the global hydrological cycle by Zhu (1987) using FGGE data showed a large area of net moisture divergence (source) over the Indian

Ocean area and net moisture convergence (sink) over Asian monsoon area consistent with Cadet and Reverdin's (1981) and Hastenrath and Lamb's (1980) regional analyses. More importantly, Zhu (1987) showed that there is an intense belt of northward moisture transport spanning from the source area to the sink area.

Zhu (1993) studied the broad-scale features of the monsoon system in a control simulation using NCAR CCM1 model, with an emphasis on the interrelationship between the large-scale monsoon circulation and the full set of atmospheric hydrological processes, i.e., evaporation, transport and precipitation. Spatially and temporally coherent variations of the hydrological cycle processes are found in association with other circulation processes. Fig. 1 shows a 3-D schematic view of the Asian monsoon system components and the interconnections between them suggesting complex interactions involving large-scale monsoon circulation, hydrological cycle and SST variations. More detailed analysis of the control experiment and the method used to identify these relationships can be found in Zhu (1993). It should be noted that the variations in SST, which is the main thrust of this current study, can influence both the surface evaporation process and the low-level flow and pressure as depicted in Fig. 1.

In this study, we focus on the relationship between the variations of SST in the southern Indian Ocean and the monsoon variations by conducting a series of SST anomaly experiments using the CCM1 model. In these experiments we not only show the "effects" of SSTA on the various atmospheric processes (i.e. the so called model response) but also give insights on the "mechanisms" through which the "effects" are realized. This is accomplished by studying the overall atmospheric response to SSTA in terms of variations of the intermediate physical processes. The key emphasis here is the hydrological cycle processes which have been identified by Zhu (1993) as key interaction agents.

In section 2, a brief description of the climate model used in this study is given together with the design of the anomaly experiment. Results will be presented in section 3. Further

discussion is given in section 4 and conclusions in section 5.

2. MODEL DESCRIPTION

The base model used in this research is the NCAR Community Climate Model (CCM1). This global climate model employs a spectral representation of the horizontal fields in terms of spherical harmonics with rhomboidal truncation at wavenumber 15. The transform grid in physical space consists of 48 longitudinal points and 40 latitudinal points (see Chervin 1986 for the exact Gaussian latitudes). The horizontal resolution is thus 7.5 degrees in the longitudinal direction and approximately 4.5 degrees in the latitudinal direction. The vertical discretization utilizes a finite difference scheme in sigma coordinate with 12 unevenly spaced layers giving higher resolution in the troposphere (see Hoerling et al. 1990 for exact sigma levels). Details of the model formulation and numerical algorithms for solution have been given by Williamson et al. (1987). Only a brief summary is intended here for the aspects of the model that are particularly relevant to this study.

The large-scale dynamics are represented by a system of governing (primitive) equations similar to those of Bourke (1974) and Hoskins and Simmons (1975). Both horizontal and vertical diffusion are included with the latter being stability dependent. Moist processes are included in an explicit specific humidity tendency equation. Cumulus convection is simulated by a moist convective adjustment scheme after Manabe et al. (1965). Stable condensation is considered when the lapse rate is stable but the moisture is supersaturated. Model cloud parameterization includes both nonconvective and convective clouds that are interactive with the radiation parameterization (Ramanathan et al., 1983). There is no diurnal cycle of solar insolation for the sake of computational efficiency (Chervin, 1986). Surface fluxes of sensible and latent heat are given by bulk aerodynamic parameterization, following Deardorff (1972). The drag coefficients are stability dependent and include a crude estimate of the effect of variable height of the planetary boundary layer. The wetness factor, which sets the surface evaporation to be a specified fraction of the evaporation from

saturated surface, is dependent on the surface type. This parameter is set to 1.0 for snow, sea ice and ocean, 0.1 for grassland and scrub, 0.01 for desert, and 0.25 for all other land types. The model also has an optional parameterization of interactive surface hydrology where the wetness factor is determined from calculated soil moistures in the model rather than being specified and fixed. However, in this current study, this option is not used for simplification and easier understanding of the results. Biological processes associated with vegetation (effects of biosphere) are not explicitly parameterized in the model, although implicitly some of these effects are represented in a limited sense by the wetness factors corresponding to different surface types.

The model includes large-scale topography as specified by the surface geopotential height obtained from the spectral representation. Other external lower boundary conditions including sea-surface temperature, sea-ice distribution and surface snow cover are prescribed using observed climatology. Surface temperatures over land and sea-ice, however, are computed from the surface-energy-balance equation assuming no heat storage below the surface. The model is integrated in seasonal mode, and the sea-surface temperatures, sea-ice locations and snow cover are changed to reflect the seasonal changes according to the observed mean seasonal variations. Solar insolation calculations in the model are also dependent on the time of the year. Thus the main time-varying external forcings of the atmosphere by the seasonal cycle of incident solar radiation and climatological sea-surface temperature are included in the model.

The model formulations described above thus include a range of fundamental interactive dynamical and physical processes of the atmosphere. The characteristic variations of the large-scale hydrological cycle components and their relationships and interactions with regard to these fundamental processes simulated by the model can therefore be evaluated in a consistent manner. One should keep in mind, however, the limitations of the model, e.g. noninteractive ocean, omission of soil moisture processes and biological evapotranspiration processes, when interpreting the results.

3. EXPERIMENT DESIGN

Two basic sets of SST anomaly experiments are conducted in this study. Each set consists of three independent four-month (May 1st through August 31st) integrations with an idealized prescribed SST anomaly (to be discussed later). Each integration was started from a different initial condition, i.e. a different year in the 10-year control run (a continuous subset of the 15-year standard CCM1 seasonal control run, see Williamson and Williamson, 1987) to ensure the effective independence between the experiment runs. The last three months (June-July-August) of each four-month integration are used in the analysis. The ensemble features of these anomaly experiments (the average of the three integrations in each set) are compared with those of the control run (the average of the 10 years).

The focus of experimental analysis is to evaluate the systematic responses (both local and remote) of the atmospheric hydrological cycle and circulation components, i.e., precipitation, evaporation, transport, atmospheric mass distribution and flow fields, etc., over the Asian monsoon region to two cases of idealized SST anomalies prescribed over the Indian Ocean area. In the first case (designated as N1), a SST anomaly of -1°C is prescribed over the southern Indian Ocean in the area from the equator to 26°S and from 40°E to 100°E (see sketch in Fig. 2). In the second case (designated as P1), an anomaly of the same pattern and magnitude as in the first case but with an opposite sign is used (i.e. $+1^{\circ}\text{C}$).

These two cases of experiments are designed to investigate the contrasting atmospheric response to SST anomalies that mimic observed patterns. The choice of magnitude, polarity and pattern of the anomaly is justified by various observational studies. For instance, the composite SST anomaly pattern compiled by Meehl (1987) demonstrated a coherent large-scale variation in the southern Indian Ocean. The anomaly area specified in this study over the Indian Ocean coincides with an area of relatively large standard deviations of monthly mean SST with values of about 1°C from May through July (Levitus, 1982). Cadet and Diehl (1984) found the SST anomaly for the

individual summer of 1956 (1972) was uniformly cold (warm) over this region with magnitudes of around 1°C .

In addition to the two basic experiments mentioned above, an additional experiment was also conducted to assess the sensitivity and linearity of the response magnitude to the anomaly strength for the cold anomaly case. The anomaly in this experiment is prescribed over the same area as in the above-mentioned cold case experiment but with a doubled magnitude. This enhanced negative anomaly case (designated as N2) is chosen to represent an enhanced "strong monsoon" scenario similar to those demonstrated by Meehl (1987) and Cadet and Diehl (1984).

The Student-t test as outlined by Chervin and Schneider (1976) was adopted to give an indication of the statistical significance of the experiment results. This statistical test provides insightful information with regard to the relative magnitude of the mean anomalous change in comparison with the natural variability (standard deviation) of a model and is also useful as a basis for comparisons between models and/or observations with different characteristic magnitudes of variability. It has been recommended in the MONEG report (1992) that the t-test be used as a standard test for model experiments. This classical approach has certain limitations, however, as it tests grid points individually and does not take into account the multi-dimensionality and the spatial correlation of the fields being tested. One should be cautious when considering the "field significance" (see discussions in Livezey and Chen, 1983).

The climatologically consistent features in the overall response patterns of the dynamically and physically interrelated processes may provide as yet another measure of the significance of the experimental results. The "physical consistency" between variables that represent the directly related physical processes may indeed indicate that the model responses would not be merely occurring by chance (see also discussions in Keshavamurty, 1982; Blasing, 1981). As it will become clear in the following analysis, the overall responses of the variables considered in our anomaly experiments do seem to vary in a physically consistent manner.

4. RESULTS

In this section results of the two basic cases (N1 and P1) of SST anomaly experiments are presented. In the discussion we focus our attention on the Asian monsoon region and the adjacent Indian Ocean area where the large-scale response patterns are most coherent and significant. There are some smaller scale features that are related to the topographic and wave type dynamics in the vicinity of the Tibetan Plateau and the area of the western Pacific along the east Asia coast. These features will not be discussed in order to focus on the large-scale responses directly related to the large-scale monsoon variations. Other features related to even larger scales will be discussed later. The anomalous responses are defined as the differences between ensemble averages of the experimental run and the control run for the summer season (June, July, August). Since the anomalous response features of positive SST anomaly experiments generally are similar in pattern but opposite in sign to the negative case, we will only discuss the results for the negative anomaly case in detail. The general characteristics of the positive anomaly case will then be briefly summarized in comparison to the negative case. Relevant observations are discussed wherever appropriate. The discussion for the case of the doubled negative anomaly will be given in section 5.2.

4.1 Hydrological cycle and atmospheric circulation responses

The precipitation anomaly for the case of the negative 1°C SST anomaly experiment (N1) is shown in Fig. 3. Areas where t-test values pass the 90% significance level are lightly shaded, and those that pass the 95% level are heavily shaded. A strong east-west oriented positive anomaly with a maximum of as much as 6 mm/day occurred over southeast Asia and extended westward to the Indian subcontinent and eastward to southern China and the western Pacific. An accompanying negative anomaly center with a maximum reaching up to 3 mm/day existed immediately to the south over the equatorial area and most of the southern Indian Ocean. Negative anomalies with similar magnitude also occurred in the area east of the

Philippines. The anomalous features are most statistically significant in southeast Asia and the equatorial area. The increase of precipitation in the areas around the Indian subcontinent and the decrease of precipitation in the southern Indian Ocean east of the Madagascar are also quite significant.

Fig. 4 shows the mean anomaly in the surface evaporation field. The most significant features are the decrease in evaporation over the southern Indian Ocean and the increase of evaporation over areas of the western and northern Indian Ocean and the South China Sea. The decrease of evaporation in the southern Indian Ocean appears directly related to the prescribed negative SST anomaly. The anomalous SST acted to reduce the surface saturation vapor pressure. The increase in evaporation in the western and northern Indian Ocean area is related to an increase in low level wind speed (see later discussion). There are also significant increases in evaporation to the northwest of the Australia and decreases to the east of the Philippines.

The 850 mb zonal wind anomaly is shown in Fig. 5. The westerly component of the southwest monsoon over the northern Indian Ocean is significantly strengthened. (Note that the areas where the pressure level is below the surface are blank in this figure and all subsequent figures.) The easterly component of the southeast trade is intensified in the Southern Indian Ocean between the latitude 10°S and 30°S. Within this region the zonal wind variability (standard deviation) is quite large which renders the t-test values small and thus statistically nonsignificant. However, the changes are physically consistent over a wide area with magnitude as large as 1 m/s.

The 850 mb meridional component of the wind shown in Fig. 6 indicates a general increase in the southerly flow over the northern Indian Ocean, which in conjunction with the increase in the zonal component, indicates an intensification of the southwest monsoon. Over the Arabian sea near the axis of the Somali jet, the northward wind speeds increased by up to 1 m/s. The strongest increases (>1 m/s) were near the longitude of 105°E. There is also a broad increase in southerly wind over the western half of the southern Indian Ocean. Although

anomaly features in most areas of the southern Indian Ocean did not pass the 95% significance criteria as did their counterparts over the northern Indian Ocean, they are consistent with the overall intensification of the low level monsoon flow which is composed of the southeast trades in the southern Indian Ocean, cross-equatorial flow near the equator, and the southwest monsoon in the northern Indian Ocean. The expected increase of the cross-equatorial flow along the east African coast is less clear in this figure, partially due to the shallowness of this anomalous near surface flow such that it would have been seen better at lower levels. For example, the vertically integrated low-level moisture transport, which includes contributions from the increases of winds below 850 mb level, shows a more distinct and significant increase as will be seen in Fig. 8. There is also an increase of the northerly wind in the eastern part of the southern Indian Ocean just west of Australia.

The zonal and meridional components of the low-level moisture transport vertically integrated from surface to 500 mb are shown in Figs. 7 and 8. The patterns bear strong resemblance to their low level wind counterparts at 850 mb. Important features are i) the consistent increase of westward transport in the southern Indian Ocean between 20-30°S latitudes (Fig. 7) associated with the consistent increase in the southeast trade winds shown earlier in Fig. 5 (smaller magnitude compared to those over the northern Indian Ocean is due to less moisture content in this area), ii) the significant increase of eastward transport north of the equator within the southwest monsoon (Fig. 7), iii) the broad increase of northward cross-equatorial transport along the western Indian Ocean which extends from the southwestern Indian Ocean east of Madagascar and maximizes near the core of Somali jet (Fig. 8), iv) the intensified northward transport near the 105°E longitude (Fig. 8).

The changes in atmospheric water vapor content (precipitable water) are shown in Fig. 9. Precipitable water is defined as the total water vapor content integrated over the entire atmospheric column. There is a general decrease in the southern Indian Ocean and in the region of the decreased rainfall in the subtropical western Pacific. Consistent with the

anomalous water vapor transports, the maximum increase occurs over the southeastern Asia. The precipitable water further northward along the eastern and western flanks of the Tibetan plateau is also significantly increased. These distribution features are closely related to those of the moisture transport and precipitation features shown earlier (cf. Figs. 8 and 3). These results indicate that the changes in moisture transport are important in influencing the distribution of both the atmospheric water vapor and the precipitation even in remote areas.

The changes in sea level pressure are shown in Fig. 10. Particularly noticeable is the decreased sea level pressure in the monsoon region over much of the Asian continent consistent with the anomalous precipitation pattern (cf. Fig. 3). Over the southern Indian Ocean where SST is decreased, particularly south of 15°S there is a broad increase in SLP of about 1 to 2 mb. These changes increase the strength of the Mascarene high and Australian high. The enhancement of the Mascarene High over southern Indian Ocean along with the deepening of the monsoon low over India and southeast Asia is consistent with the increased northward and eastward moisture transport by the low-level monsoon flow (cf. Figs. 7,8).

The model results for sea level pressure and rainfall compare well with the results of Cadet and Diehl (1984) who observed that a positive anomalous pressure of up to 1 mb occurred over the southern Indian Ocean in association with above normal monsoon rainfall and below normal southern Indian Ocean SST during the 1956 summer season. Quite similar features are also apparent in the 950 and 850 mb model height anomalies (not shown) which indicate consistent changes over the lower troposphere particularly for the eastern Asia. It is also interesting to note the study by Chervin (1989) who used a similar GCM model (a earlier version of the model used in this research) to examine the natural variability. His results suggest that part of the variance over southeast Asia may be related to the changes in the external conditions such as SST.

The change in geopotential thickness between the 950 mb and 200 mb levels (Fig. 11) reflects the change of the thermodynamic state (mean virtual temperature) within most of the total

atmospheric column and appears to be also related to the anomalous precipitation (i.e. latent heating) but with a larger overall spatial scale. Over the Asian continent, there is a broad scale increase in the geopotential thickness. This increase agrees in general with wide-spread increases of rainfall over Asian area. Stronger positive anomalies, however, occur more to the north with one situated to the east of the Himalayas maximizing near 125°E , 50°N and the other to the west around 80°E , 35°N . These two maxima are also associated with positive precipitation anomalies (cf. Fig. 3). Notice that the center near 80°E , 35°N may be overestimated as discussed before. It should also be noted that although the precipitation anomaly over southeast Asia is stronger than those further north, the response in thickness is stronger further north. This difference in response to the intensity of the precipitation anomaly (e.g.) may be attributed to the differences in characteristics of the geostrophic adjustment process in subtropics and extratropics. It is also noted that while smaller increase of thickness is associated with larger increase of precipitation in lower latitudes, the upper level divergence (shown later) is much stronger in these lower latitudes than that of the higher latitudes.

The increased thickness reflects the combination of the deepening of the surface monsoon low and the strengthening of the upper level high as manifested by, e.g. the 200 mb geopotential height (not shown). The geopotential height anomaly at the 200 mb level shows essentially the same pattern as the thickness field and indicates an increase of the large-scale geopotential height over Asian continent.

The 200 mb wind components (Figs. 12, 13) reflect a broadening and strengthening of the south Asian high. The upper level tropical easterly jet near the equatorial region has intensified (Fig. 12). The westerly wind on the northern side (north of 40°N) of the anticyclone has also intensified indicating a northward shift of the westerly jet. The most intriguing feature of the 200 mb meridional wind anomalies over the equatorial Indian Ocean area (Fig. 13) is the broad anomalous northerly flow over the equatorial Indian Ocean and South China Sea with maximum wind speeds up to 2 m/s. This is

very consistent with an anomalous thermally direct forced circulation associated with a strong positive precipitation anomaly over the Asian monsoon area north of equator and a generally negative precipitation anomaly south of the equator in the Indian Ocean (cf. Fig. 3). This anomalous southward cross-equatorial return flow at the upper level, together with the anomalous northward flow at the lower level (cf. Figs. 6, 8), manifests the three dimensionally coupled nature of the large-scale monsoon circulation. Over the southwestern Indian Ocean where the distribution of anomalous zonal wind is pretty much longitudinal, there is a strong convergence in the meridional wind. This appears linked to a downward vertical motion at 500 mb (shown later) and an intensification in the surface subtropical Mascarene high over this region (cf. Fig. 10). Notice that east-west wave type variation patterns occurred at higher latitudes in both hemispheres may indicate certain interactions of anomalous monsoon and middle and high latitude systems which is out of the scope of this study and not pursued here.

The MONEG (1992) group has suggested using the velocity potential at 200 mb as a basic diagnostic to represent the large scale changes in the upper level circulation. The potential function anomalies (Fig. 14) are negative over a banded area across India and southeast Asia indicating strong large scale anomalous divergence associated with the intensified rainfall over these regions. To the south of these regions, the positive anomalies indicate large-scale convergence over much of the southern Indian Ocean. This dipole structure is consistent with the high-level southward cross-equatorial flow (cf. Fig. 13) and, together with the low-level northward cross-equatorial flow discussed earlier, indicate a strengthened local Hadley (meridional) component of the monsoon circulation. The smaller scale convergence near 90°E , 30°N appears to result from the stronger rainfall and upper level divergence anomalies in the surrounding areas. This convergence coincides with a weak negative rainfall anomaly (cf. Fig. 3) and a weak downward motion at 500 mb (see later discussion).

The vertical motion field at 500 mb (Fig. 15) shows a band of stronger upward motion from the northern Indian Ocean to the western Pacific

including India and southeast Asia. Intensified downward motion occurs over the equatorial Indian Ocean, southwestern Indian Ocean to the east of Madagascar Island and the Australian continent. The upward motion over the southeastern part of the southern Indian Ocean appears to be related to slightly increased precipitation which in turn related to an anomalous northerly wind (cf. Fig. 8) that brings more moisture from lower latitudes into this region. As a result both temperature and humidity in the low levels are higher than normal over this region (not shown).

4.2 Overall systematic response

The above detailed analysis of the individual atmospheric component responses to the imposed SST anomaly in fact reveals a systematic change in the whole monsoon system. This overall response becomes more obvious if these anomalies are put into the context of the mean seasonal background state of the Asian summer monsoon system. Fig. 16 shows the three-dimensional mean climatological monsoon system configuration during the northern summer. As a complement of Fig. 1 which highlights the underlying coupling mechanisms, this figure is intended to show more detailed climatological flow patterns and component circulation systems in the upper and lower levels. This picture provides a convenient reference framework within which interconnections or interactions among the anomalous responses of various components of the system can be understood more easily. The prominent climatological components and salient features shown in the sketch are:

- (1) the surface Mascarene high (MH) and Australian high (AH) in the southern subtropics associated with large scale downward motions.
- (2) the southeast trades (SET) in the Southern Hemisphere and cross-equatorial flow (particularly, the Somali jet near the eastern African coast and the southerly jet near 100°E),
- (3) the southwest monsoon (SWM) over the northern Indian Ocean and the southeast monsoon (SEM) in the west Pacific related to the western Pacific subtropical high (westward extension of the north Pacific subtropical high, NPSH, in the eastern north Pacific),

(4) the monsoon low (ML) and the associated upward motion,

(5) the upper-level South Asian high (SAH) with the mid latitude westerly jet to the north and the tropical easterly jet to the south,

(6) the cross-equatorial return flow which connects to the downward motion in the Southern Hemisphere and forms the upper branch of the local Hadley type component of the monsoon circulation.

With the help of this framework, the overall anomalous response of the monsoon system to the negative SST forcing in the southern Indian Ocean can be succinctly recapped in the following: an intensified Mascarene high, stronger southeast trade in the southern Indian Ocean, stronger cross-equatorial flow and stronger southwest monsoon in northern hemisphere, increased surface evaporation along the path of the increased low level flow and subsequent moisture transport, increased monsoonal rainfall and upward motion over the area of Asian monsoon low, enhanced upper level anticyclone and tropical easterly jets, enhanced upper level return flow from the northern hemisphere that connects to the increased downward motion in the southern subtropical low level anticyclonic circulation system (Mascarene high). This series of changes thus indicate a strengthening of the overall monsoon activities. Consistent with the physical processes highlighted in Fig. 1, these systematic anomalous changes with one linked to another tend to reinforce the climatological mean circulation suggesting a positive feedback within the atmosphere triggered by the negative SST anomaly in the southern Indian Ocean.

It should be noted that the SST anomaly exhibited both local and remote effects on the atmosphere, e.g. the local intensification of the Mascarene high and southeast trades in the Southern Hemisphere and the remote impact on the increased rainfall in the Northern Hemisphere. The LHC plays an important role in the remote response of the atmosphere (in this case, to the SST anomaly in the southern Indian Ocean) by the way of increasing the evaporation and the moisture transport which resulted in precipitation increase in the Asian monsoon area. Due to the systematic changes in the LHC, an anomalous amount of latent energy is collected over a large area of ocean.

subsequently transported over long distance and finally released over more confined areas. Through these processes, SST impacts are realized in remote areas resulting in a "teleconnection" type of air-sea interaction.

This structure of atmospheric response to the external forcing due to a SST anomaly shares some similarities with the structure of the internal atmospheric variability discussed in Zhu (1993). Specifically, anomalous responses in the negative SST experiment and intensification episodes of the summer monsoon in the control simulation are both characterized by a stronger Mascarene high with enhanced descending motion, stronger cross-equatorial moisture transport, a deeper monsoon low with enhanced ascending motion and heavier rainfall. The presence of the negative SST anomaly in the experiment appears to enhance or reinforce the internal mode of variations (i.e. the couplings of the hydrological cycle and atmospheric circulation existed in the control simulation). More discussion on this will be given in section 5.1.

The atmospheric response to the positive SST anomaly experiment is largely opposite to that of the negative SST anomaly, if one focuses on the larger scale features. The main features of the positive anomaly case (P1) can be summarized (within the same framework outlined above) as the following (figures omitted due to limited space):

(1) decreased precipitation over most of the northern Indian Ocean and the Indian and southeast Asian subcontinents as well as the adjacent South China Sea areas, increased precipitation over most of southern Indian Ocean with a maximum center just south of the equator near the longitude of 100°E,

(2) decreased evaporation in the northern Indian Ocean and South China Sea, and increased evaporation in the southern Indian Ocean,

(3) general increase in sea level pressure over most of the Asian continent and decrease over most of the southern Indian Ocean including the Mascarene high area,

(4) reduced low-level monsoon westerly flow over the northern part of the Indian Ocean and reduced trade easterlies near the Mascarene high,

(5) southward cross-equatorial flow anomaly over most of the equatorial Indian Ocean except near coast of Africa,

(6) a broad scale decrease of the thickness between 200 mb and 950 mb levels over mid latitude Asian area, a broad band moderate increase over the equatorial region besides a smaller scale increase over an area near 100°E, 25°N,

(7) reduced upper-level tropical easterly jet and reduced mid latitude westerly jet to the north of the climatological Tibetan High,

(8) a reversed return flow anomaly in the upper-level over large portion of the Indian Ocean,

(9) reversed upper-level divergent flow pattern comparing to the negative case,

(10) widespread anomalous ascending motion over the southern Indian Ocean and strong descending motion over India and southeast Asia as well as the adjacent waters over the Bay of Bengal and South China Sea.

These anomalous features for the positive SST anomaly case constitute a reversed anomalous local Hadley type circulation which is most consistent over the Indian Ocean area and the southern part of the Asian continent. However, the overall significance appears to be less than that of the negative case. The changes in the northern mid latitude and west Pacific areas are more complex where wave-like structures with alternating signs are apparent, possibly caused by the nonlinearity of the wave dynamics prevailing in these areas.

Two additional points are worth mentioning. First, the local and remote impacts of an SST anomaly are clearly related. The SST anomaly may induce direct local changes in the evaporation and low-level circulations, while the subsequent remote response as described earlier may reinforce the local response through systematic changes in the anomalous Hadley circulation such as occurred in the negative anomaly experiment. The results presented here represent the net overall effects of an SST anomaly. Secondly, the SST anomalies in the experiments were kept constant and therefore were not allowed to interact with the subsequent atmospheric responses. The evolution of the SST anomalies themselves under the influence of the changes in the atmosphere originally induced by the SST anomalies (i.e. the realistic

two-way interaction between SST and the atmosphere) can not be examined in these experiments and will depend on how the changes in the atmosphere, in turn, impact on the processes that determine the SST changes, e.g., surface heat fluxes and surface wind stresses. Later in the next section, we will include a discussion about possible implications for two-way interactions from the experiment results.

5. DISCUSSION

In this section, we will discuss further some of our experiment results and their implications. We try to put these discussions into the perspective of the basic framework of the climate study and into the perspective of a broader spectrum of related climate studies. In so doing we hope that it will be helpful for understanding the current experiment results and some of the fundamental aspects of the climate system variations.

In section 4.2 we described the physics of the variations of the monsoon system relevant to the Indian Ocean SST anomaly experiments. We further discuss these experiments in relation to the physics of the climatological variations in the corresponding control simulation described by Zhu (1993). The issue of the background state climatology and the forced response anomalies are highlighted. The relationship between the strength of the SST anomaly and the response magnitude is illustrated based on the results of our doubled negative SST anomaly experiment case (N2). Changes in the net surface heat flux in the fixed SST anomaly experiments (N1 and N2) and their implications for a coupled atmosphere-ocean system are discussed. A possible global response and connection to the ENSO phenomenon will also be discussed. The issue related to multiple causes of monsoon variability is discussed by comparing our experiment results with those of Barnett et al. (1989).

5.1 Basic State Configuration and Anomalous Response

Several authors have stated that realistic simulation of the seasonal cycle is crucial even in cases where only the anomalous variations

are of major interest, such as in the case of SST anomaly experiments (Wilson and Mitchell, 1987; Boer, 1989; Kleeman, 1991; Legates and Willmott, 1992). Our current study can serve as an example in illustrating this important point. For instance, from a physics standpoint, the remote impacts of our prescribed SST anomaly are clearly dependent upon the particular mean seasonal climatological configuration of the circulation system in the Indian Ocean and Asian monsoon areas, particularly the low-level flow pattern. This is because that, to a large extent, these remote impacts are dependent on the large-scale water vapor transport, which in turn strongly dependent upon the basic flow pattern.

Zhu (1993) has shown the characteristic variations ("natural modes") of the model hydrological cycle and circulation components and has identified close relationships between these components when simulated under the normal climate conditions (represented by the long-term mean seasonal variations of solar radiation cycle and SST distribution). These characteristic variations and relationships are very important for understanding the anomalous responses ("forced modes") to SST anomaly forcing because they serve as an important background or basic state configuration upon which the anomalies of various related physical variables interact with one another. As will be clear, the anomalous response is dependent on the mean background configuration. Particularly, geographical structure and strength of the monsoon circulation system will be an important factor in determining how the "anomalous signal" (SST impact) will be "transmitted" and where the major influence areas will be located.

In the negative anomaly case, the impact of the SST anomaly in the southern Indian Ocean is reflected locally in the changes of the low level southeast trade winds and the surface Mascarene high pressure system. These changes are interconnected with changes in monsoon flow and the changes in evaporation and moisture transport along the path of the mean seasonal flow leading to remote changes in Asian monsoonal rainfall in the Northern Hemisphere. Consider the case where the characteristic seasonal mean low level flow is not reasonably simulated as directed from the

southern Indian Ocean towards the Asian monsoon region as observed. Then the path along which the moisture is transported ("signal transmission") would be different than what it should be and the area of precipitation change ("influence area"), as a direct result of the moisture transport, would also be in error.

In the same way, consider, for instance, the winter monsoon situation where the seasonal mean low-level flow is directed from the northern continent towards the southern ocean. In this winter monsoon case, the response to the same negative SST anomaly (prescribed in the southern Indian Ocean) will be totally different because the low level circulation and the associated moisture transport is almost reversed from the summer monsoon situation. (Note here the moisture transport can be thought of as a process of signal transmission with regard to the remote effects of the SST anomaly, where moisture represents the signal and the low-level flow is the carrier.) In other words, the "physics of the anomalies" which we discussed in the last section (i.e. the consistent overall anomalous Hadley type responses that consist of systematic changes in each of the related components) are closely related to the mean seasonal characteristics of the monsoon system determined by what, in contrast, might be called "physics of the normals" (or climatology).

Characteristics of the atmospheric responses ("forced modes") to the external forcing (e.g. negative SST anomaly) also may be related to the enhancements of some "natural modes" of internal variability that occur in the normal condition (e.g. control simulation without anomalous forcing). This can be seen, for instance, in the negative SST anomaly case where the anomalous hydrological cycle components are enhanced in a self-consistent way similar to the "normal" climatological variations in the control simulation as shown in Zhu.(1993). This similarity can be understood because in both cases the large-scale hydrological cycle serves as the interactive agent that results in systematic overall variations of the monsoon circulation. However, there are also some differences in the way the system components are coupled to each other. In the control simulation, the evaporation over the whole Indian Ocean is increased when the overall monsoon circulation is intensified. On

the other hand, in the negative SST anomaly case, the evaporation increases in the northern part of the Indian Ocean but decreases in the southern part of Indian Ocean where the SST anomaly is prescribed. This difference can be attributed to the dependence of the oceanic surface evaporation on both the low-level wind and SST as explained below.

In the control simulation, the SST is prescribed according to mean climatological seasonal variation. Therefore the variations in surface evaporation result solely from the changes in the low-level wind, humidity and air temperature. In the anomaly experiment, the variations in evaporation result from a combination of the external SST changes and the internal atmospheric changes, most importantly low-level wind. The relationship of a stronger surface evaporation over the northern Indian Ocean with a stronger monsoon circulation holds both in the control simulation (Zhu, 1993) and the negative SST anomaly experiment in this study. On the other hand, over the southern Indian Ocean evaporation actually decreases in the negative SST case because the increase in low-level wind (that would have increased the evaporation) is offset by the decrease in SST.

Note further that the prescribed SST anomaly in our experiments can be thought of as representing an interannual variation of SST, to a first degree of approximation, held constant (or effectively "vary" very slowly) within the summer season consistent with the longer response time scale of SST. Thus the results of our anomaly experiments can have implications with respect to the interannual air-sea interactions (see further discussion in section 5.3).

5.2 Atmospheric Response and SST Anomaly Strength

In an attempt to assess possible differences in atmospheric response to a "strong" SST anomaly scenario vs. a "normal" SST anomaly scenario, we conducted an experiment (N2) with a doubling of the SST anomaly used in the negative anomaly case (N1) discussed earlier. The results of the N2 case will be discussed here in comparison to the N1 case.

The positive evaporation anomaly of the N2 case in the western Indian Ocean near the coast of Africa and in the Arabian Sea is nearly double that in the N1 anomaly case. The positive precipitation anomaly is increased slightly in southeast Asia and extended further west. Over southern India and the adjacent waters, it is nearly double that of the N1 case. The negative rainfall anomaly over the equatorial Indian Ocean remains about the same but also extends further west. The negative rainfall anomaly within the Mascarene high area in the southwestern Indian Ocean is nearly doubled. The sea level pressure anomaly over the Asian continent is slightly reduced, but the anomalous Mascarene high is nearly doubled. An anomalous high pressure center, not present in the N1 case, now appears near 25°N, 150°E which probably results from the increased rainfall and upward motion in southeast Asia and the adjacent waters just to the west. The easterly anomaly in the southeast trade wind belt is nearly doubled while the westerly anomaly near the south coast of the Asian continent is reduced. The southerly anomaly is stronger over a large area in the southern Indian Ocean.

In general, the overall pattern especially in the near-field responses (i.e. the tropical and subtropical areas closer to the prescribed SST anomaly) remains similar to those of the N1 anomaly case with nearly doubled magnitude. The dipole pattern of precipitation anomalies over the southern part of the Asian continent and equatorial area is very robust. The low-level anomaly intensified mostly over or near the prescribed SST anomaly area, so did the precipitation across the northern Indian Ocean and the two subcontinents. These results indicate a basic linearity in terms of the intensity of the atmospheric response in relation to the strength of the SST anomaly. (Notice that the generally opposite responses to the opposite SST anomalies found in the cases N1 and P1 discussed earlier also imply a linearity.) For the far-field responses over the eastern Asian coast and the western Pacific, the changes both in pattern and magnitude reflect more complex nonlinear interactions of the internal dynamics.

5.3 Surface Fluxes and Physics of Biennial Variations

One of the most interesting features of model response lies in the evaporation anomaly field over the Indian Ocean which appears to be relevant to the interannual variability in SST observed in that region. In the negative SST anomaly case, positive evaporation anomalies occurred over western and northern Indian Ocean extending to South China Sea in contrast to the negative evaporation anomaly in the area of the reduced SST over southern Indian Ocean (Fig. 4). The one point correlation map of Newell and Wu (1992), computed from the observed monthly SSTs, shows a very similar coherent variation pattern in the areas extending from the western and northern Indian Ocean to the South China Sea. This indicates that the SST within these areas tends to vary consistently in time. As shown in Fig. 16, these areas are strongly influenced by the intense low-level monsoon flow. Systematic variations of the low-level wind in these areas would strongly impact on the evaporative cooling process at the surface and the dynamic upwelling process within the ocean (see also discussion in Joseph and Pillai, 1987) and thus could provide a explanation for the coherent spatial distributions of the observed SST variation. In our negative anomaly case, the positive evaporation anomaly mentioned above is indeed accompanied by the strengthened low-level monsoon (see e.g. Figs. 5, 6, 7, 8), although the upwelling process is absent in the model.

The anomalous net surface heat flux into the ocean in the model shows an almost identical distribution (Fig. 17) to that of the evaporation anomaly for the same negative SST experiment case shown in Fig. 4. Evaluations of each individual component of the total flux (i.e. latent and sensible heat, solar and infrared radiation) indicated that the latent heat flux is the dominant component with the other three about an order of magnitude smaller. A reversed pattern is seen in the positive SST anomaly case (not shown). These results indicate that the changes in evaporation contribute the most to the net surface heat flux changes in the model.

The above analyses have important implications regarding to air-sea interaction in a coupled ocean-atmosphere system, where the SST will respond to a change in the net surface heat flux. For an idealized 50 m mixed layer ocean, given an initial SST anomaly such as that

prescribed in negative SST anomaly experiment case, a negative (positive) surface heat flux anomaly of about 40 (20) W/m^2 over the southern (northern) Indian Ocean would produce a SST change of about $+1^\circ\text{C}$ (-0.5°C) in the southern (northern) Indian Ocean during the course of three months of the summer monsoon season. Thus, on a seasonal time scale, the atmospheric response as a result of the initial SST anomaly appears to be capable of generating a negative SST anomaly of -0.5°C in the northern Indian Ocean where there is no SST anomaly initially, and damping or even reversing the -1°C SST anomaly initially existed in the southern Indian Ocean.

If the above mixed layer ocean argument holds at least to a first order approximation, the net surface heat flux will serve as a negative feedback mechanism that could gradually reduce the magnitude of SST anomaly or even reverse the sign of the original SST anomaly if the process for a particular monsoon season is unusually strong or prolonged or vice versa. This scenario appears consistent with observational evidence showing a coherent north-south dipole pattern of SST anomaly in Indian Ocean (Weare 1979, Deng et al. 1989, Newell and Wu, 1992). Joseph and Pillai (1987) and Meehl (1987) both indicated a 2-3 year cycle of interannual variation of SST in the Indian Ocean.

It is important to note the similarities and differences between the feedback mechanism discussed here and the natural mode of internal variations discussed briefly in section 5.1 and more detailed in Zhu (1993). In both cases, the large-scale hydrological cycle have played an essential role in the enhancement of the overall Hadley type summer monsoon circulation through the interrelated changes in its component processes, i.e. the evaporation, transport and precipitation. In the negative (positive) SST anomaly experiments, the seasonal mean overall monsoon strength is enhanced (weakened) associated with increased (decreased) evaporation over Indian Ocean, increased (decreased) northward transport of moisture from the ocean to the Asian continent, and increased (decreased) precipitation in the monsoon region. Similarly, in the control simulation, the dominant (natural) mode of internal monsoon system oscillation experiences

enhanced (weakened) variation associated with increased (decreased) evaporation, transport and precipitation. However, in our anomaly experiment, the enhancement of the large-scale hydrological cycle and hence the monsoon circulation are essentially set up or controlled by the negative (positive) SST anomaly operating on an interannual time scale (consider the negative and positive anomaly experiment cases as years of colder SST and warmer SST respectively). This scenario is consistent with the longer response time scale of the oceanic system. On the other hand, in the control simulation, the enhancement or weakening of the hydrological cycle and monsoon circulation are basically a type of coherent internal system oscillation on the intraseasonal time scale consistent with the shorter response time scale of the atmospheric system. Furthermore, in both experiment and control cases, the way in which the large-scale hydrological cycle impacts on the monsoon circulation strongly depends on the basic state configuration (as discussed in section 5.1) which has a seasonal time scale. The analyses of both the anomaly experiments and the control simulation clearly showed strong interactions among the large-scale monsoon circulation, hydrological cycle and SST, among the intraseasonal, seasonal and interannual variations within the atmosphere-ocean climate system due to differences in the response time scales of each component of the system. This should serve as a useful framework for the understanding of the monsoon system variations.

It should be remembered, however, that the above discussion is based on the idealized anomaly experiments that allowed only one-way interaction. When the two-way interaction is considered, the SST anomaly itself will evolve with time as it adjust to the subsequent changes in the atmosphere. For instance, Clemens et al. (1991) argued that the colder SST in the southern subtropical Indian Ocean is associated with greater evaporation and strengthened monsoon circulation suggesting a positive feedback. Yet, Hageberg and Mix (1991) indicated that in a complex interactive monsoon system it is difficult to discern the cause and effect. As we pointed out earlier in section 5.2, while the increased low level wind may increase the surface evaporation, the decreased SST may counteract this tendency. This interaction is

also location dependent. Further investigation in coupled atmosphere-ocean models is needed to pin down the uncertainties.

5.4 Anomalous Response in Eastern Pacific

Another interesting feature of the current model experiments is the indication of a remote response in the southeastern Pacific area where changes in atmospheric conditions lead to changes in the surface evaporation thus moisture supply from the ocean to the atmosphere. In the negative Indian Ocean SST anomaly case, there was an intensification of the southeastern Pacific subtropical high with an intensified low level anticyclonic circulation and increased evaporation on the east side of the subtropical south Pacific high. These anomalies suggest a physical link between the changes in convective activity over the Asian monsoon area and the changes in sea level pressure in the southeastern Pacific. What is intriguing is that the anomalous evaporation pattern just mentioned resembles the one point correlation map of SST variation by Newell and Wu (discussed above) in that same area. This may indeed indicate one of the potential mechanisms which provides at least a partial physical explanation of the observed in-phase variations of SST in the western and northern Indian Ocean with SST along the equatorial eastern Pacific and areas southward into the subtropics (to the west of the South American coast) as have been identified by Newell and Wu (1992). An interpretation of this observed pattern is that the changes in the monsoon intensity may in fact be related to the intensity of the south Pacific subtropical high and the surface trade winds over the eastern equatorial and subtropical Pacific area.

There is much observational evidence to support the interpretation of the modeling results just presented. For instance, piecing evidence shown in Meehl (1987), Joseph and Pillai (1987), Yasunari and Seki (1992), Shen et al. (1991) and Zebiak and Cane (1987) together, they indicate a near simultaneous development of negative SST anomaly in the western and northern Indian Ocean and in the area of eastern Pacific along the western coast of South America and the equatorial region, during and just after northern summer in a strong monsoon year (corresponding to our negative anomaly case with cooling of SST over western and

northern Indian ocean during the summer, cf. Fig. 18). Yasunari and Seki (1992) showed that strong surface easterly anomalies existed near the equatorial region across the Pacific from about 150°W to about 130°E in July and August based on strong/weak monsoon composites using long term observations. These easterly anomalies tend to persist even into November. Using COADS data from 1956 to 1985, Ropelewski et al. (1992) showed an out-of-phase relationship of the surface zonal wind anomalies between the Indian Ocean and Pacific Ocean basins (e.g. a westerly anomaly in the Indian Ocean and an easterly anomaly in the Pacific) and a tendency of the sign of the anomaly to alternate from year to year. A similar situation is also true for 200 mb winds. They also indicate that this pervasive biennial pulse is related to the Southern Oscillation. The surface wind anomalies would be instrumental to ENSO development through their forcing of oceanic Kelvin waves and upwelling/downwelling, which in turn may act to reinforce the anomalies in surface heat fluxes induced by the wind anomaly, all closely related to the variations in the monsoon and Walker circulation (Wyrtki 1975, Barnett et al., 1989).

We contend that these systematic changes in low-level wind, evaporation, water vapor transport, and SST are the key factors and that they are all intimately related to the Asian summer monsoon oscillation (ASMO) and ENSO variabilities. While the moisture transport is certainly a key link between the surface evaporation over these remote oceanic areas and the monsoon rainfall over the wide area encompassing the Asian monsoon region and the western Pacific, the return flow from the latter area as manifested by the Hadley and Walker type circulation is another key link between these remote areas in the upper level.

It is interesting to note the ENSO variability has a strong tendency to be "phase-locked" with the seasonal cycle (e.g. Philander, 1990, Zebiak and Cane, 1987, Lau, 1992). One possible explanation for this tendency may indeed lie in the strong dependence of the amplifying effects of the large-scale hydrological cycle on the particular seasonal mean circulation pattern as discussed in sections 5.1, 5.3. As the season changes, the mean circulation pattern changes which may render the interactions involving

hydrological cycle circulation less effective. Presumably, during a strong monsoon year summer when the trade winds over the Pacific basin are strong, more water vapor is transported towards the Asian monsoon region resulting in more monsoonal precipitation. The overall enhancement of the monsoonal convective activity will feedback on the large scale circulation, perhaps, in a similar way as was highlighted earlier and thus lead to further intensification of the Pacific trades. This scenario is supported by the observations of Li et al. (1987) and Yasnari and Seki (1992). This again highlights the potential importance of water vapor as an active messenger or amplifier for the observed climate system "teleconnection" and the atmosphere ocean coupling. Further research emphasizing the central role of water vapor in the interacting climate system is definitely needed both in terms of real observational analysis and climate modeling to verify the links such as suggested here and clarify the many uncertainties that still exist.

5.5 Multiple Causes of Monsoon Variations

There is mention of the possibility of multiple causes of monsoon variations in the literature, e.g. Barnett et al. (1989). Here we will compare their snow-monsoon experiments with our SST-monsoon experiments to shed some light on this issue.

Barnett et al. (1989) investigated the effect of the variations in snow depth over the Eurasian continent during the previous winter on the monsoon variations in the following summer. They demonstrated an apparent snow-monsoon relationship with results from four pairs of integrations (from January through August) of the ECMWF GCM in which the premonsoon season snowfall rate was halved or doubled starting from four different years of the control run. The similarity of our experiments with positive or negative SST anomaly to their experiments with doubled or halved snowfall rate appeared to support the possibility of multiple causes for the summer monsoon variability.

In comparing our experiments with those of Barnett et al. (1989), similarities can be illustrated by comparing their halved snowfall

rate experiment and our negative SST anomaly experiment, both of which corresponds to the "strong monsoon" scenario. In their experiment with winter time snowfall rate halved, the following summertime monsoon is intensified (classified as a good monsoon year). The precipitation rate in these cases increased over the western Pacific (about 3 mm/day). Qualitatively this compares well with our results for the negative SST anomaly case both in terms of the anomaly pattern and its strength. The 200 mb zonal wind anomaly in their halved snowfall rate experiment showed an increase of up to 3 m/s in the tropical easterly jet and an increase of up to 2 m/s in the westerly jet to the north, whereas our results for the negative SST anomaly case showed the same pattern and strength of the anomaly with slightly more northward (southward) positioning for the westerly (easterly) jet. The anomalous sea level pressure over much of Asia both in their and our model is lower than normal, although their response appears too strong as compared to both the observed and our results. Their results showed an increase of surface temperature of up to 2°C over the Tibetan plateau and most of the east Asian continent whereas ours showed a similar pattern with slightly smaller amplitude (up to 1.4°C). The net surface heat flux also showed qualitative agreement over the east Asian continent and the adjacent ocean although their model has more sophisticated ground soil treatment.

These comparisons indicate that similar anomalous monsoonal states can be potentially caused by different processes, e.g. snow depth anomaly in Barnett et al. (1989) or SST anomaly in our experiments. This may be of importance to another aspect of the climate system: triggering-mechanism related to the monsoon-ENSO relationship. As shown by Barnett et al. (1989), a weak El Nino signal developed when an ocean model was driven by the model wind output from the heavy snow experiment (poor monsoon situation). A much stronger El Nino occurred in the Pacific in their corresponding coupled ocean-atmosphere model experiment (with a doubled snowfall rate). This result clearly demonstrates the importance of the atmosphere-ocean coupling in El Nino simulation. It also indicates an apparent triple interaction of snow-monsoon-El Nino. Based on the similarities of the anomalous monsoonal

responses induced by the anomalous snowfall and SST, there is likely an Indian Ocean SST-monsoon-El Nino triple connection similar to those shown by Barnett et al. (1989). However, the analogy made here should be treated with care as more quantitative evaluations and comparisons, if possible, are needed for a more firm answer. On the other hand the monsoon-ENSO relationship does seem to be supported by the observations as discussed earlier (see also discussions in Barnett et al. 1989).

In summary, based on the detailed analysis of various related fields and comparisons with observation analyses and other simulation studies, our analysis of the simulated large scale hydrological cycle and its changes in the context of anomaly experiments indicates the crucial importance of water vapor in climate system interactions and has documented relevant mechanisms which may play an important role in producing observed monsoon variability and possible links to ENSO.

6. CONCLUSIONS

The major purpose of this study is to examine the catalytic role of water vapor in the climate system, and the relationships and interactions between the large-scale hydrological cycle components, the Asian monsoon circulation, and the SST variations in the Indian Ocean. A combined approach of first examining the natural (internal) variations of the hydrological cycle and circulation in the absence of anomalous (external) forcing (discussed in Zhu, 1993) and then assessing their responses to anomalous SST forcing (in this study) is used to investigate the potential physical mechanisms responsible for the large-scale climate variations related to the hydrological cycle.

This study demonstrated the essential role of LHC in the atmospheric response in the Asian monsoon region to SST anomalies in the Indian Ocean area. Idealized SST anomaly experiments have been used to test the hypothesis that the corroborative variations in the large-scale hydrological cycle and circulation components serve as an internal feedback mechanism influencing the response of the Asian monsoon to an external forcing exerted by SST anomalies in the Indian Ocean.

The SST anomalies were chosen to mimic the major observed features of SST variation in the Indian Ocean area with magnitudes characteristic of the observed.

The results of the anomaly experiments show that, for a negative SST anomaly in the southern Indian Ocean, there are local responses including the intensification of the subtropical high and trade winds in the southern Indian Ocean and remote responses which include increased monsoon flow with increased moisture transport, and increased precipitation over the monsoonal area. The overall anomalous Hadley type circulation tends to reinforce the mean seasonal monsoon circulation resulting in a strong monsoon year scenario similar to what has been observed by Meehl (1987). The systematic changes in LHC are clearly responsible for the remote atmospheric responses to the prescribed SST anomaly. For the contrasting positive SST anomaly case, the changes described above are generally reversed resulting in a weak monsoon scenario.

These experiments highlight the catalytic role of water vapor as a messenger and enhancer which is responsible for larger scale remote atmosphere-ocean coupling, and as a feedback mechanism that activates the various linkages within the hydrological cycle. These experiments indicate that the internal intraseasonal coupling between the hydrological cycle and circulation, which is revealed by the EOF and correlation analyses of the control simulation in Zhu (1993), can have strong impacts on the longer time scale atmospheric variations when the coupling processes are enhanced or reduced by the presence of a persistent external forcing (in this case, the negative or positive SST anomalies). The prescribed SST anomalies used in the experiment are representative of the interannual variations of the SST in the southern Indian Ocean. Results of these experiments show that the interannual SST anomaly can produce systematic changes in the atmospheric circulation characteristic of the observed interannual changes in the Asian monsoon activity.

Evidence also shows that these SST anomalies could be strongly modified or even reversed due to anomalous changes in surface

heat fluxes (cf. Fig. 18 and discussion in 5.3). These changes appear to hint a type of self-repeating process in the coupled climate system where the monsoon circulation will exhibit interannual variations due to a certain SST anomaly, while the SST anomaly itself is reversely changed due to the interplay between circulation, SST and hydrological cycle process variations highlighted earlier. However, much needs to be done before the complex nature of the large-scale atmosphere-ocean interaction is fully understood.

The SST anomaly experiments indicate an important and direct role for the Indian Ocean to impact on the overall Asian monsoon variability. Furthermore, this SST-induced monsoon variability may also have the potential to trigger ENSO type climate variations in the same way as that indicated by Barnett et al. (1989).

The present experimental results are quite consistent with observations and strongly suggest a feedback mechanism responsible for the monsoonal variations that involves the large-scale hydrological cycle. Since the current model (CCM1) contains relatively crude representation of physical processes (e.g. cumulus convection), we emphasize only some general features of the large scale processes. Nonetheless, the results have provided clear insights into the importance of LHC and how the LHC might interact with the atmospheric circulation.

Similar experiments and analysis using improved models such as CCM2 with better physics and finer resolution would be desirable. This will be helpful in answering questions concerning the more detailed regional features such as rainfall distribution over India and the potential global coupling responsible for the monsoon-ENSO connection. A coupled atmosphere-ocean model will be essential in determining the evolution of a realistic two-way interaction which includes oceanic mixing, advection and wave processes. It should also be pointed out that this research is focused on the atmospheric branch of the large-scale hydrological cycle that is directly related to the latent heating and the subsequent dynamic effect of the water vapor. Other related processes such as land surface hydrology, biological

evapotranspiration processes and cloud-radiation interactions can be important and should be included in a more complete study.

Observational study regarding these issues is also crucial. It provides not only a basis for model verification but also useful guidance for model experiment design. Model simulations will help the interpretation and/or further refinement of observational analysis. Clearly a combined observational analysis and model experiment approach will be instrumental in the further understanding of climate variations and interactions.

Acknowledgments

This research was supported by National Science Foundation Grant ATM-8902849. Dr. Robert Gallimore and Ms. Linda Keller provided useful comments on interpretation of results. Also helpful were stimulating discussions on science with Dr. Pao K. Wang. We also like to thank Mr. David Lubin for helping with the final figures. Numerical calculations were performed at the Scientific Computing Division at the National Center for Atmospheric Research, which is supported by the National Science Foundation.

References

- Barnett, T. P., L. Dumenil, U. Schlese, and E. Roeckner, and M. Latif, 1989: The effect of Eurasian snow over on regional and global climate variations. *J. Atmos. Sci.* **46**(5), 661-685.
- Boer, G. J., 1989: Concerning the response of the atmosphere to a tropical sea surface temperature anomaly. *J. Atmos. Sci.*, **46**, 1898-1921.
- Bourke, W., 1974: A multi-level spectral model. I. formulation and hemispheric integrations. *Mon. Wea. Rev.*, **102**, 687-701.
- Blasing, T.J., 1981: Characteristic anomaly patterns of summer sea-level pressure for the Northern Hemisphere. *Tellus*, **33**, 428-437.

- Cadet, D. L., 1983: The monsoon over the Indian Ocean during summer 1975. Part II: break and active monsoons. *Mon. Wea. Rev.*, **111**, 95-108.
- _____, 1984: Interannual variability of surface fields over the Indian ocean during recent decades. *Mon. Wea. Rev.*, **112**, 1921-1935.
- _____, and B. C. Diehl, 1984: Interannual variability of surface fields over the Indian Ocean during recent decades. *Mon. Wea. Rev.*, **112**, 1921-1935.
- _____, and G. Reverdin, 1981: Water vapour transport over the Indian Ocean during summer 1975. *Tellus*, **33**, 476-487.
- Chervin, R. M., 1986: Interannual variability and seasonal climate predictability. *J. Atmos. Sci.*, **43**, 233-251.
- _____, and S. H. Schneider, 1976: On determining the statistical significance of climate experiments with general circulation models. *J. Atmos. Sci.*, **33**, 405-412.
- Clemens, S., W. Prell, D. Murray, G. Shimmield and G. Weedon, 1991: Forcing mechanisms of the Indian Ocean monsoon. *Nature*, **353**, 720-725.
- Deardoff, J. W., 1972: Parameterization of the planetary boundary layer for use in general circulation models. *Mon. Wea. Rev.*, **100**, 93-106.
- Deng, A., S. Tao and L. Chen, 1989: Temporal and spatial distributions of the SST in the Indian Ocean and its relationship with the precipitation in summer monsoon season in China. *Chinese J. Atmos. Sci.*, **13**, 401-410.
- Findlater, J., 1969: A major low-level air current near the Indian Ocean during the northern summer. *Quart. J. Roy. Meteorol. Soc.*, **95**, 362-380.
- Hagelberg T. and A. C. Mix. 1991: Long-term monsoon regulators. *Nature*, **253**, 703-704.
- Hastenrath, S and P. J. Lamb, 1980: On the heat budget of hydrosphere and atmosphere in the Indian Ocean. *J. Phys. Oceanogr.*, **10**, 694-708.
- Hoerling, M. P., T. K. Schaack and Donald R. Johnson, 1990: Heating distributions from January and July Simulations of NCAR community climate models. *J. Climate*, **3**, 417-434.
- Hoskins, B. J. and A. J. Simmons, 1975: A multi-layer spectral model and the semi-implicit method. *Quart. J. Roy. Meteor. Soc.*, **101**, 637-655.
- Joseph, P. V. and P. V. Pillai, 1987: Seasonal scale ocean-atmosphere interaction over tropical areas of Indian Ocean and west Pacific. In Ye, D.-Z. et al., eds.: *The Climate of China and Global Climate*. China Ocean Press, Beijing, Spring-Verlag, 1987.
- Keshavamurty, R. N., 1982: Response of the atmospheric to sea surface temperature anomalies over the equatorial pacific and the teleconnections of the southern oscillation. *J. Atmos. Sci.*, **39**, 1241-1259.
- Kleeman, R., 1991: A simple model of the atmospheric response to ENSO sea surface temperature anomalies. *J. Atmos. Sci.*, **48**, 3-18.
- Krishnamurti, T.N., J. Molinari and H. L. Pan, 1976: Numerical simulation of the Somali jet. *J. Atmos. Sci.*, **33**, 2350-2362.
- Lau, K-M. 1992: East asian summer monsoon rainfall variability and climate teleconnection. *J. Meteor. Soc. Japan*, **70**(1B), 211-242.
- Legates, D. R. and C. J. Willmott, 1992: A comparison of GCM-simulated and observed mean January and July precipitation. *Palaeogeography, Palaeoclimatology, Palaeoecology* (Global and Planetary Change Section), **97**, 345-363.
- Levitus, L., 1982: Climatological atlas of the world ocean. NOAA professional paper 13, U.S. Gov't Printing Office. 173 pp.
- Li, M., Y. Wu and J. Huang, 1987: The relationship between monsoon rainfall over

- eastern China and eastern equatorial Pacific sea surface temperature. *Chinese J. Atmos. Sci.*, **11**, 421-431.
- Livezey, R. E. and W. Y. Chen, 1983: Statistical field significance and its determination by Monte Carlo techniques. *Mon. Wea. Rev.*, **111**, 46-59.
- Manabe, S., J. Smagrinisky and R. F. Strickler, 1965: Simulated climatology of a general circulation model with a hydrologic cycle. *Mon. Wea. Rev.*, **93**, 769-798.
- Meehl, G. A., 1987: The annual cycle and international variability in the tropical pacific and Indian ocean regions. *Mon. Wea. Rev.*, **115**, 27-50.
- MONEG, 1992: Simulation of interannual and intraseasonal monsoon variability. WMO/TD-No.470, WCRP-68, World Meteorological Organization, Geneva, 185 pp.
- Newell R. E. and Z-X Wu, 1992: The interrelationship between temperature changes in the free atmosphere and sea surface temperature changes. *J. Geophys. Res.*, **97**, 3693-3709.
- Philander, S. G., 1990: El Nino, La Nina, and the Southern Oscillation. Academic Press, 1990, 293 pp.
- Ramanathan, V., E. J. Pitcher, R. C. Malone, and M. L. Blackmon, 1983: The response of a spectral general circulation model to refinements in radiative processes. *J. Atmos. Sci.*, **40**, 605-630.
- Ropelewski, C. F., M. S. Halpert, and X. Wang, 1992: Observed tropospheric biennial variability and its relationship to the southern oscillation. *J. Climate*, **5**, 594-614.
- Shen, S, K-M Lau, and F. Baer., 1991: The east Asian summer monsoon variability and tropical sea surface temperature. Preprint Volume, Fifth Conference on Climate Variations, Denver, Colorado, 14-18 October, 1991. American Meteorological Society, Boston, pp331-334.
- Weare, B. C., 1979: A statistical study of the relationships between ocean surface temperatures and the Indian Monsoon. *J. Atmos. Sci.*, **36**, 2279-2291.
- _____, J. T. Kiehl, V. Ramanathan, R. E. Dickinson and J. J. Hack, 1987: Description of NCAR community climate model (CCM1). NCAR/TN-285+STR, National Center for Atmospheric Research, Boulder, Colorado, 112pp.
- Williamson, G. S., D. L. Williamson, 1987: Circulation statistics from seasonal and perpetual January and July simulations with the NCAR community climate model (CCM1) : R15. NCAR Tech Note, NCAR/TN-302+STR, National Center for Atmospheric Research, Boulder, Colorado, 199pp.
- Wilson, C. A. and J. F. B. Mitchell, 1987: A doubled CO2 climate sensitivity experiment with a global climate model including a simple ocean. *J. Geophys. Res.*, **92**, D11, 13315-13343.
- Wyrtki, K., 1975: El Nino - the dynamic response of the equatorial Pacific ocean to atmospheric forcing. *J. Phys. Ocean.*, **5**, 572-584.
- Yasunari, T. and Y. Seki, 1992: Role of the Asian monsoon on the international variability of the global climate system. *J. Meteor. Soc. Japan*, **70**, 177-189.
- Zebiak, S. E. and M. A. Cane., 1987: A model El Nino-Southern Oscillation. *Mon. Wea. Rev.*, **115**, 2262-2278.
- Zhu, Y. L., 1987: Global water vapor transport and its relationship with hydrological cycle and latent heating: A preliminary result for July, 1979. MS thesis, Dept. of Meteor., Univ. of Wisconsin, Madison, Wisc., 63 pp.
- _____, 1993: The large-scale hydrological cycle and its role in Asian summer monsoon variations induced by Indian Ocean sea surface temperature anomalies. PhD Thesis, Department of Atmospheric and Oceanic Sciences, University of Wisconsin-Madison, 205pp.

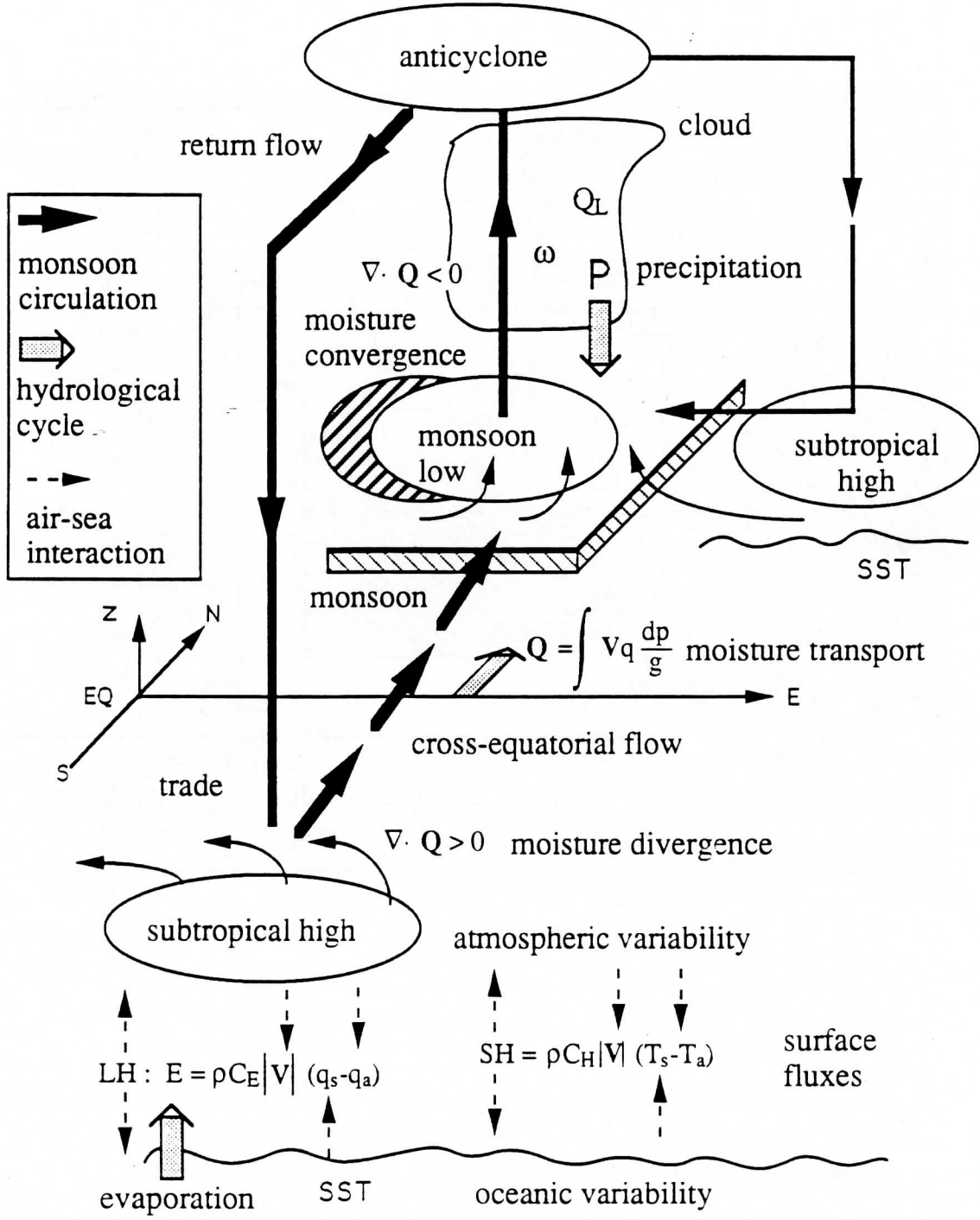


Fig. 1 Schematic representation of the basic elements and potential interactions of the Asian summer monsoon system.



Fig. 2 The area where SST anomalies are specified in the anomaly experiments (shaded).

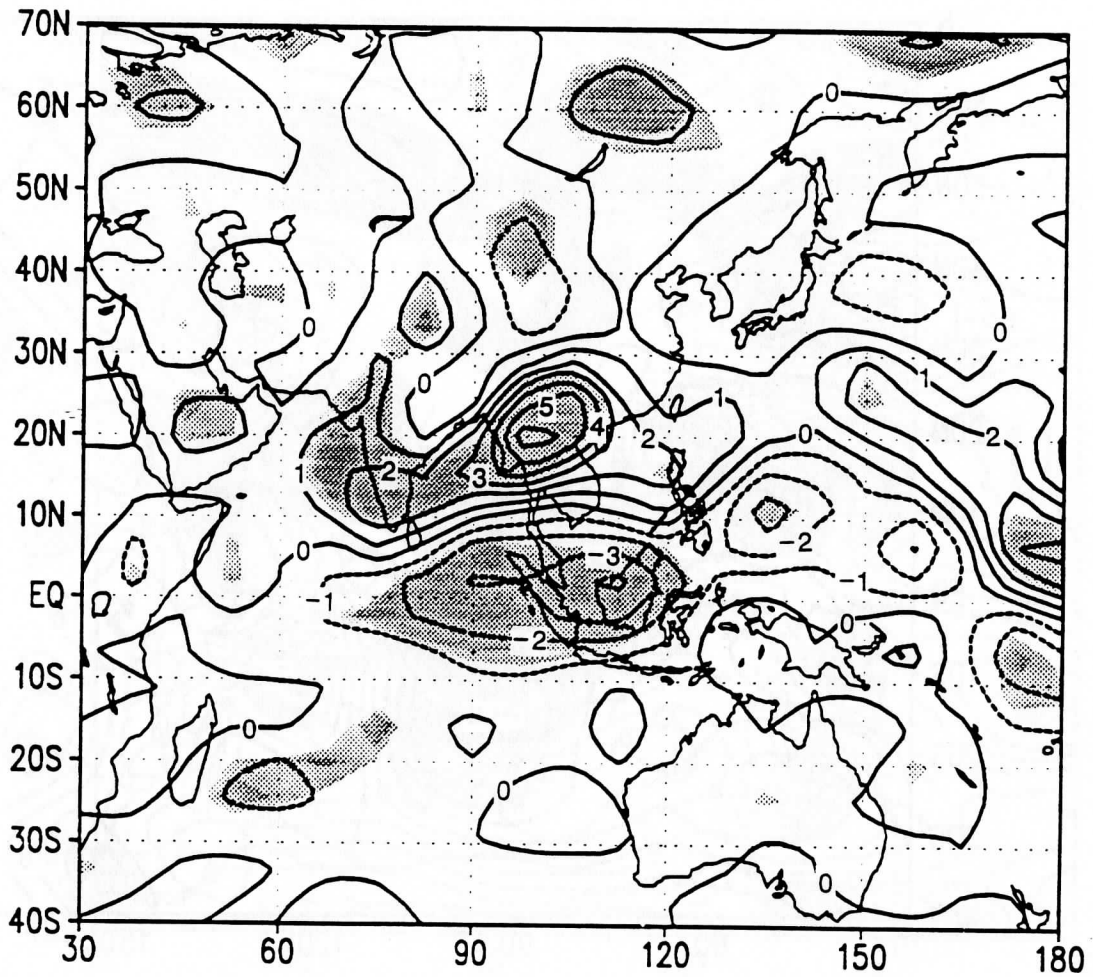


Fig. 3 Seasonal mean (Jun-Jul-Aug) anomaly for precipitation in the negative one degree SST anomaly case experiment. (Units: mm/day) Dashed-line indicates negative contours. Light-shading indicates areas where t-test significance level exceeds 90%, heavy-shading indicates significance level exceeds 95%.

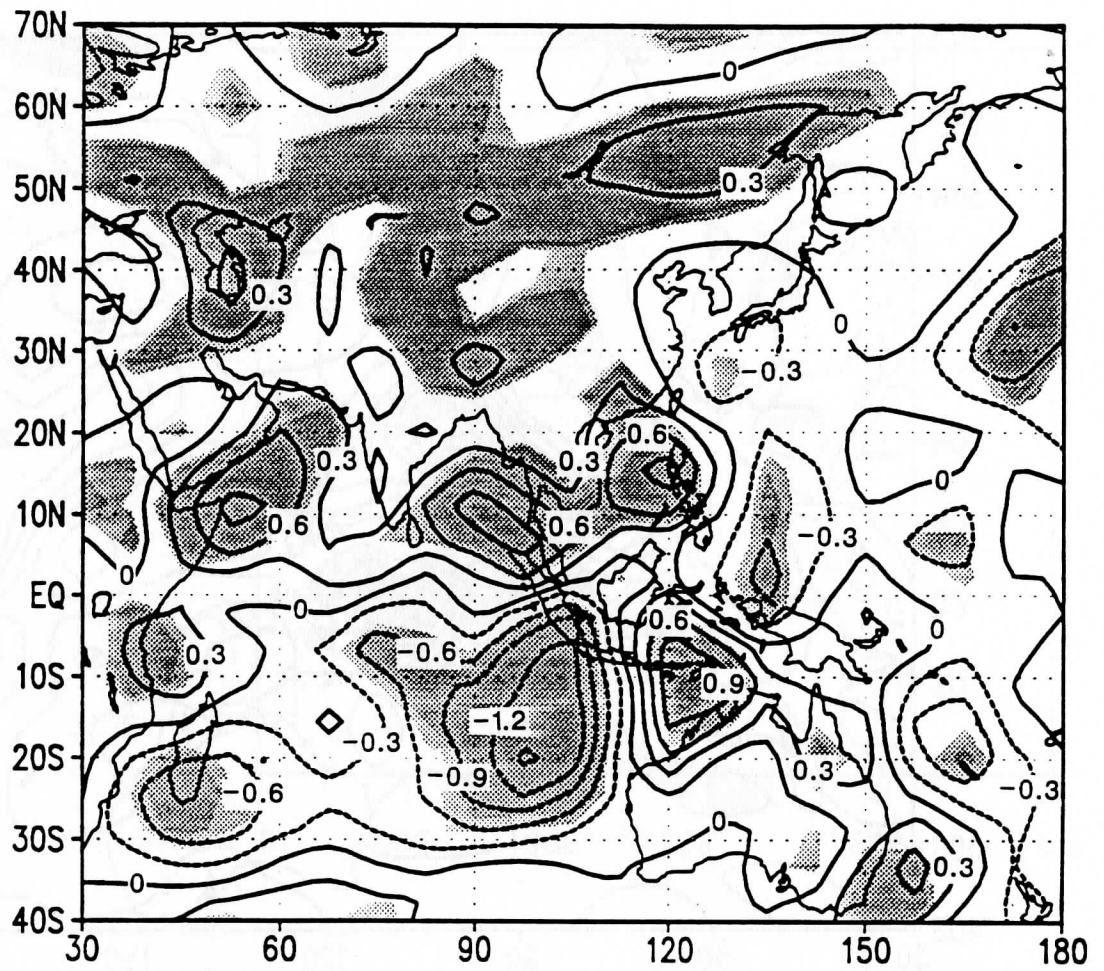


Fig. 4 Same as Fig. 3, but for evaporation. (Units: mm/day)

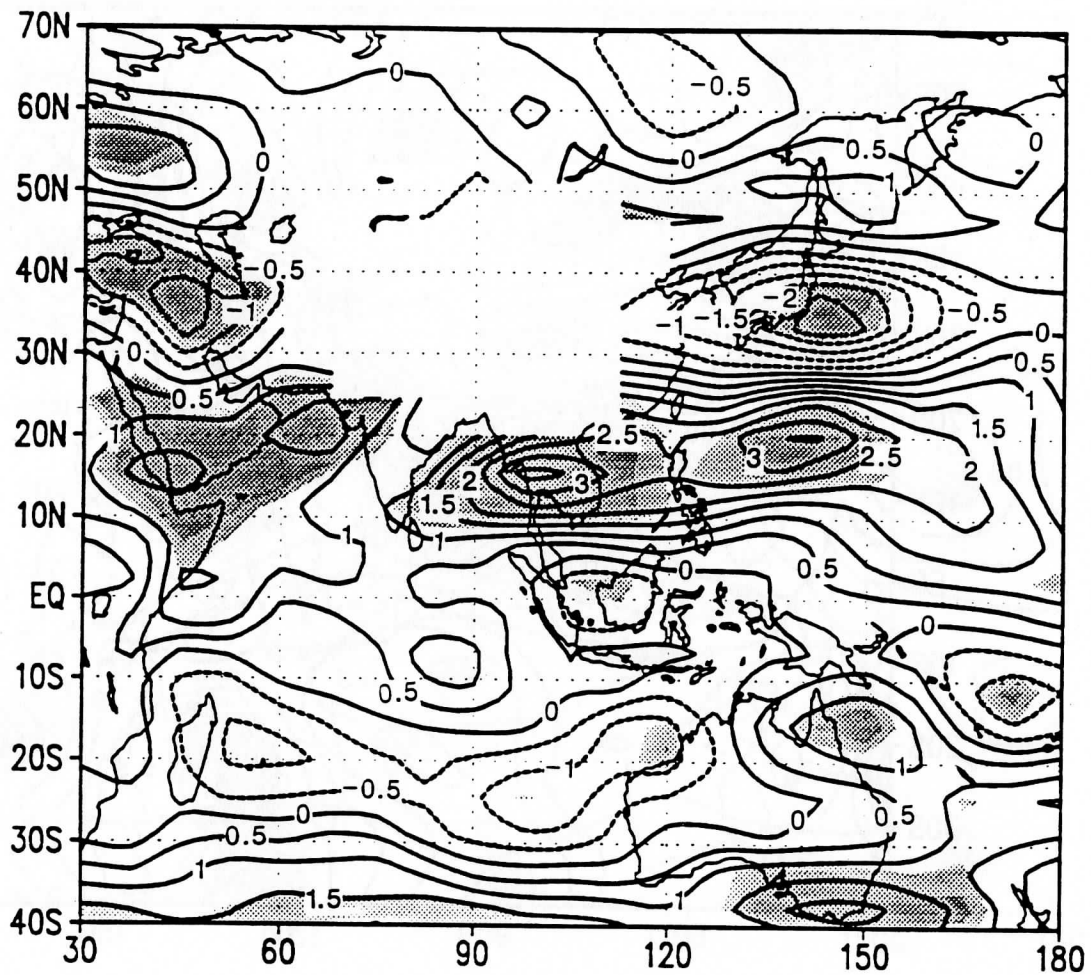


Fig. 5 Same as Fig. 3, but for the zonal wind at 850 mb.

(Units: m/s)

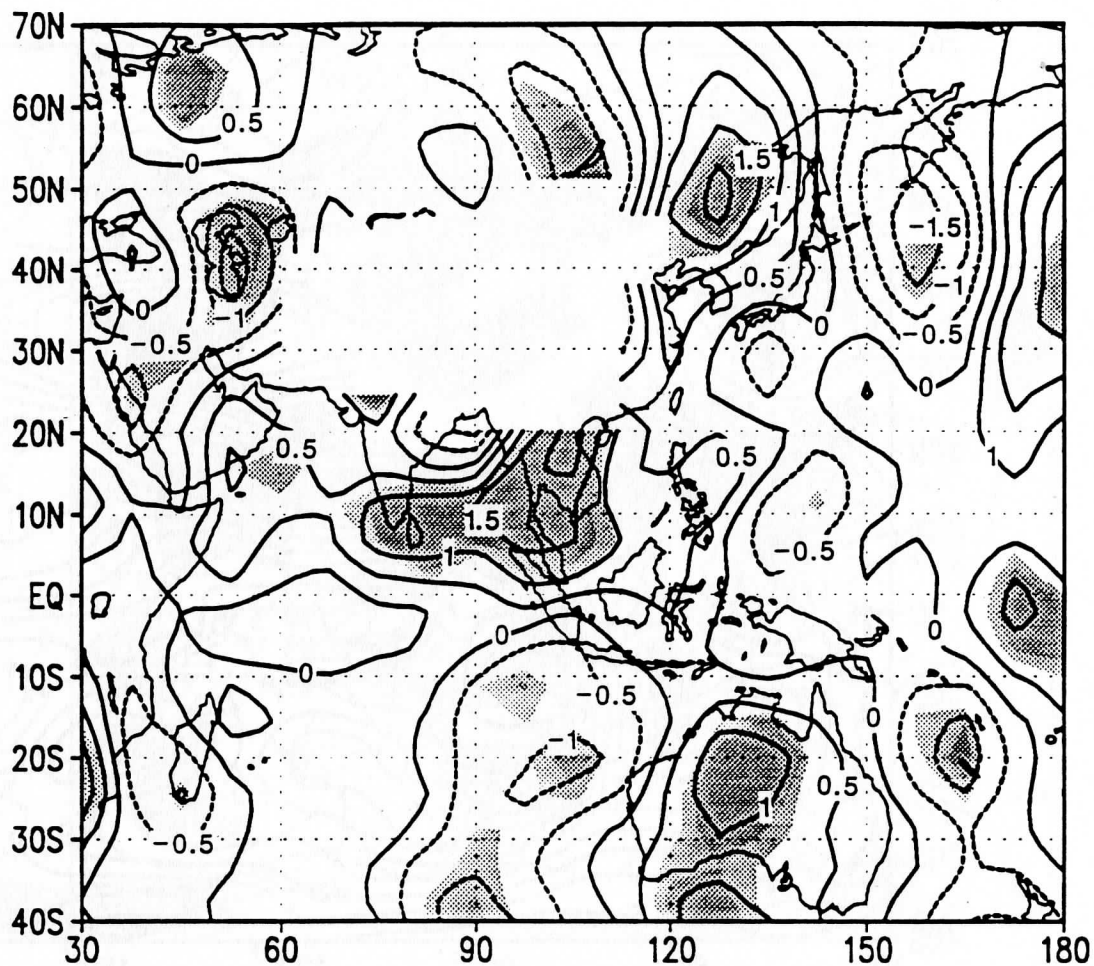


Fig. 6 Same as Fig. 3, but for the meridional wind at 850 mb. (Units: m/s)

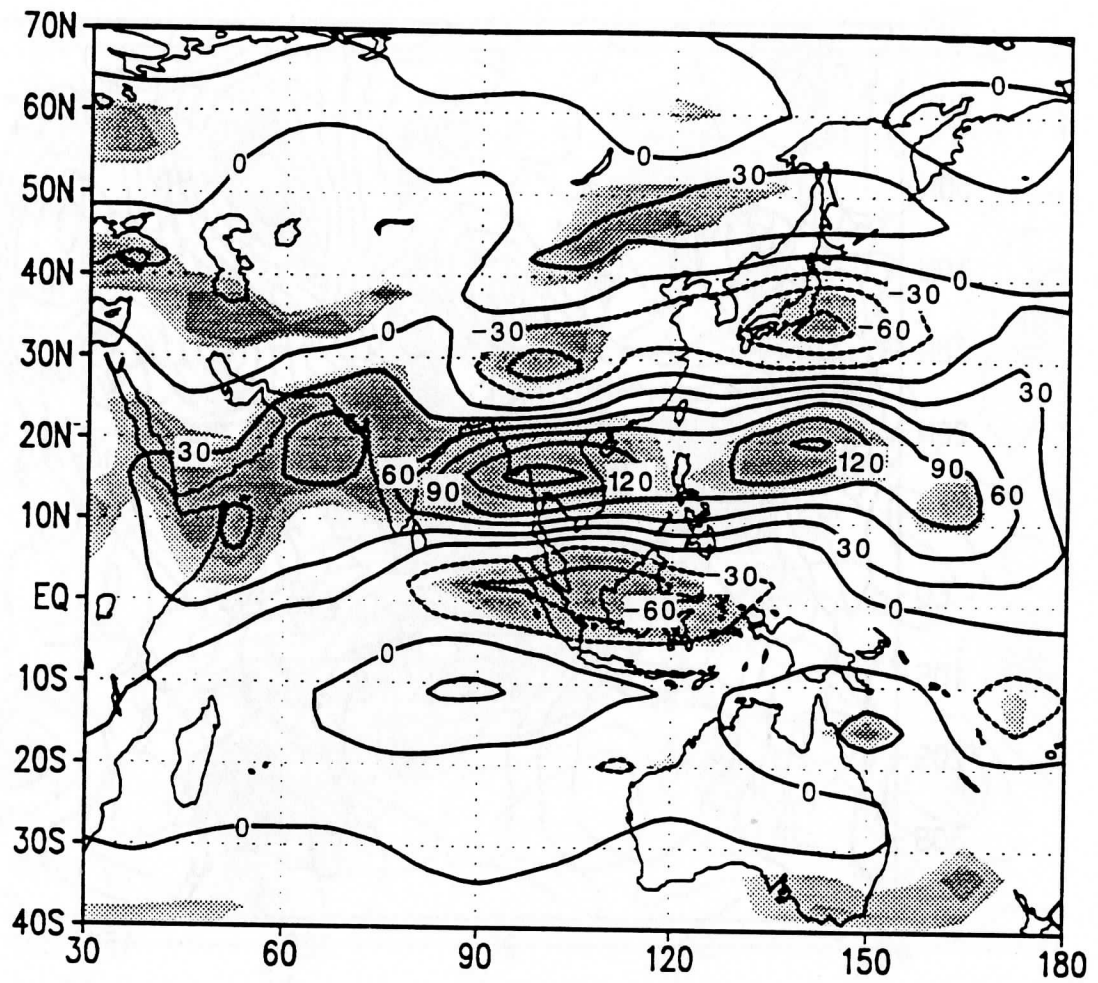


Fig. 7 Same as Fig. 3, but for the zonal component of the vertically integrated water vapor transport.
(Units: kg/m*s)

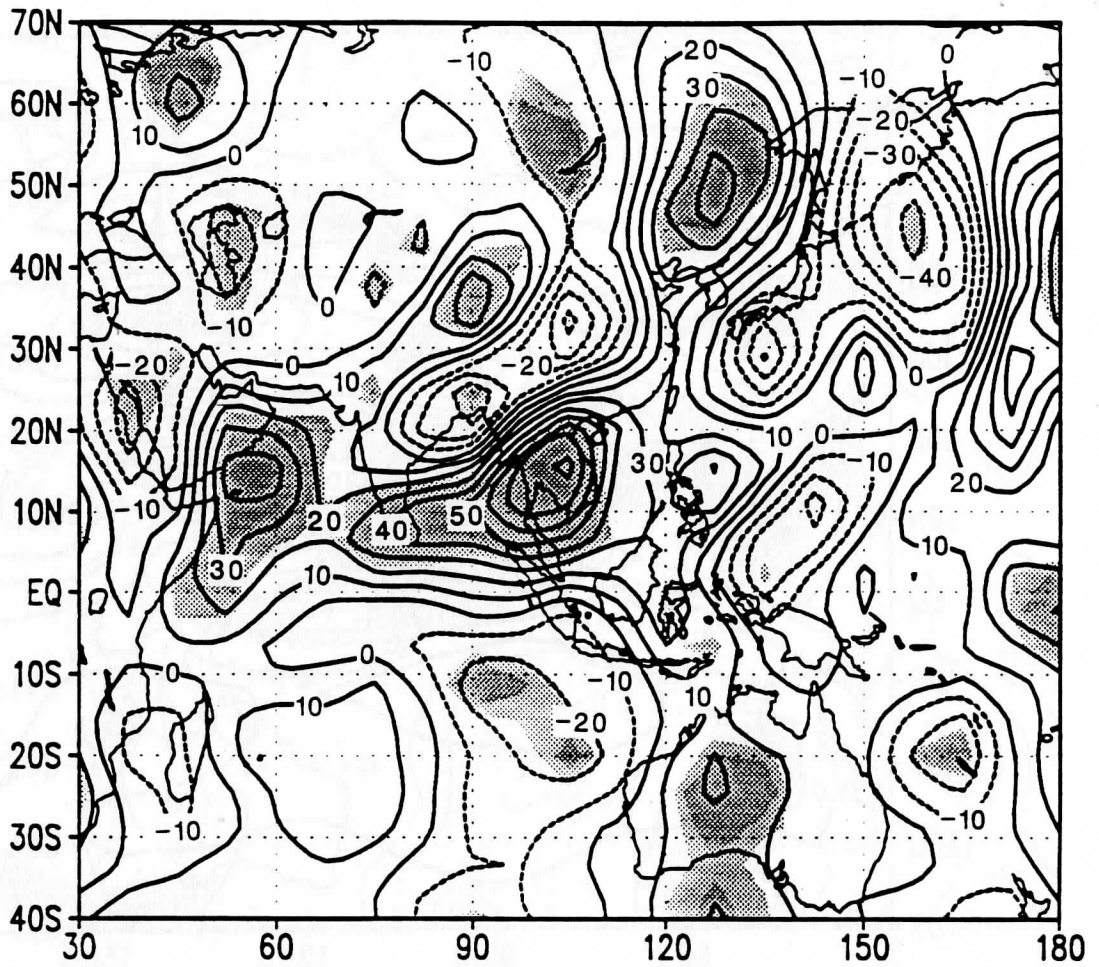


Fig. 8 Same as Fig. 3, but for the meridional component of the vertically integrated water vapor transport.
(Units: $\text{kg}/\text{m}^2\text{s}$)

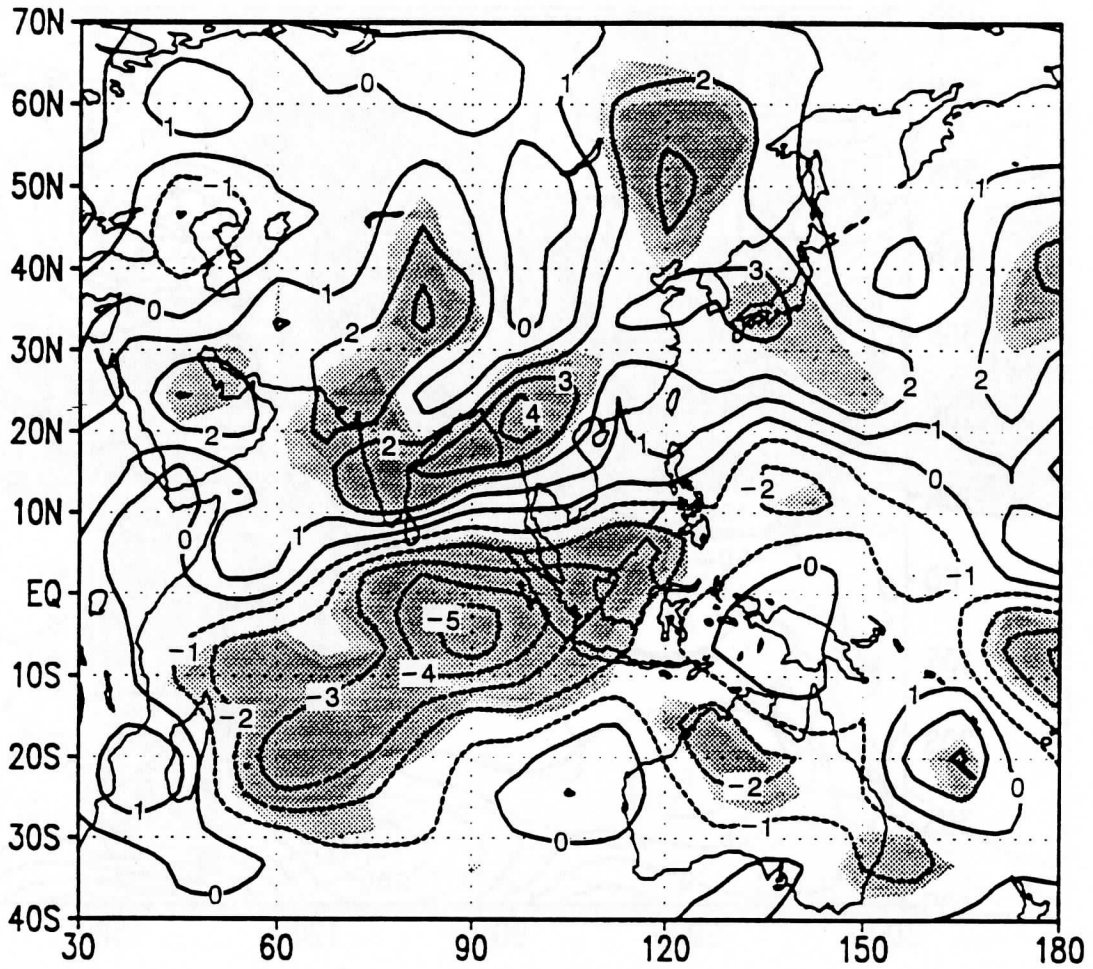


Fig. 9 Same as Fig. 3, but for precipitable water. (Units: kg/m^2)

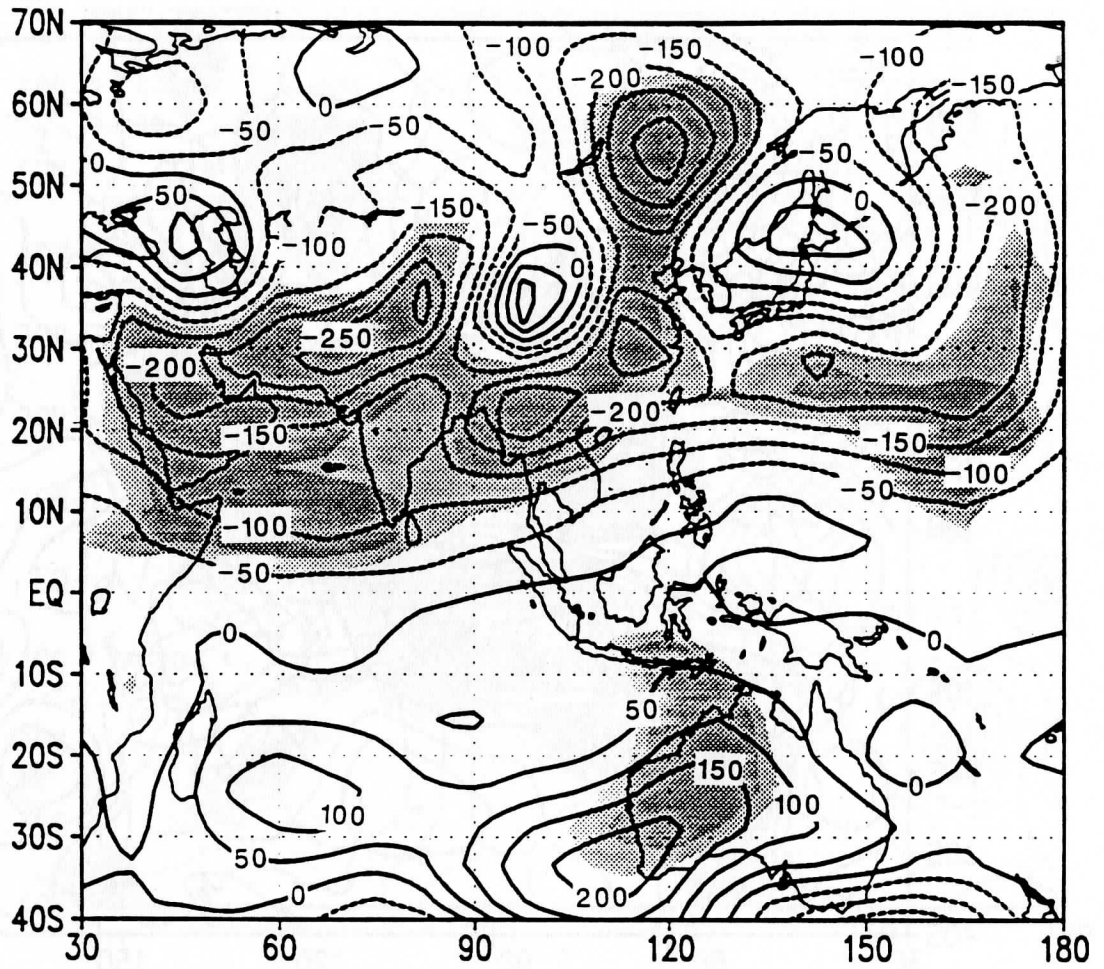


Fig. 10 Same as Fig. 3, but for sea level pressure.

(Units: Pa)

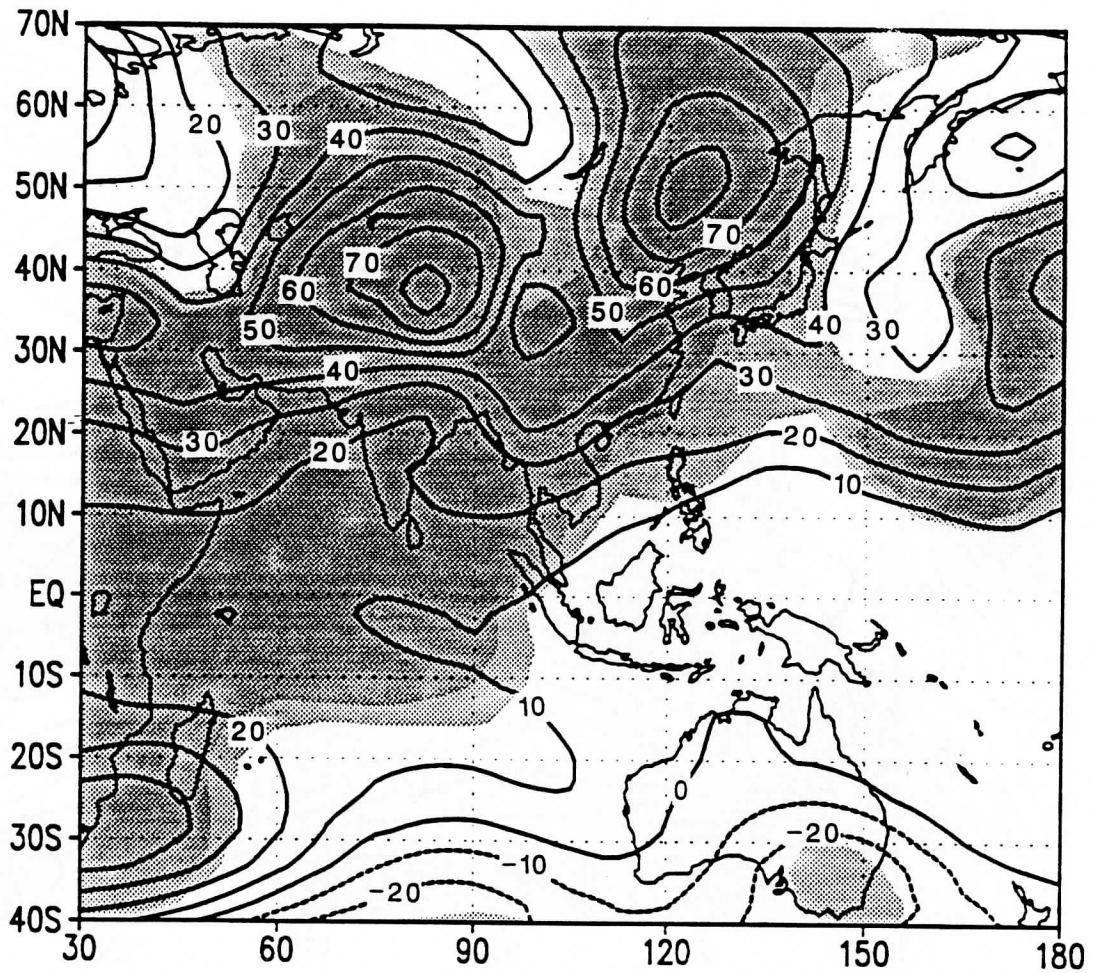


Fig. 11 Same as Fig. 3, but for thickness between 200 mb and 950 mb levels. (Units: m)

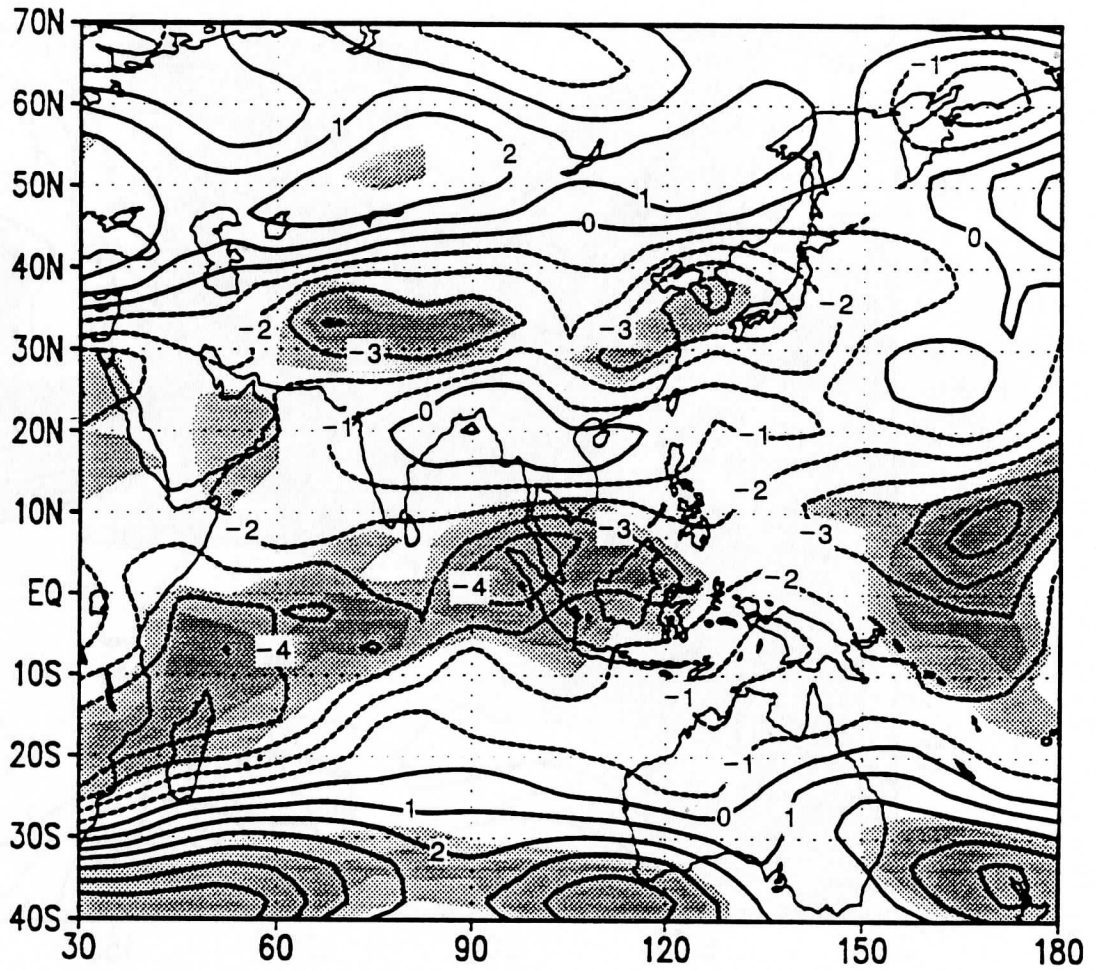


Fig. 12 Same as Fig. 3, but for the zonal wind at 200 mb.

(Units: m/s)

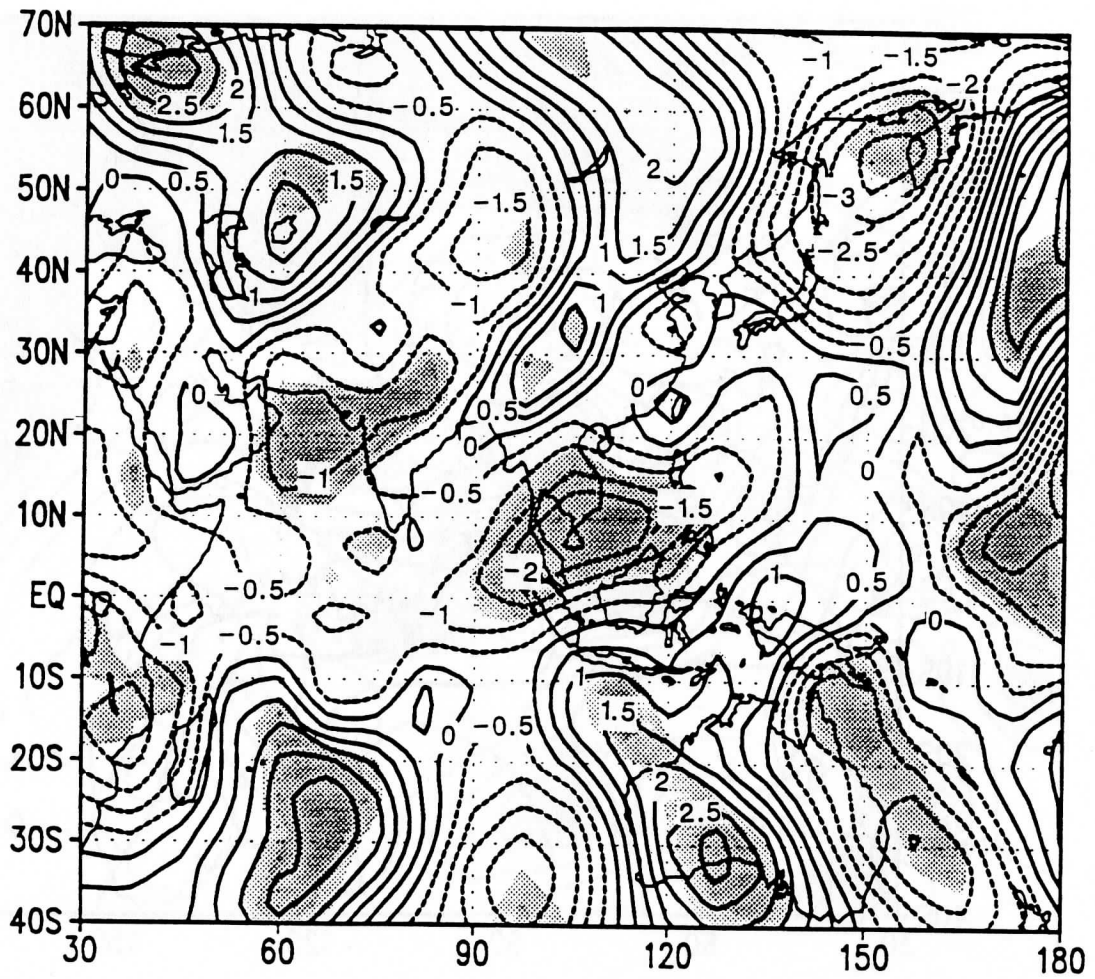


Fig. 13 Same as Fig. 3, but for meridional wind at 200 mb.

(Units: m/s)

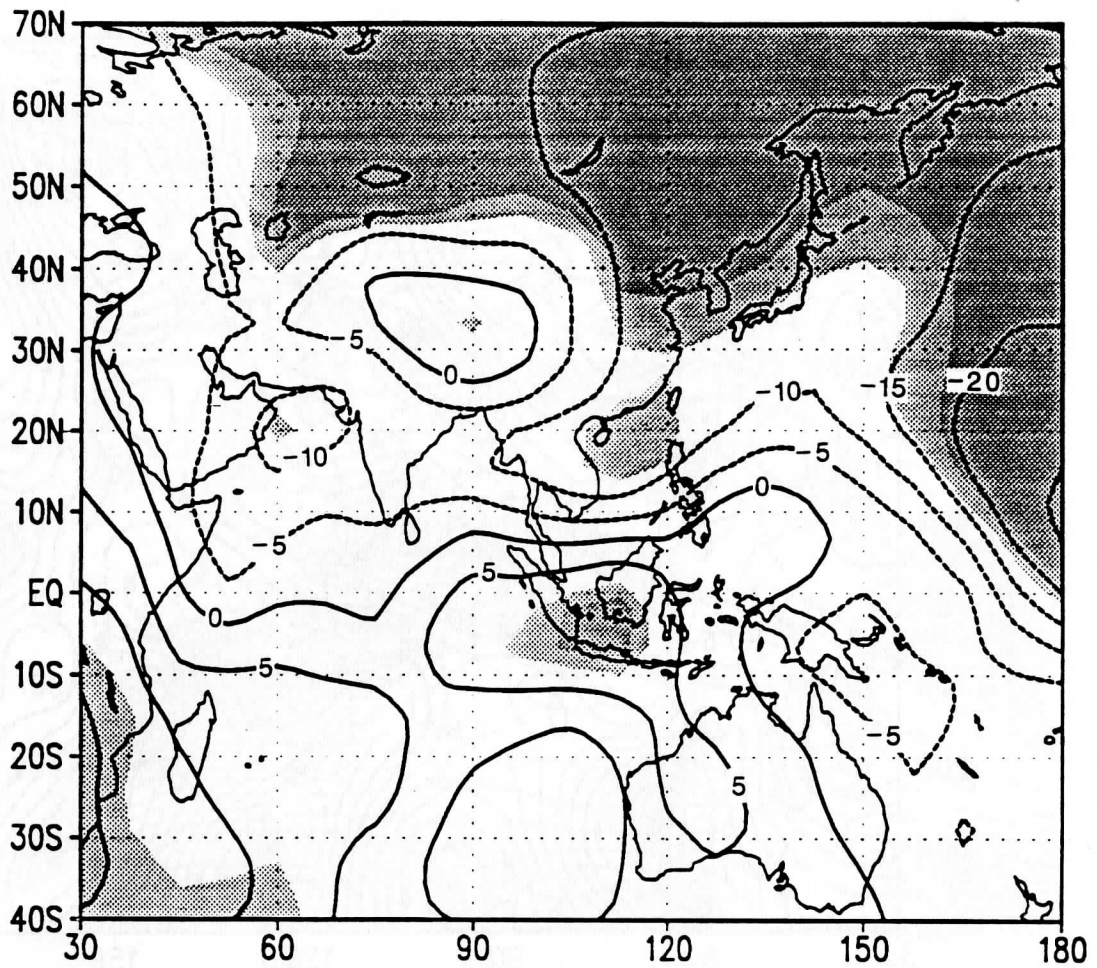


Fig. 14 Same as Fig. 3, but for 200 mb velocity potential.

(Units: $10^5 \text{ m}^2/\text{s}$)

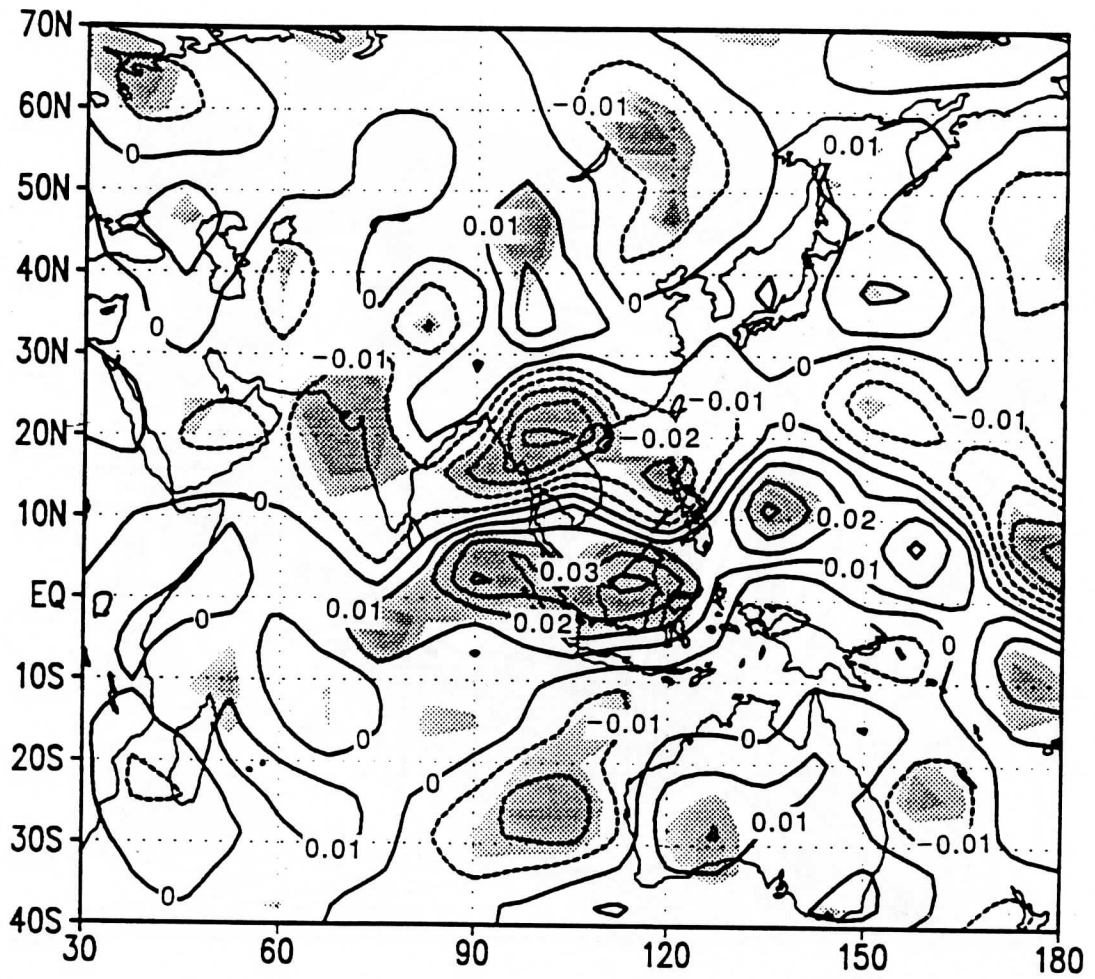


Fig. 15 Same as Fig. 3, but for vertical motion at 500 mb.

(Units: Pa/s)

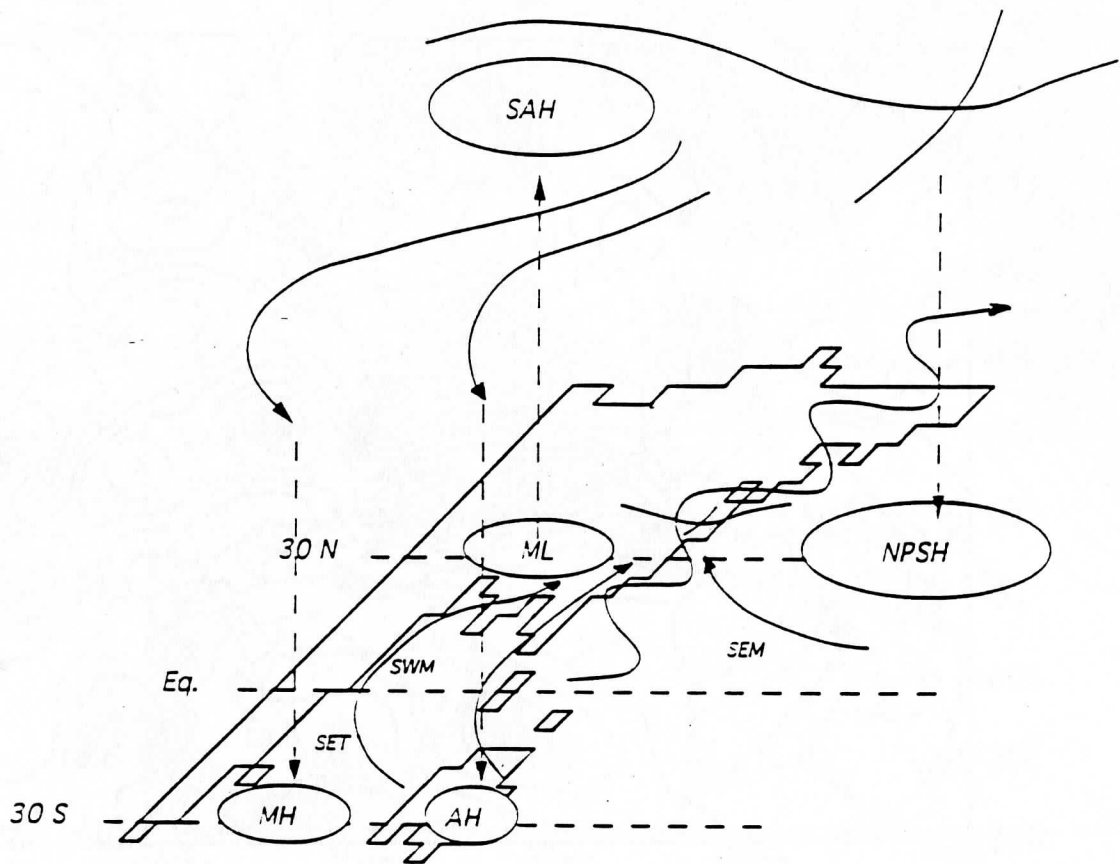


Fig. 16 The three-dimensional mean summertime climatological configuration of the pressure systems and motion fields in the Asian monsoon region. (Acronyms are defined in the text)

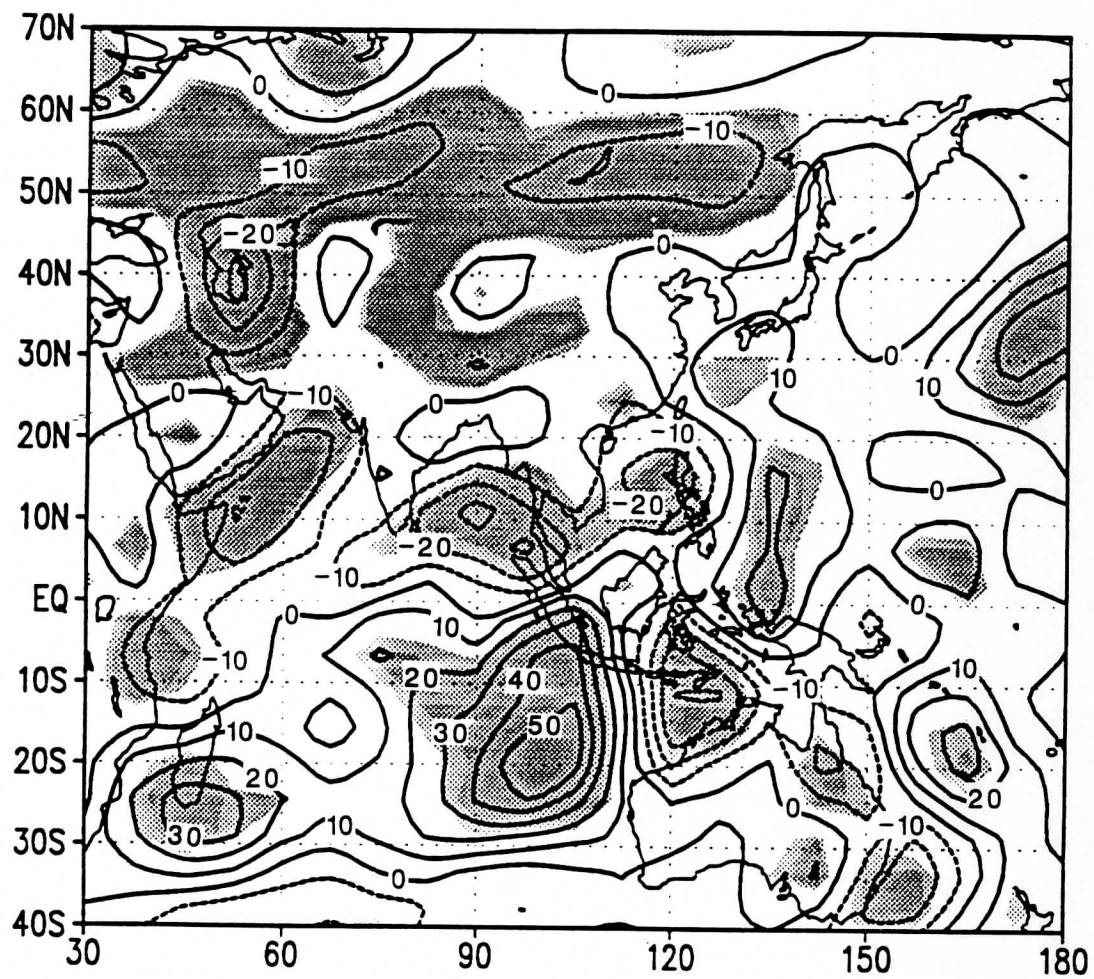


Fig. 17 Seasonal mean (Jun-Jul-Aug) anomaly for net surface heat flux in the negative one degree SST anomaly case (Units: W/m^2)